THE UNIVERSITY OF CALGARY

Molecular Determinants of Calcium Channel Inactivation

By

Renée Spaetgens

A THESIS

SUBMITTED TO THE FACULTY OF GRADUATE STUDIES

IN PARTIAL FULFILLMENT OF THE REQUIREMENTS FOR THE

DEGREE OF MASTER OF SCIENCE

DEPARTMENT OF NEUROSCIENCE

CALGARY, ALBERTA

SEPTEMBER, 1999

Abstract

R-type (α_{1E}) and L-type (α_{1C}) calcium channels exhibit dramatically different inactivation properties. To define structural determinants which govern these intrinsic differences, a series of chimeric calcium channel α_1 subunits was created which combines the major structural domains of the two wild-type channels. Results from whole-cell voltage clamp experiments indicate that each of the four domains help to determine the voltage-dependence of steady-state inactivation, and that inactivation rate is governed by domains II, III and IV. A second series of chimeras in which the II S6 and III S6 segments were individually switched amongst the two parent channels revealed that the these segments play an important role in determining inactivation rate, but have little influence on steady state inactivation profiles. Thus, voltage-dependent inactivation of the α_{1E} channels appears to be a complex process involving multiple structural domains and possibly a global conformational change at the pore as seen for C-type potassium channel inactivation.

Acknowledgments

I would like to thank my supervisor, Dr. Gerald Zamponi for his guidance and support over the past two years, as well as my committee members, Dr. Peter Light and Dr. William Cole for their assistance. I would also like to thank Dr. Jawed Hamid, Scott Jarvis, and Aaron Beedle who have helped me many times along the way, and particularly Stephanie Stotz who did the recordings for the second set of chimeras. In addition I would like to thank my parents for their support and encouragement.

Table of Contents

List of Tables

List of Figures

INTRODUCTION

Calcium channels are voltage-dependent ion channels which allow the entry of calcium ions into cells upon membrane depolarization. These channels are ubiquitous to all excitable cells including skeletal, smooth and cardiac muscle, neurons, and a wide range of cells that secrete hormones and neuromodulators. In these cells, calcium channels mediate a critical role in maintaining and regulating internal calcium levels. Calcium is somewhat unique among permeant ions in that calcium ions themselves serve many crucial functions within the cell, in addition to carrying electrical charge. Actions of calcium ions within the cell include the activation of second messenger cascades and calcium-dependent enzymes, release of calcium from internal stores, control of gene transcription levels, excitation-contraction coupling in heart and muscle, neurite proliferation, and control of neurotransmitter release (Marty, 1989; Pelzer *et. al.*, 1990). They also play a role in controlling the activity of other ion channels, including the calcium-activated potassium and chloride channels. Under normal physiological conditions, intracellular calcium levels are maintained at exceedingly low levels (~10 - 100 nM), in comparison to the extracellular space, where the calcium ion concentration is in the one to two mM range. During increases in voltage-dependent calcium channel activity, the cytosolic calcium levels can reach concentrations of 100 μM in the vicinity of the plasma membrane (De Waard *et. al.*, 1996). Thus, the flux of calcium through a population of conducting calcium channels, in addition to depolarizing the membrane,

also alters the intracellular calcium concentration by more than two orders of magnitude, allowing calcium to trigger one or more of the above cellular events.

Biophysical and Pharmacological Diversity of Calcium Channels

Several types of calcium channels, distinguished by biophysical and pharmacological properties as well as cellular distribution, have been identified to date. Traditionally calcium channels have been grouped into two major categories according to their kinetics and voltage-dependent properties: high voltage-activated (HVA) channels, and low voltage-activated (LVA) channels (Birnbaumer *et. al.*, 1994).

The HVA channels activate at depolarized membrane potentials (between -30 and 0 mV), and include N-, P-, Q-, L-, and R-type channels. Within the HVA class, the channel subtypes are distinguished by their pharmacological profiles, biophysical properties (i.e., activation and inactivation kinetics), and relative permeabilities to divalent cations. The N-type channels are rapidly inactivating, and are irreversibly blocked by ω-conotoxin GVIA, a calcium channel antagonist isolated from the venom of the *Conus geographus* marine snail (Plummer *et. al.*, 1989). They are localized to presynaptic nerve terminals where they play a key role in neurotransmission (Hirning *et. al.*, 1988; Tsien *et. al.*, 1988; Robitaille *et. al.*, 1990; Westenbroek *et. al.*, 1992). P- and Q-type channels are also located at presynaptic nerve terminals where they are implicated in neurotransmitter release (Takahashi and Momiyama, 1993; Wheeler *et. al.*, 1994). Both P- and Q-type channels are blocked by ω-agatoxin IVA, a toxin from a funnel web

spider, with the P-type channels showing a ~100-fold higher sensitivity (Mintz *et. al.*, 1992b). In addition, these channels exhibit different biophysical properties. The P-type channels, first identified in Purkinje neurons, show no or very little time-dependent inactivation in comparison with the Q-type channels which exhibit rapid inactivation kinetics (Regan *et. al.*, 1991; Mintz *et. al.*, 1992a). The L-type channels exhibit very slow inactivation kinetics and are sensitive to dihydropyridines (Soldatov *et. al.*, 1988; Murphy *et. al.*, 1990). Neuronal L-type channels are localized to cell bodies and proximal dendrites, where they likely play an important role in regulation of basal cellular activity (Westenbroek *et. al.*, 1990; Hell *et. al.*, 1993). In addition, L-type channels are the major calcium channel subtype found in cardiac, smooth, and skeletal muscle cells, where they mediate excitation-contraction coupling by triggering calcium release from the sarcoplasmic reticulum through the ryanodine receptor (Tanabe *et. al.*, 1990; Catterall, 1991). R-type channels reside in nerve terminals and along dendrites, and are defined by their resistance to the common calcium channel blockers (Randall *et. al.*, 1993). They activate at relatively negative potentials and inactivate rapidly. It is thought that the R-type channels may be a heterogeneous population of calcium channels characterized mainly by their lack of sensitivity to specific calcium channel antagonists (Randall *et. al.*, 1993; Tottene *et. al.*, 1996).

The other major group of calcium channels are the low-voltage activated channels (LVA), also referred to as T-type channels. These low threshold channels are transiently activated by relatively small depolarizations (in the -75 to -50 mV range) and inactivate very rapidly over a time course of less than 100 ms (Cribbs *et. al.*, 1998; Perez-

Reyes *et. al.*, 1998; Lee *et. al.*, 1999). T-type calcium channels have been identified in several tissue types including neuronal, and smooth, cardiac and skeletal muscle (Cribbs *et. al.*, 1998; Talley *et. al.*, 1999). They are thought to be involved in pacemaker activity, low threshold calcium spikes, neuronal oscillations, and resonance and rebound firing (Hagiwara *et. al.*, 1988; Huguenard, 1996). To date, no specific antagonist for T channels has been identified, although commonly they are thought to exhibit a higher sensitivity to block by nickel ions than the HVA channels.

Subunit Structure of Voltage-Dependent Calcium Channels

Calcium Channels are Multi-Subunit Proteins

Molecular cloning and functional expression studies have immensely advanced our understanding of calcium channel structure and function. Studies carried out over the past 10 years have shown that calcium channels, like other ionic channels, are membrane spanning proteins that consist of several subunits (see Fig. 1). The α_1 subunit is the pore forming subunit and has a molecular weight between 200 and 250 kD. It is thought to be the primary determinant of the biophysical and pharmacological properties of a calcium channel. Expression of the α_1 subunit alone can result in functional calcium channel activity; however, three accessory subunits associate with the α_1 subunit and modulate its activity.

All HVA channels contain cytoplasmic β subunits as an element of the channel protein complex. β subunits are 50-70 kD proteins. They contain no putative

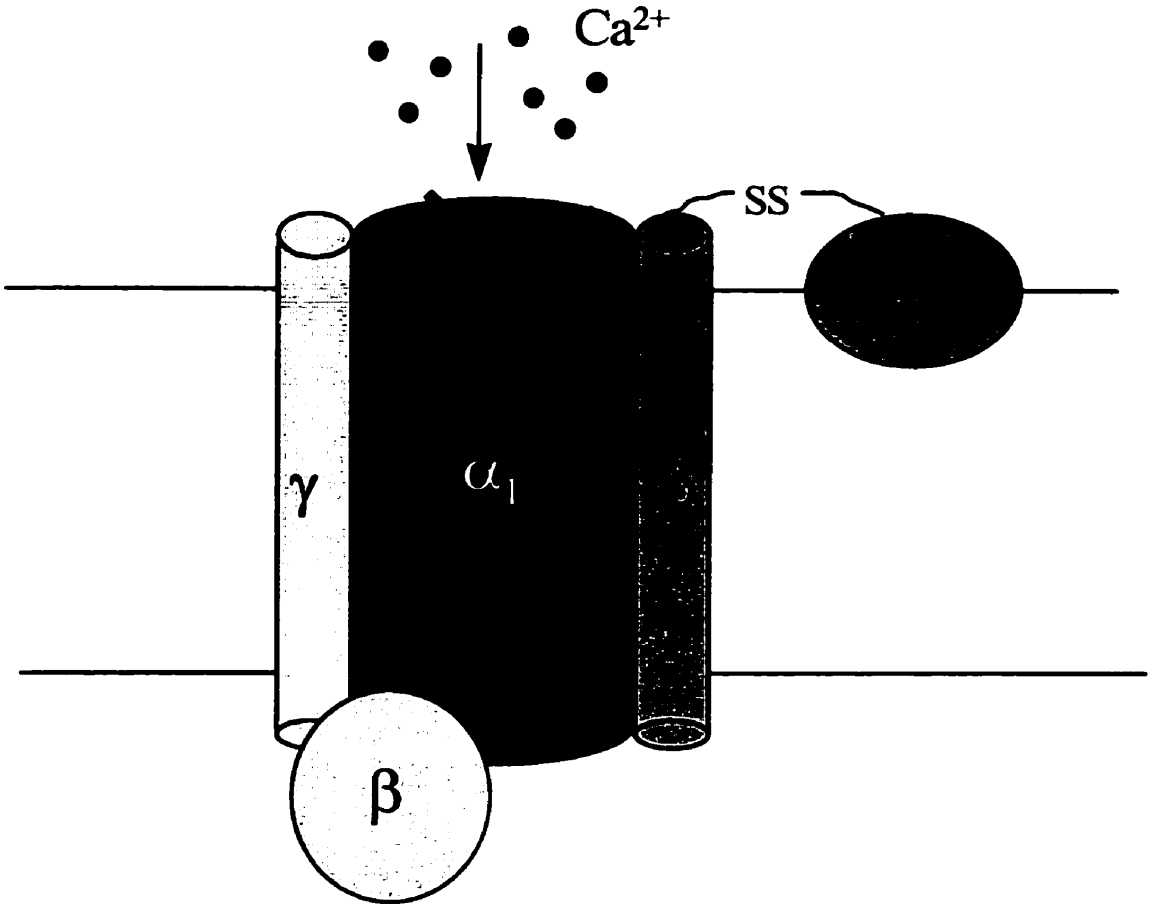

Figure 1 - Calcium Channel Subunit Composition

Calcium channels are comprised of four protein subunits. The pore-forming α_1 subunit (200 - 250 kD) associates with an intracellular β (50-70 kD) and the transmembrane α_2-δ (170 kD) and γ (25 kD) subunits.

transmembrane domains, and likely associate with the α_1 subunit at the cytoplasmic side of the channel. β subunit structure is unknown, but sequence predictions suggest a series of α-helices (Walker and De Waard, 1998). Four different genes encoding for different calcium channel β subunits (termed β_1 - β_4) have been identified, all of which are expressed in the brain as well as in many other tissues including skeletal, smooth and cardiac muscle (Hullin *et. al.*, 1992). β subunit co-expression substantially increases the level of current amplitude of calcium channels, but the mechanism by which this is mediated is not well understood. Direct interaction of the β subunit with α_1 could result in an increase in conductance or open probability of the channel by inducing a conformational change in the pore subunit. Alternatively, there is strong evidence that β subunits aid in targeting the α_1 subunit to the plasma membrane (Josephson and Varadi, 1996; Kamp *et. al.*, 1996; Brice *et. al.*, 1997; Chien *et. al.*, 1998). The β subunits are also important modulators of the biophysical properties calcium channels. They modify the kinetics and voltage-dependence of activation and inactivation, with different β subunits having distinct effects in this regard (Soong *et. al.*, 1993; Stea *et. al.*, 1993; DeWaard and Campbell, 1995). For example, the β_1 and β_3 subunits accelerate inactivation kinetics, whereas coexpression with the β_2 subunit dramatically slows inactivation of calcium channels (Ellinor *et. al.*, 1993; Sather *et. al.*, 1993). Finally, β subunits have also been shown to modulate the pharmacological properties of the α_1 subunits (i.e., Zamponi *et. al.*, 1996).

Calcium channel α_1 subunits are associated with a third subunit called α_2-δ (170 kD). It is a membrane spanning subunit composed of an α_2 and a δ protein which are encoded by one gene, posttranslationally cleaved and then relinked by a disulfide bond (Ellis *et. al.*, 1988; De Jongh *et. al.*, 1990; Jay *et. al.*, 1991). Structurally, the α_2-δ is heavily glycosylated, and it is the δ component that anchors the α_2 to the membrane via a single transmembrane segment (Gurnett *et. al.*, 1996). The α_2-δ subunit is well conserved across many different tissues, including heart, brain, and skeletal muscle. To date three genes have been identified which encode the protein (Klugbauer *et. al.*, 1999). The effects of the α_2-δ subunit on channel activity are not as dramatic as the effects of the β subunits. The α_2-δ seems to mediate an increase in current amplitude, and has small effects on activation/inactivation kinetics, but these effects are dependent on β subunit coexpression. Otherwise the role of this subunit is not well understood (Felix *et. al.*, 1997, Klugbauer *et. al.*, 1999).

All calcium channels are formed by a combination of the α_1 subunit with the β and α_2-δ subunits, except for the skeletal L-type channels which also include a fourth subunit. The γ subunit is a membrane spanning protein with a molecular weight of approximately 25 kD. It is very hydrophobic and extensively glycosylated (Eberst *et. al.*, 1997). The function of this subunit is still incompletely understood. Recently, a novel neuronal form of the γ subunit was identified (Letts *et. al.*, 1998). The 36 kD protein, called stargazin, is brain specific and shows structural similarity to the γ subunit of skeletal muscle. Disrupted expression of the stargazin gene (by insertion of an early

transposon leads to a form of genetic epilepsy in a mouse mutant called stargazer, presumably by allowing in appropriate calcium entry into neurons. The stargazer phenotype closely resembles that observed in humans with absence (or petit mal) epilepsy. In contrast with the high voltage activated channels, the T-type channels do not appear to be associated with any ancillary subunits.

The α_1 Subunit Determines Pharmacological and Biophysical Properties

The biophysical and pharmacological properties of a given calcium channel are primarily determined by the α_1 subunit. To date, the primary structures of 10 different neuronal calcium channel α_1 subunits (termed α_{1A} through α_{1I}) have been identified. α_{1C}, α_{1D}, and α_{1F} encode L-type channels (Williams *et. al.*, 1992a; Tomlinson *et. al.*, 1993; Bech-Hansen *et. al.*, 1998), α_{1B} defines N-type channels (Dubel *et. al.*, 1992; Williams *et. al.*, 1992b; Fujita *et. al.*, 1993), different splice variants of α_{1A} encode P- and Q-type channels (Mori *et. al.*, 1991; Sather *et. al.*, 1993; Stea *et. al.*, 1994; Bourinet *et. al.*, 1996; Sutton *et. al.*, 1998; Bourinet *et. al.*, 1999), α_{1G}, α_{1H} and α_{1I} form T-type channels (Cribbs *et. al.*, 1998; Perez-Reyes *et. al.*, 1998; Lee *et. al.*, 1999), and α_{1E} likely encodes a component of the resistant (R-type) current identified in several neuronal preparations (Soong *et. al.*, 1993; Williams *et. al.*, 1994; Tottene *et. al.*, 1997). Finally, an additional α_1 subunit encoding the skeletal muscle L-type channel has been identified and termed α_{1S} (Ellis *et. al.*, 1988; Morton and Froehner, 1989). Alternative splicing of these 10 transcripts produces at least 20 structurally distinct α_1 subunits to substantially increase

the diversity of calcium channel phenotypes. Overall, the channels can be grouped into three phylogenetically related groups (see Fig. 2) - the L-type channels (α_{1C}, α_{1D}, α_{1F}, α_{1S}), the non-L-type high voltage activated channels (α_{1A}, α_{1B}, α_{1E}), and the low voltage activated channels (α_{1G}, α_{1H}, α_{1I}). Within each of these groups, there is a relatively high degree of identity (~65%) whereas less than 40% identity is observed across the three groups (De Waard *et. al.*, 1996).

Calcium channel α_1 subunits are structurally similar to the α subunit of sodium channels. The predicted transmembrane topology of the α_1 subunit indicates that the protein is comprised of four major transmembrane regions termed domains I-IV, which are connected via cytoplasmic linkers (see Fig. 3). Within each domain there are six transmembrane segments which are referred to as S1-S6 in each domain. The structure also includes an intracellular amino-terminus and a longer intracellular carboxyl terminus. The transmembrane sequences are highly conserved with most of the sequence variability arising in the intracellular loops connecting the segments and in the carboxyl terminus.

Several structural features of the calcium channel α_1 subunit have been associated with various calcium channel functions to date. For example; (a) the fourth segment in each domain (S4) is 20 amino acids in length and contains repeated motifs of one positively charged amino acid at every third or forth position followed by several hydrophobic amino acids. Site-directed mutagenesis of the positively charged amino acids of the S4 segment of sodium channels has revealed that these segments likely

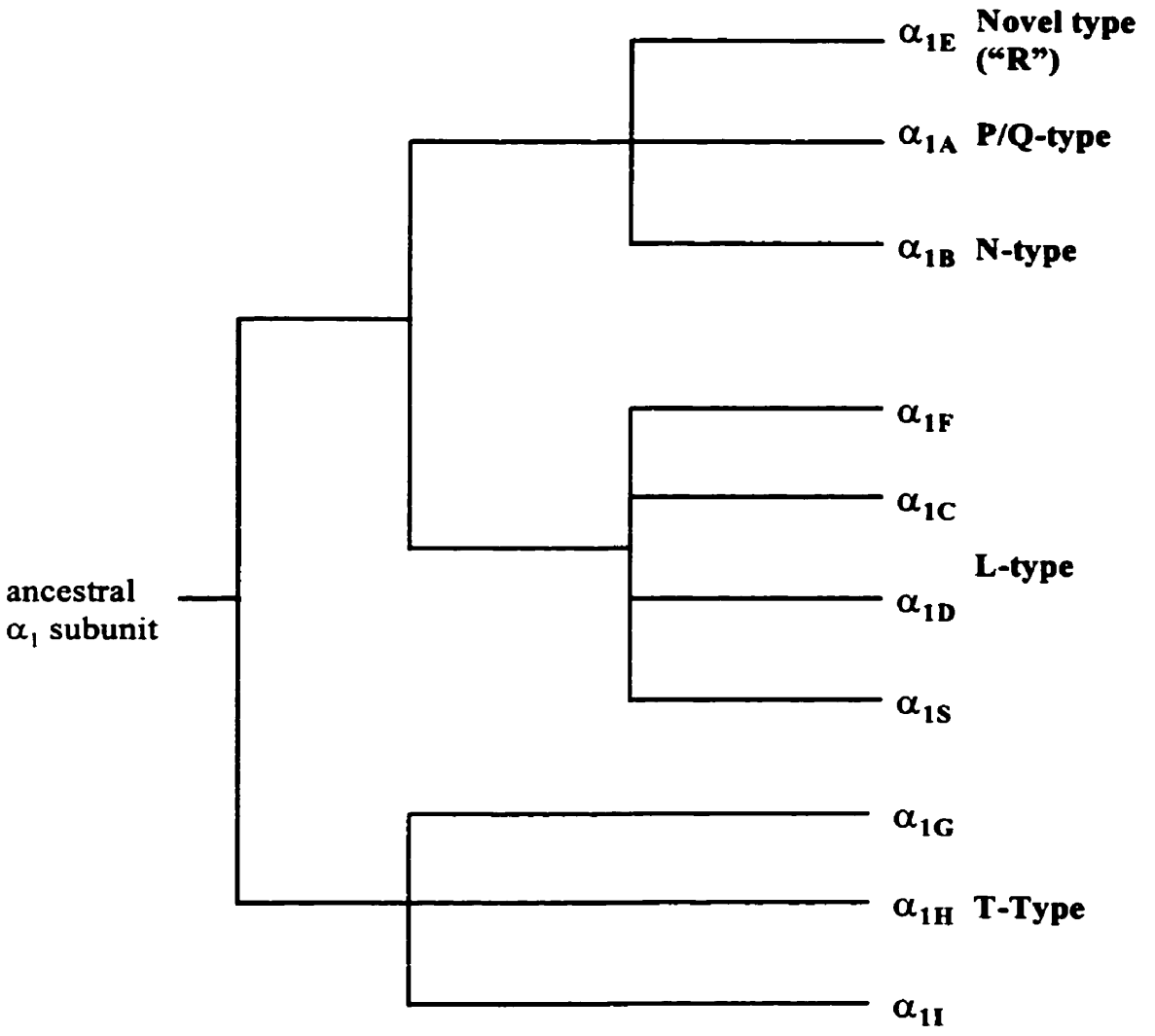

Figure 2 - Classification and Gene Family Tree of Calcium Channel α_1 Subunits

Relationship of the α_1 subunit genes that form calcium channels. Degree of relatedness is based on amino acid identity. Channel subtypes for each α_1 gene(s) are listed on the right hand side of the figure.

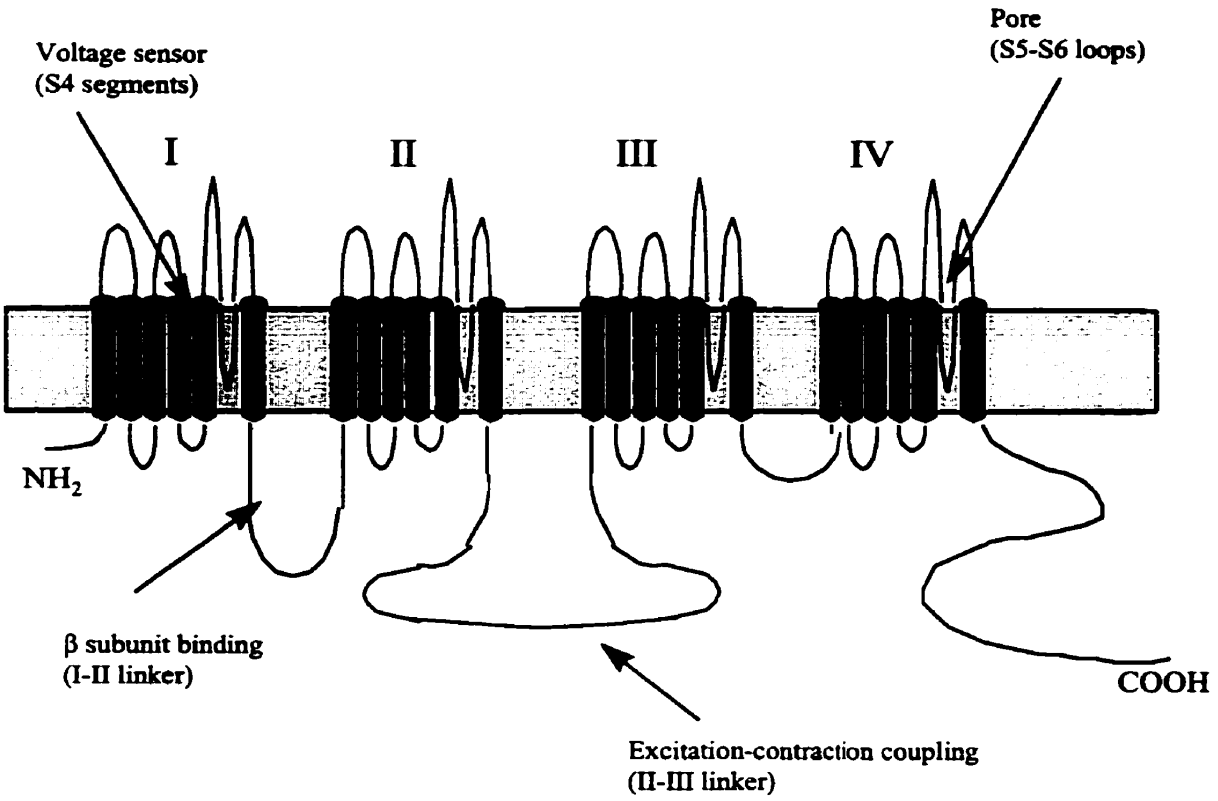

Figure 3 - Transmembrane Topology of Calcium Channel α_1 Subunits

Calcium channel α_1 subunits contain four major transmembrane domains, each having six membrane spanning segments. The amino- and carboxyl- terminal ends, as well as the linkers which join the major domains, are cytoplasmic. Some of the structures which are related to functions of the calcium channel are noted with arrows.

represent portions of the voltage sensors that initiate channel opening during activation (Stuhmer *et. al.*, 1989). Similar studies have been carried out to show that the S4 segments of calcium channels also act as voltage sensors (Catterall, 1988). (b) The permeation pore is formed by the SS1 and SS2 segments (two short segments located between S5 and S6 in each of the four transmembrane domains) and the S5 and S6 segments (Guy and Conti, 1990; Striessnig *et. al.*, 1990; Catterall *et. al.*, 1992). Highly conserved glutamate residues located within the SS2 segments of each domain serve as the major determinants of ion selectivity (Yang *et. al.*, 1993; Sather *et. al.*, 1994; Yatani *et. al.*, 1994a; Ellinor *et. al.*, 1995). Single amino acid mutations to glutamate residues within the SS2 segments of sodium channels can alter ion selectivity of the pore, effectively converting the sodium channel into a calcium channel (Heinemann *et. al.*, 1992). (c) The site of β subunit interaction with the α_1 subunit is located in the I-II linker (the intracellular loop between domains I and II) of all the HVA channels, a motif which is lacking in LVA channels (Pragnell *et. al.*, 1994). The β subunit binding site is formed by a cluster of 18 amino acids (of which nine are conserved among the HVA channels) located 23 amino acids downstream of domain I on the α_1 subunit.

Besides these properties which are common to most α_1 subunits, there must also be differences in the structures which lead to the diverse pharmacological and biophysical properties of the different α_1 subunit subtypes. For example, specific amino acid residues in the pore-forming region of domains III and IV of L-type α_1 subunits are responsible for conferring dihydropyridine sensitivity to these channels (Tang *et. al.*,

1993; Hering *et. al.*, 1998). Furthermore, the I-II linker region of N- and P-type channels contains a binding site for $G_{\beta\gamma}$ proteins which bind to and inhibit calcium channels via a membrane delimited pathway (Herlitze *et. al.*, 1996; 1997; de Waard *et. al.*, 1997; Zamponi *et. al.*, 1997). The II-III linker of the α_{1S} calcium channel determines the EC coupling properties of the skeletal muscle L-type channels and is thought to interact directly with the ryanodine receptor (Tanabe *et. al.*, 1990; Catterall, 1991). Syntaxin (a protein required for neurotransmitter release at the synapse) interacts with the II-III linker of the N-type and P/Q-type channels to allow formation of the tight exocytosis complex which facilitates calcium-dependent neurotransmitter release (Sollner *et. al.*, 1993; Sheng *et. al.*, 1994). There are however, many other functional properties which have not been mapped to particular amino acid sequences of the channel protein. Currently, it is a major goal of calcium channel research to correlate these observed differences among the channels subtypes with the structures of their α_1 subunits.

Ion Channel Inactivation

Voltage-dependent ion channels, including calcium channels, respond to electrical stimuli to cause conformational changes which result in the opening of a pore and the flux of ions down an electrochemical gradient. After a channel has opened, it may enter one of two possible gating conformations. If the membrane potential quickly returns to resting potential, then channels will deactivate (or close) and return to the resting state. This is analogous to 'turning off' the current through the channel. Alternatively, if

membrane depolarization is sustained, some ion channels will eventually shut down through a process termed inactivation (Hille, 1992). Compared to deactivation, inactivation is slower, and can develop with different kinetics depending on the ion channel subtype. Once a channel is inactivated it is unavailable for opening, and to remove inactivation, the membrane must be repolarized. Like activation, inactivation of ion channels is primarily regulated by membrane potential and is therefore a voltage-dependent process. Inactivation processes are not always intrinsically voltage-dependent however. For example, coupling of inactivation to voltage-dependent activation results in the appearance of a voltage-dependent inactivation mechanism. The mechanism of inactivation however, is distinct from that which controls the activation process. Inactivation is an important biophysical feature of ion channels, and it has significant physiological implications. For example, sodium channel inactivation contributes to the repolarizing phase of an action potential, and is a key determinant of action potential duration. Sodium channel inactivation also accounts for the loss of excitability that occurs if the resting potential of a cell falls by as little as 10 or 15 mV, which can result from elevated extracellular potassium ion concentrations, or after prolonged anoxia or metabolic block (Hille, 1992).

Calcium Channel Inactivation is an Important Determinant of Calcium Entry

In calcium channels, the process of inactivation serves several important functions. Firstly it is a key mechanism by which calcium channels are able to achieve a tight regulation of internal calcium levels. The inactivation of calcium channels is

important in determining (and limiting) the amount of calcium entry during electrical activity and its resulting impact on the diverse cellular events in which calcium plays a role. It is also a critical determinant of the temporal precision of calcium signals. Another important function of calcium channel inactivation is the prevention of long-term increases in intracellular calcium levels (Choi, 1988; Orrenius *et. al.*, 1989; Orrenius and Nicotera, 1994). Perturbation of intracellular calcium homeostasis is a common step in the development of cytotoxicity, particularly in the central nervous system (CNS) and immune system. Sustained increases in intracellular calcium can lead to the activation of degradative enzymes such as phospholipases, proteases, endonucleases, and to mitochondrial dysfunction and the disruption of cytoskeletal organization, as well as induces free radical formation. Calcium overload plays a critical role in ischemic damage, as well as in various neurodegenerative disorders.

In addition to preventing calcium-mediated cytotoxicity, calcium channel inactivation has other important physiological consequences, particularly in the CNS where calcium channels are abundant. Within the context of the role of calcium channels in neurotransmission, calcium channel properties, including inactivation, are an important determinant of synaptic efficacy. This has been demonstrated at the giant synapse in the rat brainstem. At this excitatory glutamatergic synapse, calcium channel inactivation (through a combination of both calcium- and voltage-dependent mechanisms) and slow recovery from inactivation has been observed (Forsythe *et. al.*, 1998). The slow recovery allows inactivation to accumulate over a train of action potentials, thereby contributing to post-tetanic depression at the synapse. Consequently, in addition to triggering exocytosis

of vesicles containing neurotransmitter, presynaptic calcium channels also play an important role in short term plasticity due to their inactivation properties. Functional significance of calcium channel inactivation has also been demonstrated in nerve terminals of the neurohypophysis. These nerve terminals are responsible for secretion of oxytocin and vasopressin in response to action potentials, and they show a decline of secretion in response to sustained high-frequency stimulation. Branchaw *et. al.* (1997) have shown that the depression of hormone secretion results from the accumulation of calcium channel inactivation which occurs during high frequency stimulation. Their results suggest that calcium current inactivation can vary significantly depending on stimulation frequency and duration, and on the subunit composition of the calcium channel (Patil *et. al.*, 1998). These variations in calcium channel activity influence neuropeptide secretion and likely neurotransmitter secretion as well. Thus calcium channel inactivation is one of a variety of mechanisms which comes into play in determining how neurohormone secretion and neurotransmitter release will vary with different forms of electrical activity at the synapse.

Molecular Mechanisms of Inactivation

"Hinged-Lid" Inactivation - Sodium Channel Fast Inactivation

The process of inactivation is highly variable in many of its properties and in its mechanisms. Sodium and potassium channels both undergo well characterized forms of fast inactivation in which inactivation occurs by occlusion of open channels from the cytoplasmic side of the channel by a tethered gate. Initial investigations of both sodium

and potassium channel inactivation showed that their inactivation processes were specifically prevented by intracellular proteolytic treatment, the effect of which was to cleave a cytoplasmic inactivation particle (Armstrong *et. al.*, 1973; Hoshi *et. al.*, 1990). Identification of the sodium channel segments required for fast inactivation was achieved by using a panel of site-directed anti-peptide antibodies against short (15 - 20 residues) peptide segments of the α subunit. Only the antibody directed against the short intracellular loop between domains III and IV inhibited inactivation, suggesting that this region was the locus for inactivation in sodium channels (Vassilev *et. al.*, 1988; 1989). In another study, expression of the sodium channel α subunit as two pieces (cut between domains III and IV) resulted in channels that activate normally but inactivate 20 times more slowly than normal, confirming the III-IV linker as the inactivation particle (Stuhmer *et. al.*, 1989). The inactivation gating loop in the III-IV linker contains highly conserved clusters of positively charged and hydrophobic amino acid residues, however it is a cluster of only 10 amino acids at the amino-terminal end of the III-IV loop that are responsible for mediating inactivation, as deletion of this cluster completely prevents fast inactivation. Mutation of hydrophobic residues in this region to the hydrophilic uncharged glutamine residue demonstrated key roles for three residues. Mutation of the three residue cluster isoleucine-phenylalanine-methionine (IFM motif) to glutamines completely blocked fast inactivation (West *et. al.*, 1992). The single phenylalanine in the center of the cluster appears to be the critical residue, as its conversion to glutamine is sufficient to prevent channel inactivation almost completely. Later experiments showed

that a synthetic peptide containing the IFM sequence motif could restore fast inactivation to mutant sodium channels having defective inactivation gates and to wild type sodium channels whose inactivation was slowed by α scorpion toxin (Eaholtz *et. al.*, 1994). Synthetic peptides containing the mutation that prevents fast inactivation (IQM) were unable to restore inactivation. The interaction of the IFM residues with the receptor for the inactivation gating particle is likely to be hydrophobic because there is a close correlation between the hydrophobicity of the residues and the extent of channel inactivation (McPhee *et. al.*, 1994; 1995). A "hinged-lid" model for sodium channel fast inactivation is proposed whereby the III-IV linker serves as a rigid lid that closes over the intracellular mouth of the sodium channel in the open state to prevent permeation of the channel (Fig. 4A).

"Ball and Chain" Inactivation - Potassium Channel Fast Inactivation

Like sodium channels, fast inactivation of potassium channels also occurs by occlusion of the intracellular mouth of the pore by a cytoplasmic inactivation particle (Armstrong *et. al.*, 1973; Hoshi *et. al.*, 1990; Isacoff *et. al.*, 1991). In contrast though, the potassium channel inactivation particle is located at the amino terminus of the polypeptide prior to the first transmembrane segment. Evidence of an amino-terminus inactivation particle came from experiments which showed that deletion of the amino-terminus prevented fast inactivation (Hoshi *et. al.*, 1990; Demo and Yellen, 1991). Smaller scale deletions demonstrated that the first 22 amino acids formed the inactivation

Figure 4 - Mechanisms of Inactivation of Sodium and Potassium Channels

(A) The "hinged-lid" mechanism of sodium channel inactivation: The intracellular loop connecting domains III and IV of the sodium channel forms a hinged lid and blocks the pore intracellularly to inactivate the channel. The three residue cluster, isoleucine-phenylalanine-methionine (IFM motif) plays a critical role in the inactivation process. **(B)** The "ball and chain" mechanism of potassium channel inactivation: The amino terminal segment of each subunit acts as an inactivation particle tethered on the end of a long chain of amino acids. Basic residues of the inactivation particle facilitate interaction with the inner vestibule of the channel to cause inactivation.

A

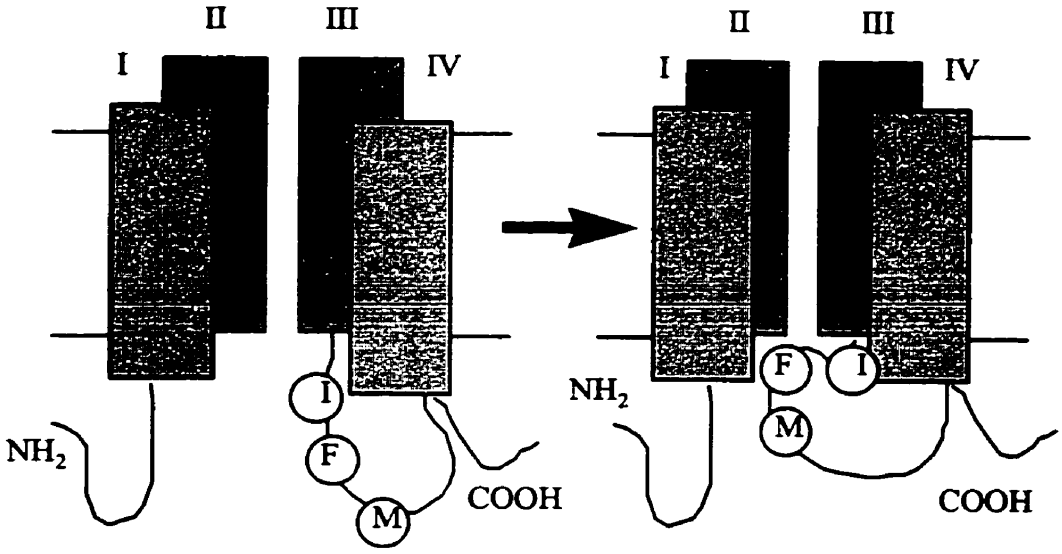

B

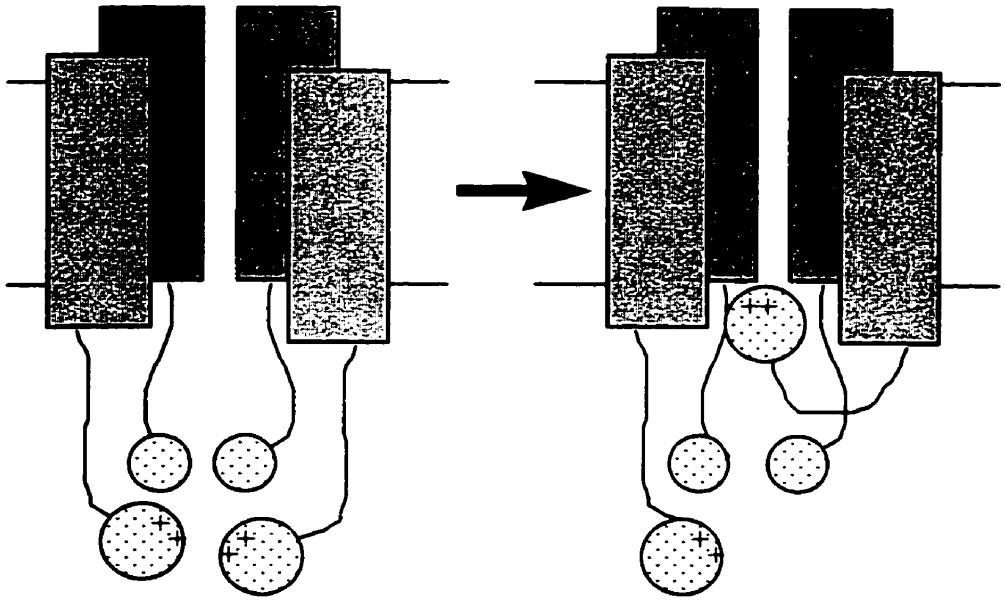

particle. Inactivation can be restored in non-inactivating amino-terminal deletion mutants by exogenous application of short peptides derived from the amino-terminus sequence, confirming the role of this region in the inactivation process (Zagotta *et. al.*, 1990). A leucine residue at position 7 was identified as a critical residue in mediating fast inactivation, as mutation of Leu 7 to a hydrophilic residue prevents fast inactivation almost completely (Hoshi *et. al.*, 1990). These results have led to the proposal of a "ball and chain" model of inactivation, in which the amino-terminal segment of the potassium channel is envisioned as an inactivation particle tethered on the end of a long chain of amino acids (Fig. 4B). When in the closed conformation, the inner vestibule of the pore is unable to bind the chained ball. Upon activation, the conformational change associated with the transition to the open state renders the inner vestibule of the pore available for binding to the inactivation ball which is able to diffuse into the receptor. Diffusion is facilitated by electrostatic interaction between basic residues in the ball peptide and acidic residues in the channel vestibule. Hydrophobic residues stabilize the bound peptide in the inner mouth of the pore, where it hinders the passage of potassium ions. Although each channel has four amino-termini and therefore four independent inactivation particles, only one inactivation ball interacts with the mouth of the pore to cause inactivation of the channel (MacKinnon *et. al.*, 1993).

"C-Type" Inactivation - Potassium Channel Slow Inactivation

In addition to the rapid inactivation of potassium channels mediated by the amino-terminal inactivation particle (N-type inactivation), potassium channels also undergo a

slower inactivation mechanism termed C-type inactivation. C-type inactivation requires specific amino acid residues at the extracellular end of the S6 segment which is proposed to comprise part of the pore of the channel (Hoshi *et. al.*, 1991; Lopez *et. al.*, 1994). C-type inactivation is sometimes referred to as slow inactivation because its kinetics are often, but not always, slower than N-type inactivation. In addition to involvement of the S6 segment, specific residues in the extracellular H5-S6 loop are also importantly involved in mediating C-type inactivation (Lopez-Barneo *et. al.*, 1993). Internal TEA, which competes with the amino-terminal peptide ball for its lodging site at the inner mouth of the pore in N-type inactivation, does not modify C-type inactivation. However, externally applied TEA, as well as high external permeant ion concentrations interfere with inactivation, suggesting inactivation occurs by a mechanism involving closure of the extracellular mouth of the pore (Choi *et. al.*, 1991). These results are consistent with a simple 'foot in the door' model whereby a channel cannot close when occupied by a blocker or permeant ion. Consequently a model for C-type inactivation was proposed in which conformational changes near the external mouth prevent permeation of the channel. Yellen *et. al.* (1994) and Liu *et. al.* (1996) demonstrated that C-type inactivation changes external solute accessibility of a limited number of residues near the external mouth of the *Shaker* potassium channel supporting the view that conformational changes mediate C-type inactivation. Constriction of the pore by conformational change involves cooperative interactions between all four subunits to cause inactivation (Ogielska *et. al.*, 1995; Panyi *et. al.*, 1995). A slow inactivation process is also observed

in sodium channels, and is thought to occur by a mechanism resembling C-type inactivation (Balser *et. al.*, 1996; Wang and Wang, 1997).

Calcium Channels Undergo Two Forms of Inactivation

Calcium channels undergo two types of inactivation. Voltage-dependent inactivation has been found in all calcium channel subtypes, however the kinetics of inactivation differ considerably between subtypes as described previously. A second type of inactivation, driven by intracellular calcium concentration, is restricted to L-type calcium channels and is termed calcium-dependent inactivation. Calcium-dependent inactivation is mediated by intracellular calcium ions which bind to a specific site on L-type channels causing the inactivation of the channel (Imredy and Yue, 1994). It is observed only with calcium as the charge carrier, unlike voltage-dependent inactivation which is present with either calcium or barium as charge carriers. Calcium-dependent inactivation is proposed to arise from a mechanism that is fundamentally different from that underlying voltage-dependent inactivation, and has been localized to the carboxyl terminal region of the α_1 subunit (de Leon *et. al.*, 1995). Recently, calmodulin has been identified as the calcium sensor for calcium-dependent inactivation (Peterson *et. al.*, 1999; Qin *et. al.*, 1999; Zuhlke *et. al.*, 1999). It is proposed that calmodulin is constitutively tethered to the channel complex and that inactivation occurs by a calcium-facilitated interaction of the tethered calmodulin with an IQ-calmodulin binding motif on the carboxyl-terminal of the α_{1C} subunit to prevent ion flow through the channel.

Fast, voltage-dependent inactivation of calcium channels does not appear to occur by the same mechanisms as observed in sodium and potassium channels. Structures analogous to a single inactivation "ball" or "lid" have not been identified in calcium channel proteins. Instead it appears that the molecular mechanisms for calcium channel inactivation may be distributed across calcium channel subunits and it seems that these mechanisms are likely to be complex, multiple and interacting in contrast to the previously described mechanisms.

Voltage-Dependent Inactivation of Calcium Channels

Studies performed to date on calcium channel inactivation have not provided a clear and coherent model describing the molecular basis of voltage-dependent inactivation of calcium channels. One of the first studies which specifically investigated the molecular mechanisms of calcium channel voltage-dependent inactivation suggested that the domain I S6 region (I S6) is a critical determinant of the differences in voltage-dependent inactivation properties observed with marine ray (doe-I) α_{1E} and rabbit brain (BI) α_{1A} calcium channels (Zhang *et. al.*, 1994a). Chimeric calcium channels in which a 200 amino acid segment from doe-I (including the I S6 and stretching 19 amino acids into the I-II linker) were inserted into the α_{1A} channel exhibited the faster inactivation properties seen with the doe-I phenotype. These findings were later validated in a study by Parent *et. al.* (1995), using L-type cardiac calcium channels (α_{1C}), which undergo predominantly calcium-dependent inactivation and little voltage-dependent inactivation,

and the L-type skeletal calcium channels (α_{1S}) whose inactivation is primarily voltage-dependent. They found that the replacement of domain I of the α_{1C} subunit with domain I from the α_{1S} channel resulted in the emergence of voltage-dependent inactivation, suggesting the locus for voltage-dependent inactivation is located in domain I.

Elsewhere within the α_1 subunit, five independent studies have indicated that the intracellular loop connecting domains I and II has a role in mediating voltage-dependent inactivation. Chimeras containing the I-II linker of α_{1B} inserted into α_{1E} produced a current phenotype with inactivation kinetics intermediate between α_{1E} and α_{1B} (Page *et. al.*, 1997). Insertion of the I-II linker of α_{1A} into α_{1E} caused a similar slowing of inactivation in comparison to the wild type α_{1E} (Page *et. al.*, 1997). In a different study, the I-II linker of α_{1C} was replaced by the corresponding region from α_{1S}, resulting in a construct with slower inactivation kinetics than the wild-type α_{1C} (Adams and Tanabe, 1997). It is interesting to note that in the study by Parent *et. al.* (1995), the exchange of domain I of α_{1C} with that of α_{1S} caused a speeding of inactivation in comparison to the wild-type α_{1C} channel, however when the I-II linker of α_{1C} was replaced with its counterpart from α_{1S}, inactivation was slowed in comparison to the wild-type α_{1C}. Recently, Cens *et. al.* (1999) have also demonstrated involvement of the I-II linker in the inactivation process by showing that overexpression of the I-II linker from either α_{1C} or α_{1A} speeds up the inactivation of α_{1A} in oocytes, with the α_{1A} I-II linker being more effective at accelerating inactivation.

A number of studies have identified individual amino acid residues in the I-II linker which govern inactivation processes. An arginine residue in the G-βγ binding motif (QXXER) in the I-II linker of α_{1A} appears to mediate its fast voltage-dependent inactivation kinetics, as when it is replaced with a glutamate residue (the corresponding residue from the slowly inactivating α_{1C} channel), steady-state inactivation is shifted to more depolarized potentials, and inactivation is significantly slowed so that inactivation kinetics resemble those of α_{1C} (Herlitze *et. al.*, 1996). Conversely, a mutation of the glutamate residue at the same position in α_{1C} to an arginine (as in α_{1A}) speeds up inactivation and shifts steady state inactivation in the hyperpolarizing direction. In another study, the difference in inactivation properties between the rapidly inactivating Q-type and very slowly inactivating P-type calcium channels (both of which are encoded by the α_{1A} subunit) has been shown to be due to alternative splicing in which a valine insertion in the I-II linker ($\alpha_{1A\text{-}2}$) changes inactivation kinetics from fast to slow (Q- to P-type) (Bourinet *et. al.*, 1999). This single residue located at position 421 (18 residues carboxyl to the β subunit binding site) appears to be responsible for the distinct inactivation profiles of the two channel subtypes.

Recently, studies which have attempted to locate the binding sites of the calcium channel antagonists 1,4-dihydropyridines, benzothiazepines, and phenylalkylamines on the α_{1C} subunit, have revealed additional information about possible mechanisms of calcium channel inactivation. Several groups have shown that the III S6 segment, as well as the pore forming segment in domain III, is involved in voltage-dependent inactivation.

The domain III SS2-S6 region from α_{1A} speeds up inactivation when inserted into the α_{1C} subunit showing that extracellular regions near the pore could contribute to inactivation in calcium channels (Tang *et. al.*, 1993; Yang *et. al.*, 1994). These findings were supported by independent studies in which the putative pore-lining residues in the III S6 segment of α_{1C} were mutated to alanines, resulting in slowed inactivation rates and shifted steady-state inactivation to more positive potentials (Hering *et. al.*, 1997; Hockerman *et. al.*, 1997). The IV S6 segments have been similarly implicated in playing a role in voltage-dependent inactivation of calcium channels. The pore-forming segment from the end of IV S5 to the beginning of IV S6 of α_{1A} is able to confer fast inactivation kinetics on the α_{1C} channel (Yatani *et. al.*, 1994b). A change in inactivation kinetics is also seen by introducing L-type sequence into α_{1A} in this region. Interestingly, the implantation of the transmembrane segment IV S6 from the slowly inactivating α_{1C} did not result in transfer of the slower L-type inactivation kinetics onto the faster inactivating α_{1A}. The sequence substitution unexpectedly accelerated the inactivation kinetics compared to that of α_{1A} (Doring *et. al.*, 1996). This effect was subsequently narrowed down to three amino acid residues from the IV S6 segment of α_{1C} (methionine, alanine, and isoleucine) which were able to accelerate voltage-dependent inactivation of α_{1A} (Hering *et. al.*, 1996).

Finally, residues in the intracellular carboxyl terminal of the α_{1C} subunit also appear to play a role in calcium channel voltage-dependent inactivation processes. Point mutations of a glutamate residue (E1537) in the EF hand motif of α_{1C} surprisingly

reduced voltage-dependent inactivation instead of affecting calcium-dependent inactivation as was hypothesized, suggesting that this region may contribute to voltage-dependent inactivation processes as well as calcium-dependent inactivation (Bernatchez *et. al.*, 1998). In addition, alternative splicing of the α_{1C} has revealed a carboxyl terminal splice variant which contains a replacement of 80 amino acids in the second quarter of the carboxyl terminal with 81 non-identical amino acids. This construct exhibits 10 times faster voltage-dependent inactivation than the conventional α_{1C} channel lending further support to the hypothesis that the carboxyl terminal contributes to voltage-dependent inactivation (Soldatov *et. al.*, 1997; 1998).

It is evident from the many studies performed during the last 10 years that the molecular mechanisms of calcium channel inactivation are not as clear cut as the previously described inactivation mechanisms of sodium and potassium channels. The combined results of these calcium channel studies indicate that the structures responsible for inactivation might be distributed across the α_1 subunit and that the actual mechanism is likely complex, with multiple interactions. Taken together, these observations support the idea that voltage-dependent inactivation of calcium channels involves multiple structural elements. However, with the exception of the study by Zhang *et. al.* (1994a) there has to date been no systematic attempt to identify these elements. In order to do just that, I have investigated how each of the major transmembrane domains participate in the inactivation process. Using a chimeric approach with a systematic permutation of the major transmembrane domains of the rapidly inactivating R-type α_{1E} and the relatively

weakly-inactivating L-type α_{1C} calcium channels, enabled the identification of some of the structural features of the calcium channel α_1 subunit which mediate the rapid inactivation of α_{1E}. This type of approach, where the contribution of each of the major domains is examined, allows "scanning" of the calcium channel protein to see which of the major structural regions are involved, and narrows down the regions which can be subsequently examined in more detail to identify more detailed molecular mechanisms of inactivation.

Standard molecular biology techniques and procedures were employed in creating chimeras between the α_{1C} and α_{1E} calcium channels subunits. Subsequently, the inactivation properties of the chimeras were examined by whole cell patch clamp methods to determine two different inactivation parameters (described in detail in the Methods section). Both rates of inactivation as well as steady-state inactivation were used as measures of inactivation properties. Based on these measures, functional roles for inactivation were assigned to individual transmembrane domain(s) of the calcium channel α_1 subunit.

METHODS and MATERIALS

Molecular Biology: α_{1E}/α_{1C} Chimeras

Overview

In order to examine the structural features which underlie voltage-dependent inactivation in calcium channels, I created a series of chimeras between the α_{1E} and α_{1C} subunits. Each chimeric construct consists of a different combination of the four major transmembrane domains of the two parent channels (see illustrations in Fig. 5). An experimental strategy based on the introduction of complimentary, unique restriction enzyme sites in both channel genes by site-directed mutagenesis was used to accomplish the construction of the chimeras. Restriction sites at exactly complimentary positions in each of the parent channels are required in order to exchange domains between them. Since convenient restriction sites do not occur naturally in the same locations in both sequences, unique restriction sites were added to both channels in the cytoplasmic linker regions connecting the individual transmembrane domains. Figure 6 illustrates the distribution of these unique restriction sites along the cDNA sequences of both α_{1E} and α_{1C} subunits. The sites were designed such that they immediately follow the S6 segment of each domain; an *Avr II* site at the beginning of the I-II linker, a *Sal I* site at the beginning of the II-III linker, and an *Mlu I* site about 30 amino acids into the III-IV linker. It is important to note that the restriction sites were inserted at exactly complimentary positions in the cDNA sequences of rbE-II (α_{1E}) and rbC-II (α_{1C}) such that

Figure 5 - α_{1C}/α_{1E} Chimeras

The wild-type α_{1C} (black) and α_{1E} (white) calcium channels and fourteen α_{1C}/α_{1E} chimeras are depicted. Each chimera is comprised of a combination of transmembrane domains of the two parent channels.

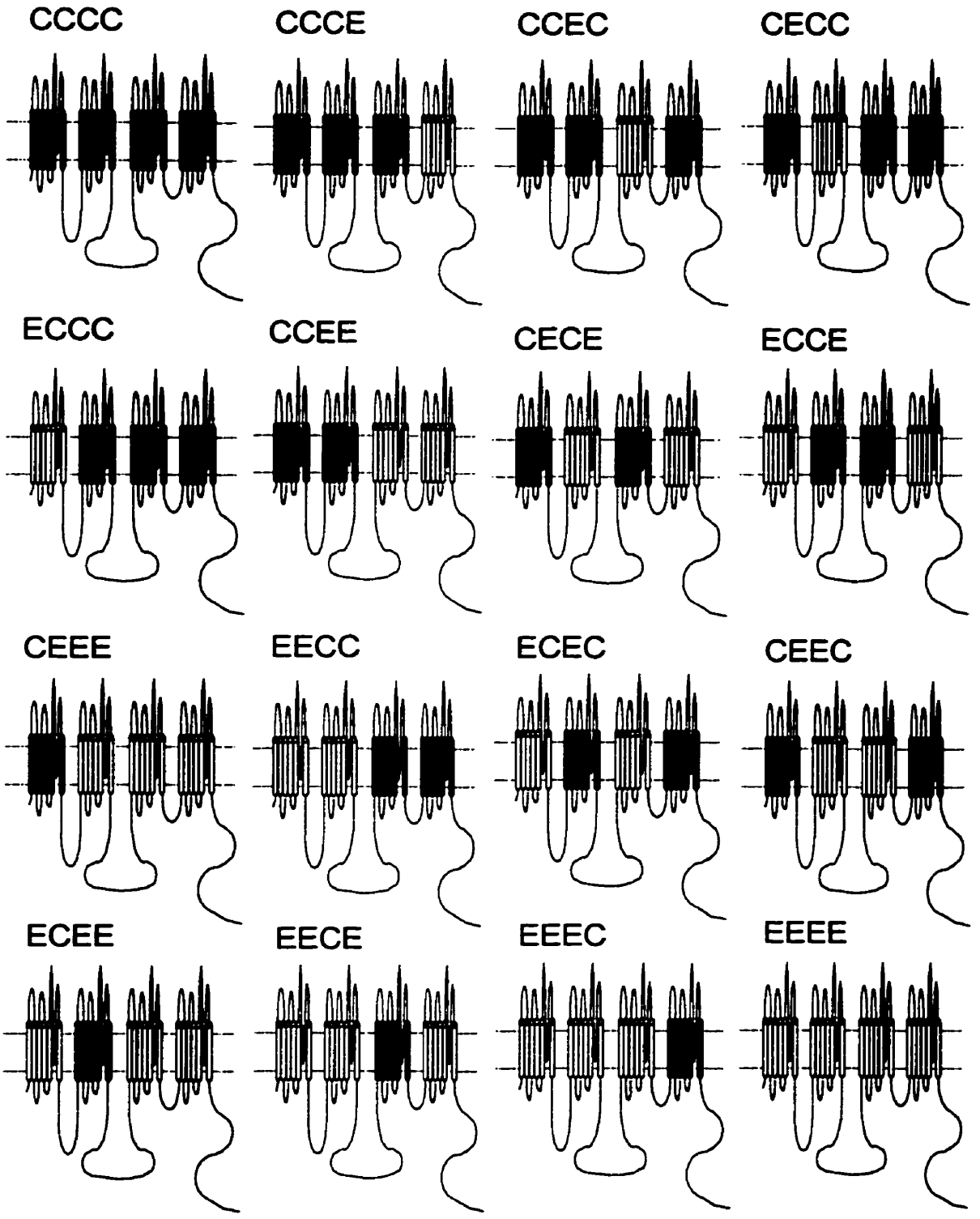
CCCC
CCCE
CCEC
CECC
ECCC
CCEE
CECE
ECCE
CEEE
EECC
ECEC
CEEC
ECEE
EECE
EEEC
EEEE

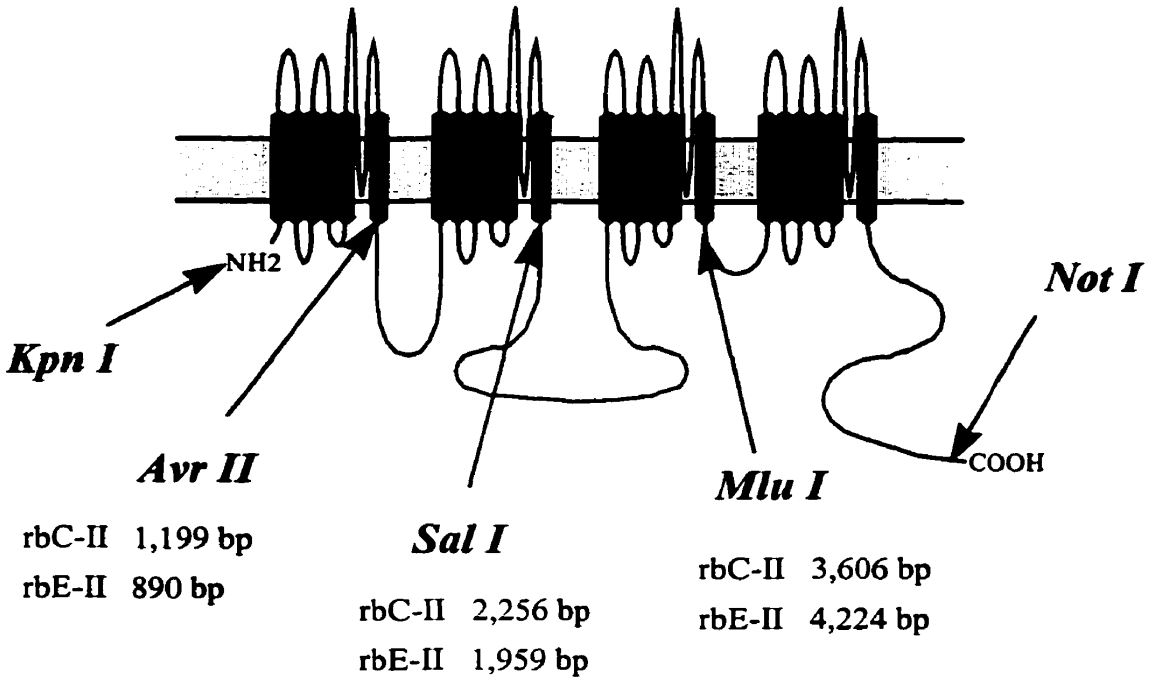

Figure 6 - Mutagenesis Sites in rbC-II and rbE-II

Unique restriction enzyme sites were introduced into rbC-II and rbE-II cDNA constructs via site-directed mutagenesis at exactly complimentary positions at; the beginning of the domain I-II linker (*Avr II*), at the beginning of the domain II-III linker (*Sal I*), and 33 amino acid residues into the domain III-IV linker (*Mlu I*). Both constructs are flanked by, respectively, *Kpn I* and *Not I* sites at the 5' and 3'ends. Note that because of the location of the restriction enzyme sites, each domain remains associated with the linker preceding it in the chimeric constructs.

once the chimeras were made, no frameshifts, redundancies or deletions in the coding sequence occurred. The mutations used to create the desired restriction sites were silent mutations in all cases except for the insertion of an *Mlu I* site in rbC-II. In this case an amino acid change occurred which replaced an arginine with a threonine (the complimentary residue from α_{1E}). In this way the mutation becomes silent when it is in a construct containing a junction between domains III and IV. For all chimeras lacking the transition between domains III and IV, an rbC-II construct missing the *Mlu I* mutation was used as the parent channel, thus preventing the inclusion of the non-silent mutation. In addition to the unique restriction sites within the coding sequence, each cDNA is flanked by a unique *Kpn I* site at the 5' end in the untranslated region (UTR), and a unique *Not I* site at the 3' end in the UTR. These sites permit the isolation of domain I (with the *Kpn I* site) and domain IV (with the *Not I* site), and also allow for subcloning of the entire coding sequence of the chimeric constructs into mammalian expression vectors.

Site-Directed Mutagenesis

All site-directed mutagenesis was carried out using the QuikChange Site-Directed Mutagenesis Kit (purchased from Stratagene). This technique uses a non-PCR mechanism, and the high fidelity thermostable Pfu DNA polymerase to minimize unwanted mutations. The basic procedure utilizes a double stranded DNA (dsDNA) template and two synthetic oligonucleotide primers containing the desired mutation (Fig. 7). The oligonucleotide primers, complementary to opposite strands of the template,

Figure 7 - Overview of QuikChange Site-Directed Mutagenesis Method

The basic procedure utilizes a dsDNA template (thick black lines), and two synthetic oligonucleotide primers containing the desired mutations. The primers extend during thermal cycling by means of a Pfu polymerase, thereby incorporating the mutation into the daughter strands (thin black lines). The daughter strands are later selected for by degrading the parental DNA with *Dpn I*, and the remaining DNA is transformed into XL1-Blue supercompetent cells to repair nicks.

I 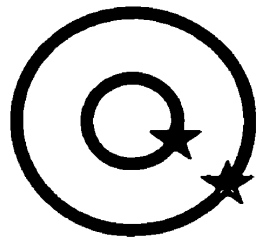

ds DNA template with target site (★) for mutation

II 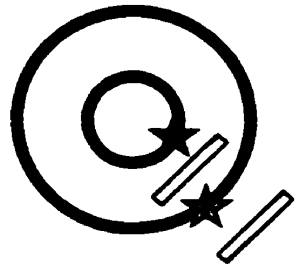

Denature plasmid and anneal mutagenic primers containing mutation (▭)

III 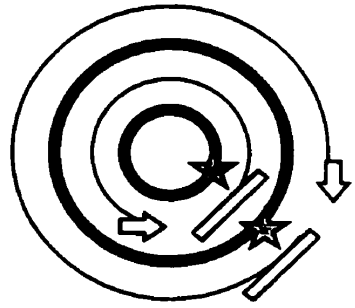

Extend and incorporate the mutagenic primers with Pfu polymerase to give nicked circular strands

IV 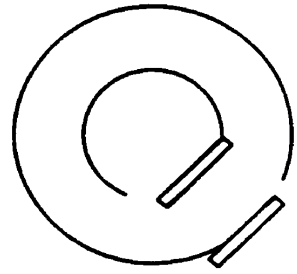

Digest methylated, nonmutated parental DNA with DpnI, so that only mutated plasmid is left (nicked circular strand)

V 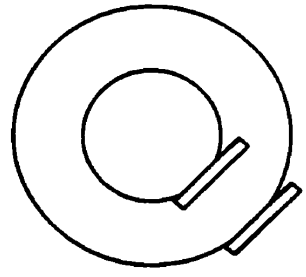

Transform the circular nicked DNA into XL-1 Blue cells (which repair the nicks in the mutated plasmid)

extend during temperature cycling by means of the Pfu polymerase. Upon incorporation of the primers, a mutated plasmid containing staggered nicks is generated. The nicked circular strands cannot be replicated, leaving only the parent strands to be used as template, further minimizing unwanted mutations. To select for the daughter strands of DNA that contain the desired mutation, the reaction mix is treated with *Dpn I* following temperature cycling. *Dpn I* is an endonuclease specific for methylated DNA, and is used to digest the parental DNA template without degrading the newly synthesized daughter strands. DNA isolated from almost all *Escherichia coli* strands is *dam* methylated and therefore susceptible to *Dpn I* digestion. Because the newly synthesized strands have not been grown in *E. coli*, they are not *dam* methylated and, thus, remain undigested. In the final step, the nicked vector DNA containing the desired mutation is transformed into *E. coli*, where the nick is repaired and the plasmid can be replicated and then isolated.

α_{1C} Mutagenesis

The α_{1C} subunit used in the following procedure was cloned from rat brain and was kindly donated by Dr. T.P. Snutch (rbC-II: GenBank accession number M67515). The parent rbC-II clone (7.4 Kb) was originally subcloned into the Bluescript -KS vector (2.9 Kb). This construct contained *Sal I* sites in the 5' UTR and in the polylinker at the 5' end of the insert (refer to Fig. 8). Because *Sal I* was to be one of the unique restriction sites created by site-directed mutagenesis, the elimination of these additional sites was necessary. To eliminate both unwanted sites, the plasmid was digested with *Sal I* and the

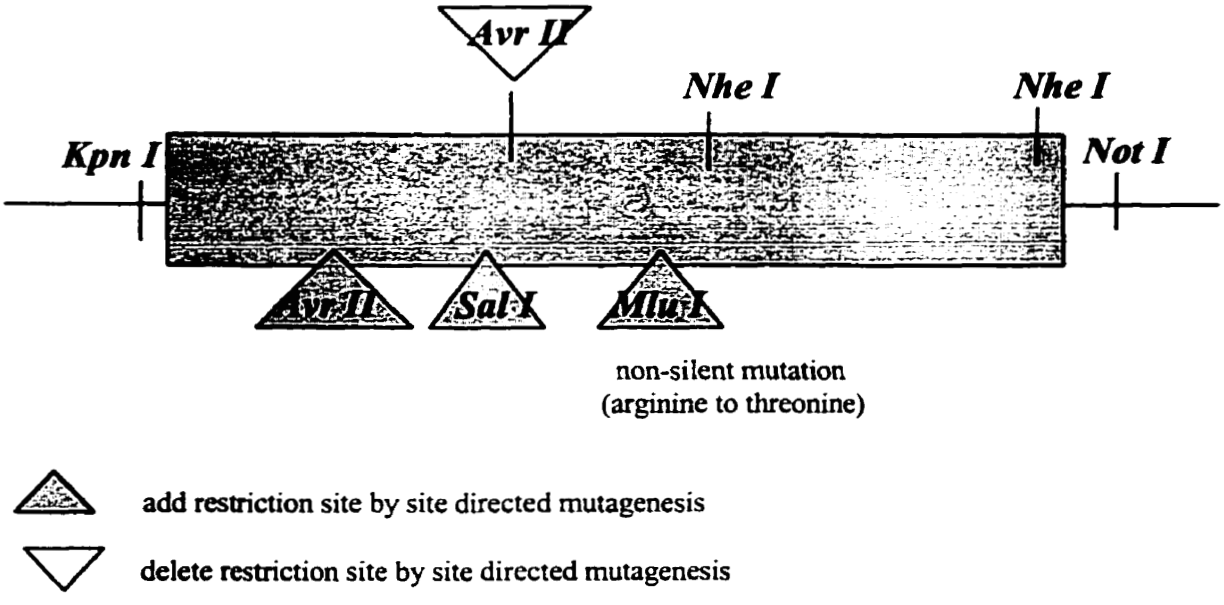

Figure 8 - rbC-II Mutagenesis

The full-length rbC-II cDNA (7.4 Kb) in Bluescript -KS originally had two *Sal I* sites (5' polylinker and 5' UTR). rbC-II was cut with *Sal I*, blunted and religated to eliminate both sites. Temporary elimination of an *Nhe I* fragment (4,274 bp - 6,941 bp) reduced the size of the clone by ~ 2.7 Kb. This shortened construct was used as the template for 4 rounds of mutagenesis; addition of *Avr II*, *Sal I*, and *Mlu I* restriction sites, and elimination of a previously existing *Avr II* site.

overhanging ends were blunted and then re-ligated. For the purposes of doing mutagenesis, it is advantageous to use shorter rather than longer templates (shorter extension times, and less template to be subject to possible unwanted mutations). To shorten the total length of the 10 Kb plasmid, it was cut with *Nhe I* and recircularized. This temporarily reduced the size of the clone to ~7.5 Kb by removal of a 2.5 Kb fragment from the 3' end. This shortened construct was used as the template for all subsequent rounds of mutagenesis. Using the QuikChange kit, the following mutations were created: silent mutation at bp 1199 to create an *Avr II* site; silent mutation at bp 2256 to generate a *Sal I* site; and a silent mutation at bp 2804 to eliminate an undesired endogenous *Avr II* site. Additionally in a fourth round of mutagenesis, a non-silent mutation to create a *Mlu I* site at bp 3606 was also carried out. Table 1 shows the oligonucleotide primers which were used to introduce/delete the above restriction sites. As previously mentioned, the mutation (arginine to threonine substitution) was to the corresponding amino acid residue found in rbE-II, and the rbC-II construct containing the *Mlu I* site was used only to make chimeras that involved transitions between domains III and IV. The successful addition/deletion of restriction sites was first confirmed by restriction digests, and the complete coding region was sequenced to confirm the absence of errors. For both constructs, the excised 2.5 Kb *Nhe I* fragment was re-introduced to yield two full length clones in Bluescript containing the unique restriction sites (CCCC, and CCCC(+*Mlu I*)). CCCC was subcloned into pMT2 (XS) using the *Kpn I* and *Not I* sites flanking the 5' and 3' ends of the clone respectively.

Table 1: α_{1C} Mutagenesis Primers

Oligonucleotide primers used for the insertion of unique *Avr II, Sal I, Mlu I, Kpn I and Not I* restriction enzyme sites by site-directed mutagenesis (QuikChange Site-Directed Mutagenesis Kit). Sequences are read from 5' to 3' with the top sequence of each pair being the forward primer (i.e. mutA primers). Numbers in brackets are the base pair positions of the restriction site. Bolded base pairs highlight the restriction site sequence, and italicized letters above show where the oligonucleotide sequences differ from the wild-type sequence. Note that a non-silent mutation (arginine to threonine) was created by insertion of an *Mlu I* site into the rbC-II sequence.

Table 1: α_{1C} Mutagenesis Primers

***Avr II* insertion:**

	T C
CII-*Avr II*-mutA (1,119)	CTA AAT CTG GTC **CTA GGT** GTT TTG AGC GGA GAG
CII-*Avr II*-mtuB	CTC TCC GCT CAA AAC **ACC TAG** GAC CAG ATT TAG

***Sal I* insertion:**

	G
CII-*Sal I*-mutA (2,256)	CC ATT GCG **GTC GAC** AAC CTG GCT GAT GC
CII-*Sal I*-mutB	GC ATC AGC CAG GTT **GTC GAC** CGC AAT GG

***Mlu I* insertion:**

	**CGA A G*
CII-*Mlu I*-mutA (3,606)	GCC CTC AAG GCC CGA CCC TTG **ACG CGT** TAC ATC CCC AAG AAC C
CII-*Mlu I*-mutB	G GTT CTT GGG GAT GTA **ACG CGT** CAA GGG TCG GGC CTT GAG GGC

* arginine to threonine mutation

***Avr II* elimination:**

	A
CII-Δ*Avr II*-mutA (2,804)	CC TTC AGG AAC CAC ATC **CTG GGC** AAT GCA GAC
CII-Δ*Avr II*-mutB	GTC TGC ATT GCC **CAG GAT** GTG GTT CCT GAA GG

α_{1E} Mutagenesis

The α_{1E} subunit used in the following procedure was cloned from rat brain and was kindly donated by Dr. T.P. Snutch (rbE-II: GenBank accession number L15453). The original rbE-II clone (6.8 Kb) was subcloned into the Bluescript -SK vector (2.9 Kb). This sequence contained a *Not I* site in the 5'UTR (about 150 bases into the clone), and in the polylinker at the 5' end (refer to Fig. 9). Because of the requirement to use the *Not I* site in later steps to isolate domain IV, and to cut out the whole coding sequence for rbE-II, the second *Not I* site was eliminated. This was accomplished by cutting the plasmid with *Not I* and re-ligating, leaving only a single *Not I* site. To temporarily reduce the size of the clone to simplify the mutagenesis, the rbE-II construct was cut with *Xho I* and recircularized, resulting in the temporary removal of a 1.7 Kb fragment from the 3' end of the clone. The remaining 8 Kb plasmid was used as the template for all subsequent rounds of mutagenesis. Using the QuikChange kit, the following silent mutations were created: addition of an *Avr II* site at bp 890; addition of a *Sal I* site at bp 1959, and addition of an *Mlu I* site at bp 4,224 (see Table 2 for mutagenesis primers). The original rbE-II insert in Bluescript -KS was flanked at the 5' and 3' ends, respectively, by *Not I* and *Kpn I*, which was exactly opposite compared to the rbC-II construct. For purposes of creating the chimeras it was therefore necessary to generate identical flanking sites in both constructs. Thus, two additional rounds of mutagenesis were carried out to replace the *Not I* and *Kpn I* sites flanking rbE-II with respectively *Kpn*

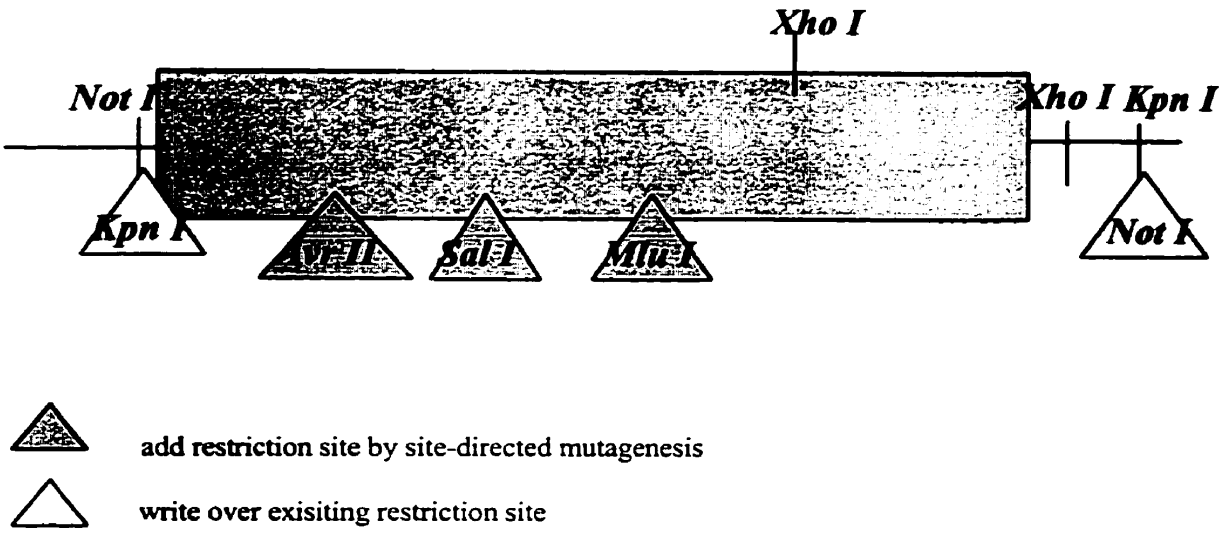

Figure 9 - rbE-II Mutagenesis

The full length rbE-II cDNA (6.8 Kb) in Bluescript -SK originally had two *Not I* sites (5'polylinker and 5' UTR). rbE-II was cut with *Not I* and religated to leave only one *Not I* site. Temporary elimination of an *Xho I* fragment (5,044 bp - 3' polylinker) reduced the size of the clone by ~1.7 Kb. This shortened construct was used as the template for 5 rounds of site-directed mutagenesis; addition of *Avr II*, *Sal I*, and *Mlu I* restriction sites, and overwriting of *Not I* and *Kpn I* sites at the 5' and 3' ends with *Kpn I* and *Not I* respectively.

Table 2: α_{1E} Mutagenesis Primers

Oligonucleotide primers used for the insertion of unique *Avr II, Sal I, and Mlu I* restriction enzyme sites, and deletion of an endogenous *Avr II* site by site-directed mutagenesis (QuikChange Site-Directed Mutagenesis Kit). Sequences are read from 5' to 3' with the top sequence of each pair being the forward primer (i.e. mutA primers). Numbers in brackets are the base pair positions of the restriction site. Bolded base pairs highlight the restriction site sequence, and italicized letters above show where the oligonucleotide sequences differ from the wild-type sequence. Note that the introduction of the *Kpn I* site in the 5' UTR was over a *Not I* site, and conversely the introduction of the *Not I* site in the 3' UTR was over a *Kpn I* site, so that the rbE-II clone is flanked by a *Kpn I* site at the 5' end and a NotI site at the 3' end.

Table 2: α_{1E} Mutagenesis Primers

***Avr II* insertion:**

	G
EII-*Avr II*-mutA (890)	CTC AAC CTT GT**C CTA GG**C GTG CTT TCC GGG
EII-*Avr II*-mutB	CCC GGA AAG CAC G**CC TAG** GAC AAG GTT GAG

***Sal I* insertion:**

	G
EII-*Sal I*-mutA (1,959)	G GCT ATC GCT **GTC GAC** AAT CTC GCC AAT GCC
EII-*Sal I*-mutB	GGC ATT GGC GAG ATT **GTC GAC** AGC GAT AGC C

***Mlu I* insertion:**

	C C
EII-*Mlu I*-mutA (4,224)	GCC AAA CCT CTC **ACG CGT** TAC ATG CCA CAG AAC
EII-*Mlu I*-mutB	GTT CTG TGG CAT GTA **ACG CGT** GAG AGG TTT GGC

***Kpn I* insertion:**

	CG G
EII-*Kpn I*-mutA (5' UTR)	GC TCC ACC GCG GTG **GGT ACC** GCC TAC AAG CAG
EII-*Kpn I*-mutB	CTG CTT GTA GGC **GGT ACC** CAC CGC GGT GGA GC

***Not I* insertion:**

	GT A CA
EII-*Not I*-mutA (3' UTR)	C GAG GGG GGG CCC **GCG GCC GCA** TTC GCC CTA TAG TG
EII-*Not I*-mutB	CA CTA TAG GGC GAA **TGC GGC CGC** GGG CCC CCC CTC G

I and *Not I*. The successful completion of the five rounds of mutagenesis were confirmed via restriction digests. The excised 1.7 Kb *Xho I* fragment was re-introduced to yield the full length clone EEEE in Bluescript. This construct was completely sequenced from the 5' end to the first *Xho I* site (bp 5,044) to ensure that no unwanted mutations were created during site-directed mutagenesis. Finally the insert was subcloned into pMT2 (XS) using the *Kpn I* and *Not I* sites.

Construction of α_{1E}/α_{1C} Chimeras

CCCE/EEEC: These chimeras were assembled in Bluescript using CCCC (+*Mlu I*) and EEEE by switching the *Mlu I - Not I* fragments (containing domain IV) among the parent channels. Both chimeras (CCCE and EEEC in Bluescript) were subsequently subcloned into the pMT2 (XS) expression vector using *Kpn I* and *Not I*. Note again that in these two chimeras the non-silent *Mlu I* mutation in CCCC (+*Mlu I*) becomes silent.

The remaining 12 chimeras were assembled in pMT2. The pMT2 vector contains a restriction sequence for *Avr II* about 900 bp upstream of the 5' polylinker, allowing isolation of a fragment containing domain I by digestion with *Avr II* (Fig. 10). In addition, the pMT2 vector also contains a unique restriction sequence for *Sal I* in the 3' polylinker, so that digestion with *Sal I* yields a fragment containing domains III and IV. Digests and ligations with *Avr II* or *Sal I* were therefore used to construct the remaining 12 chimeras. Correct orientation of the ligated fragments was confirmed with restriction digests and, in some cases, was validated by sequencing.

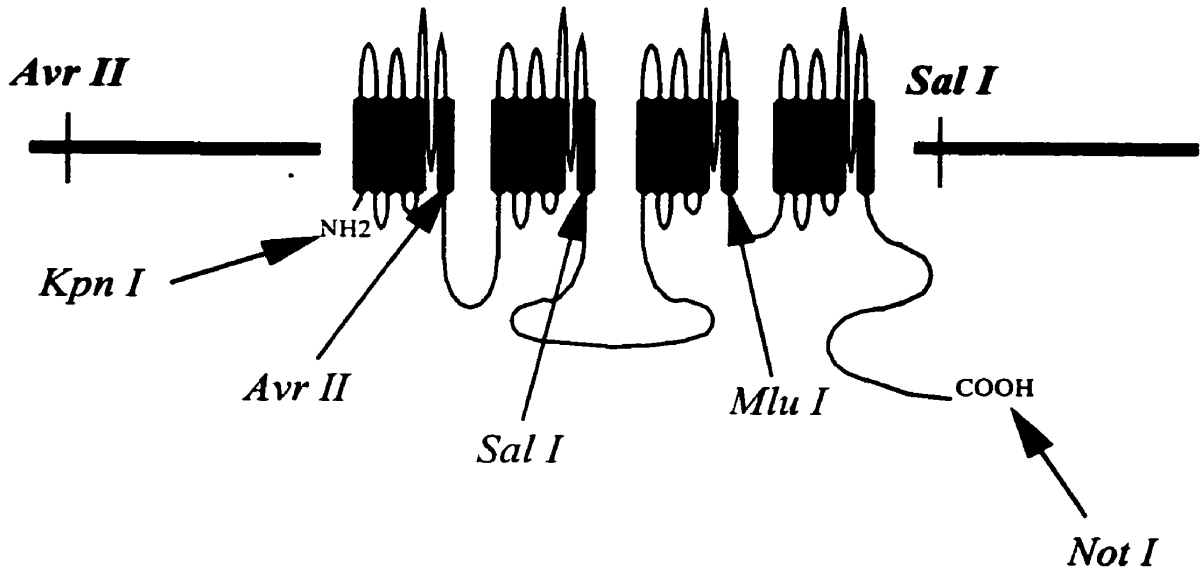

Figure 10 - α_1 Subunit in pMT2 (XS) Expression Vector

rbE-II and rbC-II constructs containing unique restriction sites (EEEE and CCCC respectively) were subcloned into the pMT2 (XS) expression vector (5 Kb) to construct chimeras. An *Avr II* site in the vector (about 900 bp upstream of the polylinker) allows isolation of a fragment containing domain I by a single *Avr II* digestion. Similarly, a *Sal I* site in the 3' polylinker of the vector allows isolation of a fragment containing domains III and IV by a single *Sal I* digestion. These sites were used in exchanging domains between the chimeras.

CCEC: Replacement of a *Sal I* fragment from CCCC (containing domains III and IV) with the corresponding fragment from EEEC in pMT2.

EECE: Replacement of a *Sal I* fragment from EEEE (domains III and IV) with the corresponding fragment from CCCE in pMT2.

CEEC: Replacement of an *Avr II* fragment from EEEC (containing domain I) with the corresponding fragment from CCCC in pMT2.

ECCE: Replacement of an *Avr II* fragment from CCCE (domain I) with the corresponding fragment from EEEE in pMT2.

CEEE/ECCC: Domains I of EEEE and CCCC were swapped via excision and ligation of the *Avr II* fragments from both constructs.

EECC/CCEE: Domains III and IV of EEEE and CCCC were swapped via excision and ligation of the *Sal I* fragments from both constructs.

ECEE: Replacement of a *Sal I* fragment from ECCC (domains III and IV) with the corresponding fragment from EEEE in pMT2.

CECC: Replacement of a *Sal I* fragment from CEEE (domains III and IV) with the corresponding fragment from CCCC in pMT2.

ECEC: Replacement of a *Sal I* fragment from ECCC (domains III and IV) with the corresponding fragment from EEEC.

CECE: Replacement of a *Sal I* fragment from CEEE (domains III and IV) with the corresponding fragment from CCCE.

II S6 and III S6 Chimeras

Four additional calcium channel α_1 subunit chimeras were constructed containing individually, the II S6 and III S6 segments of α_{1C} inserted into α_{1E}, and the II S6 and III S6 segments of α_{1E} inserted into α_{1C} (Fig. 11). Experimental design was once again based on a strategy in which unique restriction enzyme sites were introduced at complimentary positions in the α_{1E} and α_{1C} cDNA sequences to permit isolation and subsequent subcloning of the S6 segments. An *Age I* restriction site was introduced at a position about 20 amino acids 5' to the beginning of the II S6 segment to switch this segment among the parent channels. To switch the III S6 segment, an *Aat II* restriction site was introduced at a position about 15 amino acids 5' to the beginning of the III S6 segment. Figure 12 illustrates the distribution of these unique restriction sites along the cDNA sequences of the α_{1E} and α_{1C} subunits.

II S6 Chimeras - Mutagenesis and Molecular Biology

The EECC and CCEE chimeras (in the pMT2 expression vector) were used as the templates for mutagenesis to introduce unique *Age I* sites at the beginning of the II S6 segments. Both constructs were first cut with *Sal I* and recircularized to reduce their length by about five Kb before proceeding with mutagenesis. Using the QuikChange kit, the following mutations were created; silent mutations as bp 2109 of CCEE and bp 1815 of EECC (see Table 3 for mutagenesis primers). Successful addition of the sites was confirmed by restriction digests, and the coding region was sequenced to confirm the

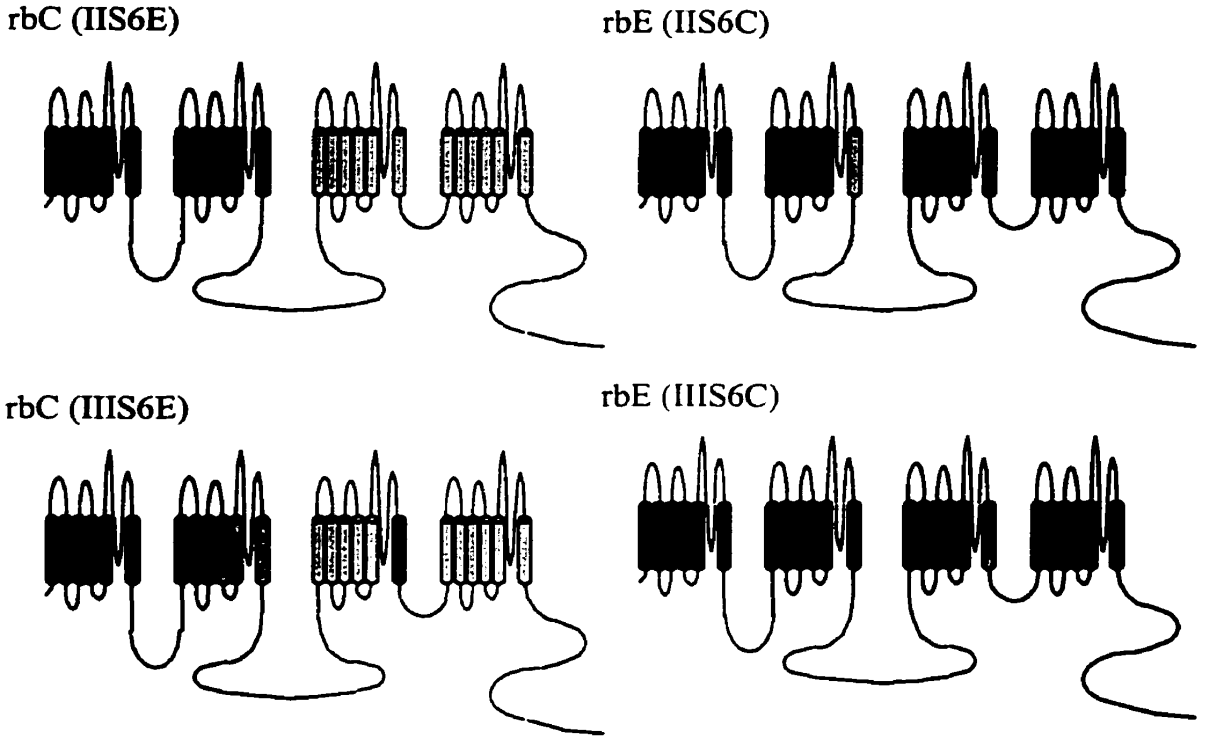

Figure 11 - S6 Chimeras: Membrane Topology

Transmembrane topology of each of the four S6 chimeras is depicted. Each contains an exchanged S6 transmembrane segment in either domain II or III. α_{1C} channel regions are shown in grey, and α_{1E} channel regions are shown in black.

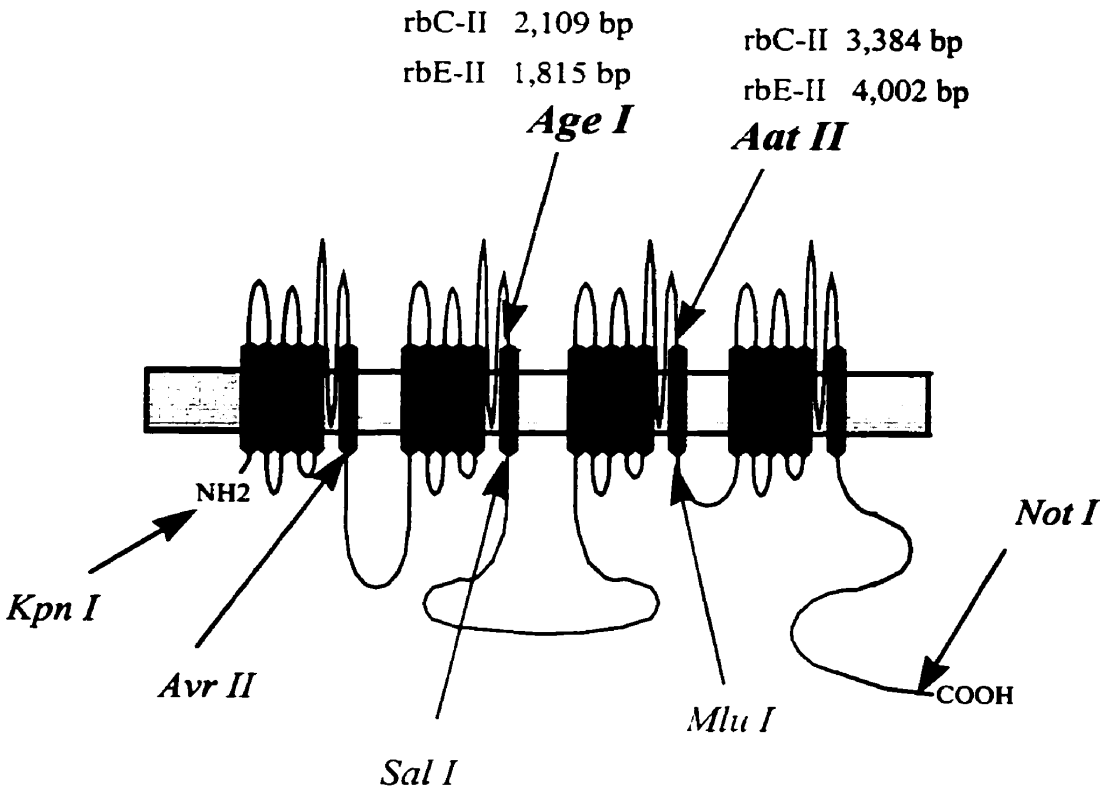

Figure 12 - Mutagenesis Sites for S6 Chimeras

Unique restriction enzyme sites were introduced into rbC-II and rbE-II sequences via site-directed mutagenesis at exactly complimentary positions at the following locations; 20 amino acid residues into the domain II S6 segment (*Age I*), and 15 amino acids into the beginning of the domain III S6 segment (*Aat II*). *Age I* was introduced into the CCEE and EECC constructs, and *Aat II* was introduced into the CCCE and EEEC constructs. Note the position of other unique restriction sites which were used in assembly of the chimeras.

Table 3: Mutagenesis Primers for IIS6/IIIS6 Chimeras

Oligonucleotide primers used for the insertion of unique *Age I* and *Aat II* restriction enzyme sites in α_{1E} and α_{1C} sequences by site-directed mutagenesis (QuikChange Site-Directed Mutagenesis Kit). Sequences are read from 5' to 3' with the top sequence of each pair being the forward primer (i.e. mutA primers). Numbers in brackets are the base pair positions of the restriction site. Bolded base pairs highlight the restriction site sequence, and italicized letters above show where the oligonucleotide sequences differ from the wild-type sequence. Note that a non-silent mutation (serine to valine) was created by introduction of an *Aat II* site into the rbC-II sequence.

Table 3: Mutagenesis Primers for IIS6/IIIS6 Chimeras

α_{1E} *Age I* insertion:

	G G
EII-*Age I*-mutA (1,815)	GTG TTC CAG ATC CTG **ACC GGT** GAA GAC TGG AAT GAA A
EII-*Age I*-mutB	C TTC ATT CCA GTC TTC **ACC GGT** CAG GAT CTG GAA CAC

α_{1C} *Age I* insertion:

	G
CII-*Age I*-mutA (2,109)	GTG TTT CAG ATC CTG **ACC GGT** GAG GAC TGG AAT TCG
CII-*Age I*-mutB	CGA ATT CCA GTC CTC **ACC GGT** CAG GAT CTG AAA CAC

α_{1E} *Aat II* insertion:

	T G
EII-*Aat II*-mutA (4,002)	CTG CAG CAC TCG GTA **GAC GTC** ACA GAG GAG GAC AGA GGC
EII-*Aat II*-mutB	GCC TCT GTC CTC CTC TGT **GAC GTC** TAC CGA GTG CTG CAG

α_{1C} *Aat II* insertion:

	* *T C*
CII-*Aat II*-mutA (3,384)	CTG TAC CGC TCC ATT **GAC GTC** CAC ACA GAA GAC AAG
CII-*Aat II*-mutB	CTT GTC TTC TGT GTG **GAC GTC** AAT GGA GCG GTA CAG

* serine to valine mutation

absence of errors. To construct the chimeras, CCEE + *Age I*, and EECC + *Age I* were cut with *Kpn I* and *Age I* restriction enzymes, and the resulting 2 Kb fragments from each were exchanged. Finally, the excised 5 Kb *Sal I* fragment was reintroduced into both constructs to yield two full length clones: rbE (IIS6C)/pMT2 and rbC (IIS6E)/pMT2 (Fig 13A).

III S6 Chimeras - Mutagenesis and Molecular Biology

The EEEC and CCCE chimeras (in the pMT2 expression vector) were used as the templates for mutagenesis to introduce unique *Aat II* sites at the beginning of the III S6 segments. Using the QuikChange kit, the following mutations were created; a silent mutation at bp 4,002 of EEEC, and a non-silent mutation at bp 3,384 of CCCE (see Table 3 for mutagenesis primers). The mutation of a serine residue in rbC-II was to the corresponding amino acid (valine) from the rbE-II sequence, so that in the III S6 chimeras, the mutation becomes silent. Successful addition of the sites was confirmed by restriction digests, and the coding region was sequenced to confirm the absence of errors. To construct the chimeras, CCCE + *Aat II*, and EEEC + *Aat II* were cut with *Not I* and *Aat II* restriction enzymes, and the resulting four Kb fragments from each were exchanged and religated to yield two full length clones: rbE (IIS6C)/pMT2 and rbC (IIS6E)/pMT2 (Fig. 13B).

Figure 13 - Assembly of S6 Chimeric Calcium Channels

(A) α_{1E} and α_{1C} constructs containing exchanged II S6 segments were assembled by exchange of the *Kpn I-Age I* fragments of CCEE + *Age I* and EECC + *Age I*. The 2 Kb *Kpn I-Age I* fragments contain domains I and II minus the II S6 segment. Exchange and ligation of this fragment gives the chimeras; rbC (IIS6E) and rbE (IIS6C). **(B)** α_{1E} and α_{1C} constructs containing exchanged III S6 segments were assembled by exchange of the *Aat II-Not I* fragments of CCCE + *Aat II* and EEEC + *Aat II*. The 4 Kb *Aat II-Not I* fragments contain domain IV plus the III S6 segment. Exchange and ligation of this fragment gives the chimeras; rbC (IIIS6E) and rbE (IIIS6C).

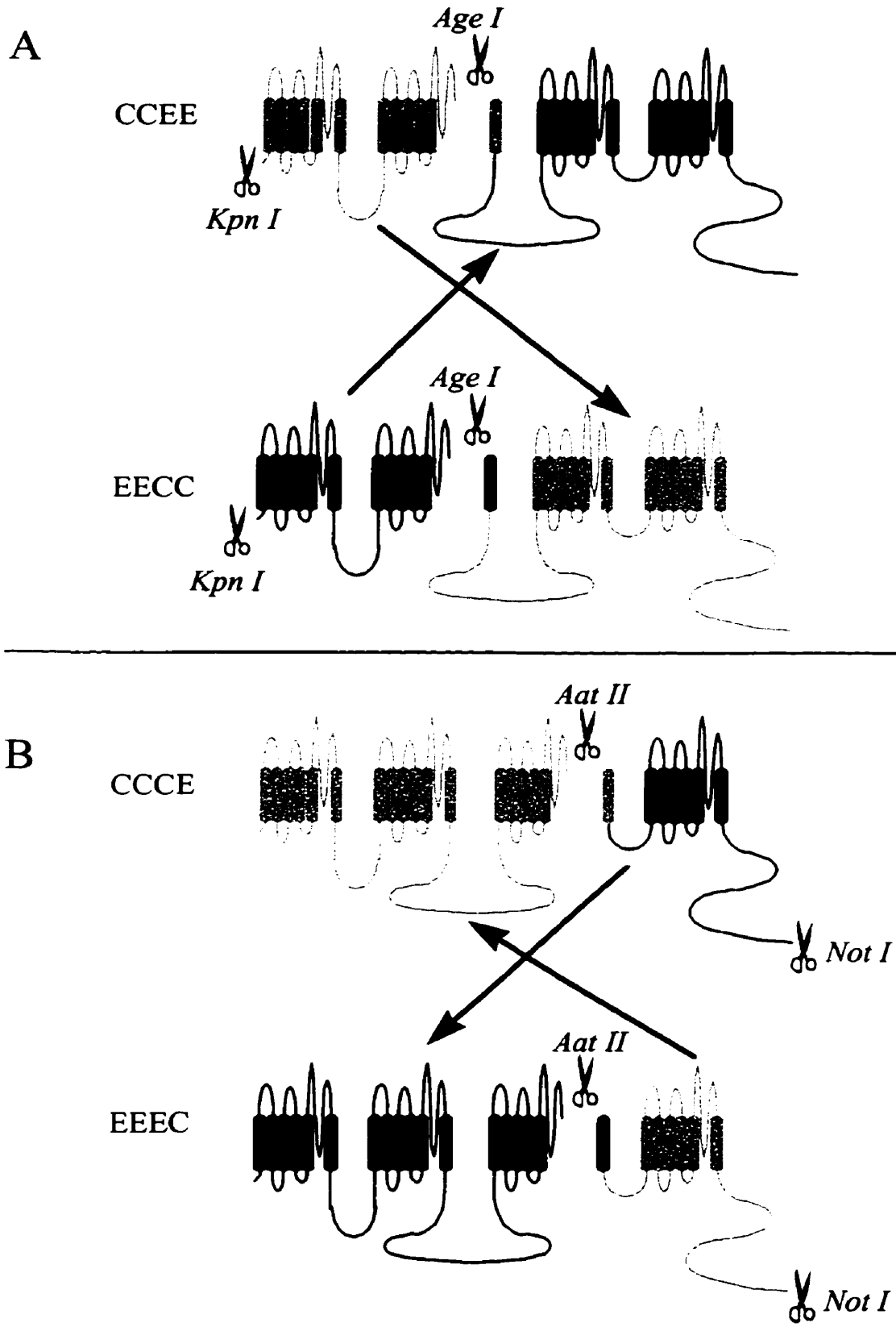
A
Age I
CCEE
Kpn I
Age I
EECC
Kpn I
B
Aat II
CCCE
Not I
Aat II
EEEC
Not I

Expression and Electrophysiology

Transient Transfection

To obtain expression of wild type α_{1E} and α_{1C} channels, and the α_{1E}/α_{1C} chimeras, a human embryonic kidney (HEK) cell expression system was used. HEK cell lines have traditionally served as efficient test systems for functional and biochemical studies of ion channel proteins and calcium channels in particular. It is a suitable system in that it is of mammalian origin (as are the calcium channel α_1 subunits - rat brain), and it does not contain endogenous calcium current, as determined from recordings obtained from both non-transfected HEK cells and HEK cells transfected only with β_{1b} and α_2-δ (personal communication with Dr. G. Zamponi). HEK tSA-201 cells were grown in standard DMEM medium, supplemented with 10% fetal bovine serum, 0.5 mg/ml penicillin-streptomycin and 0.4 mg/ml neomycin. Cells were grown to 85% confluency, split with trypsin-EDTA and plated on glass coverslips at 10% confluency 12 hours prior to transfection. Immediately before transfection, the medium was replaced with fresh DMEM, and a standard calcium phosphate protocol was used to transiently transfect the cells with cDNA constructs encoding for calcium channel α_1, β_{1b}, and $\alpha_{2\text{-}\delta}$ subunits, and green fluorescent protein (7,7,7 and 4 μg respectively). Coexpression with β_{1b} and $\alpha_{2\text{-}\delta}$ is used to increase the expression of functional channels. The GFP protein fluoresces under UV light and was used as a selection tool to indicate cells which had been transfected. After 12 hours, cells were washed with fresh DMEM and were allowed to recover for 12

hours. Subsequently the cells were incubated at 28°C in 5% CO_2 for one to three days prior to recording.

Electrophysiology

Immediately prior to recording, individual coverslips were transferred to a 3.5 cm culture dish containing external recording solution comprised of 20 mM $BaCl_2$, 1 mM $MgCl_2$, 10 mM HEPES, 40 mM TEACl, 10 mM glucose and 65 mM CsCl (pH 7.2). Barium was used as the charge carrier rather than calcium to eliminate calcium-dependent inactivation which exists in the L-type α_{1C} channel. As mentioned previously, calcium-sensitive inactivation has been localized to the carboxyl-terminus, so any chimera containing domain IV from α_{1C} would also be subject to effects of calcium. Whole cell patch clamp recordings were performed using an Axopatch 200B amplifier (Axon Instruments, Foster City, CA) linked to a personal computer equipped with pCLAMP v 6.0. Patch pipettes (Sutter borosilicate glass, BF150-86-15) were pulled using a Sutter P-87 microelectrode puller, fire polished using a Narashige microforge, and showed a typical resistance of about 3 - 4 MΩ. For α_{1C}/α_{1E} chimeras, the internal pipette solution contained 105 mM CsCl, 25 mM TEACl, 11 mM EGTA, and 10 mM HEPES (pH 7.2). Recordings of the S6 chimeras used an internal pipette solution containing 108 mM CsMS, 4 mM $MgCl_2$, 9 mM EGTA, 9 mM HEPES (pH 7.2). Recordings were made from cells expressing the GFP gene as visualized by a fluorescence signal. The bath was connected to ground via a 3M CsCl AGAR bridge. Seals were formed directly in the

external control solution. After seal formation, diffusion of cytoplasmic contents and internal recording solution was allowed to proceed for 5 to 10 minutes before recordings were performed. Unless stated otherwise, currents were typically elicited from a holding potential of -100 mV to various test potentials using Clampex software (Axon Instruments). Only negligible leak currents were observed. Outward currents, carried presumably by cesium ions could be observed at potentials more positive than the reversal potential. Contamination of calcium currents with the cesium currents likely also occurs at potentials near the reversal potentials, however these did not affect the determination of the reversal potential because data points close to reversal were not considered for fitting of macroscopic current-voltage relations.

The series resistance for each cell was typically around 8 MΩ. Because most currents were smaller than one nA at the peak of the current voltage relation, voltage errors were calculated to be less than 10 mV in the worst case. For steady-state inactivation curves, this has little effect on the half-inactivation potential for two reasons: First, the conditioning potential is not affected by voltage errors, because with the exception of one chimera (ECEE) there was little current activation during the conditioning pulses. Secondly, the test potential used during the recording of the steady-state inactivation curves (+10 or +20 mV) was typically 10 mV to 20 mV more positive than the peak of the I-V relation, resulting in smaller currents and, thus, smaller voltage errors. Any remaining errors may cause a slight skewing of the shape of the steady-state inactivation curve in the initial falling phase, but very little effect on the measured half-

inactivation potential. Consistent with this notion, for any given channel construct no correlation between half-inactivation potential and current size was found.

Steady state inactivation was assessed by holding the cells at various conditioning potentials for five seconds prior to stepping to a test potential of +10 or +20 mV. The rate of inactivation was assessed by using the percentage of current which had inactivated over a time course of 150 ms rather than utilizing exponential fits to the time course of inactivation. This was necessary because it was not always possible to fit the time course of inactivation with only a single exponential. Typically, currents were elicited by stepping from -100 mV to a series of test depolarizations.

Data were filtered at 1 kHz and recorded directly onto a personal computer. Data were analyzed using Clampfit (Axon Instruments). All curve fitting was carried out in Sigmaplot 4.0 (Jandel Scientific). Steady state inactivation curves were fitted to the Boltzman equation I_{peak} (normalized) = C + (1-C)/(1 + exp ((V- V_h) z/25.6)), where V and V_h are respectively the conditioning and the half-inactivation potential, z is a slope factor and C is the non-inactivating fraction. Current voltage relations were fitted according to the equation I_{peak}= (V-E_{rev})G(1/(1+exp (V_a-V)/S)) where E_{rev} is the reversal potential, V_a is the half-activation potential, G is the maximum chord conductance and S is a slope factor which is inversely proportional to the effective gating charge. Unless stated otherwise, all error bars are standard errors, numbers in parentheses displayed in the figures reflect numbers of experiments, and p values given reflect Student's t-tests.

RESULTS

Wild-Type α_{1E} and α_{1C} Channels Exhibit Distinct Voltage-Dependent Inactivation Properties

It is well established that neuronal (L-type) α_{1C} calcium channels undergo little voltage-dependent inactivation in response to membrane depolarization. In contrast, α_{1E} channels are among the most rapidly inactivating high voltage-activated calcium channel isoforms. Figure 14 illustrates these intrinsic differences between α_{1C} and α_{1E} (both coexpressed in HEK cells with ancillary α_2-δ and β_{1b} subunits). As seen in Figure 14A, α_{1E} channels inactivate much more rapidly than the α_{1C} isoform, and this difference is maintained over a large range of test potentials (Fig. 14C). Generally, some variability was observed in the number of time constants required for fitting the time course of inactivation of α_{1E} (i.e., while in the majority of cases, a single exponential yielded a satisfactory fit, in some cases two exponentials were required). Hence, in order to facilitate comparison among the wild type and chimeric calcium channels, the rate of inactivation is reflected, in Figure 14C and throughout the text, as the percentage of peak current that had inactivated over a time course of 150 ms. Over the voltage range from -20 mV to +30mV, the inactivation rate of α_{1E} ranged from 52 to 74 percent, whereas α_{1C} exhibited inactivation rates between 6 and 22 percent. Note that because barium was used as the external charge carrier, and due to effective buffering of intracellular calcium with EGTA, voltage-dependent inactivation processes were not contaminated by the

Figure 14. Comparison of Kinetic Properties of Wild-Type rbC-II and rbE-II Calcium Channels

Inset: Proposed transmembrane topology of voltage-dependent calcium channels. Throughout the manuscript, transmembrane domains of the parent α_{1C} channel are depicted in black, the four letter code (CCCC, EEEE) refers to the origin of the four individual transmembrane domains. **(A)** Representative whole cell current traces (I_{Ba}) of rbC-II *(upper panel)* and rbE-II *(lower panel)* in 20mM Ba^{2+}. Currents were elicited by a 250 ms step depolarization to +10 mV from a holding potential of -100 mV. The traces were leak subtracted on-line using a p/5 protocol. Note that α_{1E} inactivates much more rapidly than α_{1C}. **(B)** Representative current-voltage relations of rbC-II *(upper panel)* and rbE-II *(lower panel)* in 20mM Ba^{2+} from a holding potential of -100 mV. The I-V plots were fitted as outlined in the Methods section, the half-activation potential of α_{1E} was typically about 10 mV more negative than that of α_{1C} (α_{1C} V_a= -11.2 ± 2.4 mV; α_{1E} V_a = -20.6 ± 3.2). **(C)** Voltage-dependence of the inactivation rates (as determined by the fraction of current inactivated during the course of a 150 ms test depolarization) for rbC-II (circles, n=9) and rbE-II (triangles, n=11). **(D)** Comparison of steady state inactivation properties of rbC-II (circles, n=9) and rbE-II (triangles, n=14). Peak current amplitude was measured immediately following a 5 s conditioning potential. The data were fitted using the Boltzman equation. The half-inactivation potentials obtained from the fits were, respectively -16 mV (z=3.0) and -58 mV (z=3.1) for rbC-II and rbE-II. Error bars reflect standard errors.

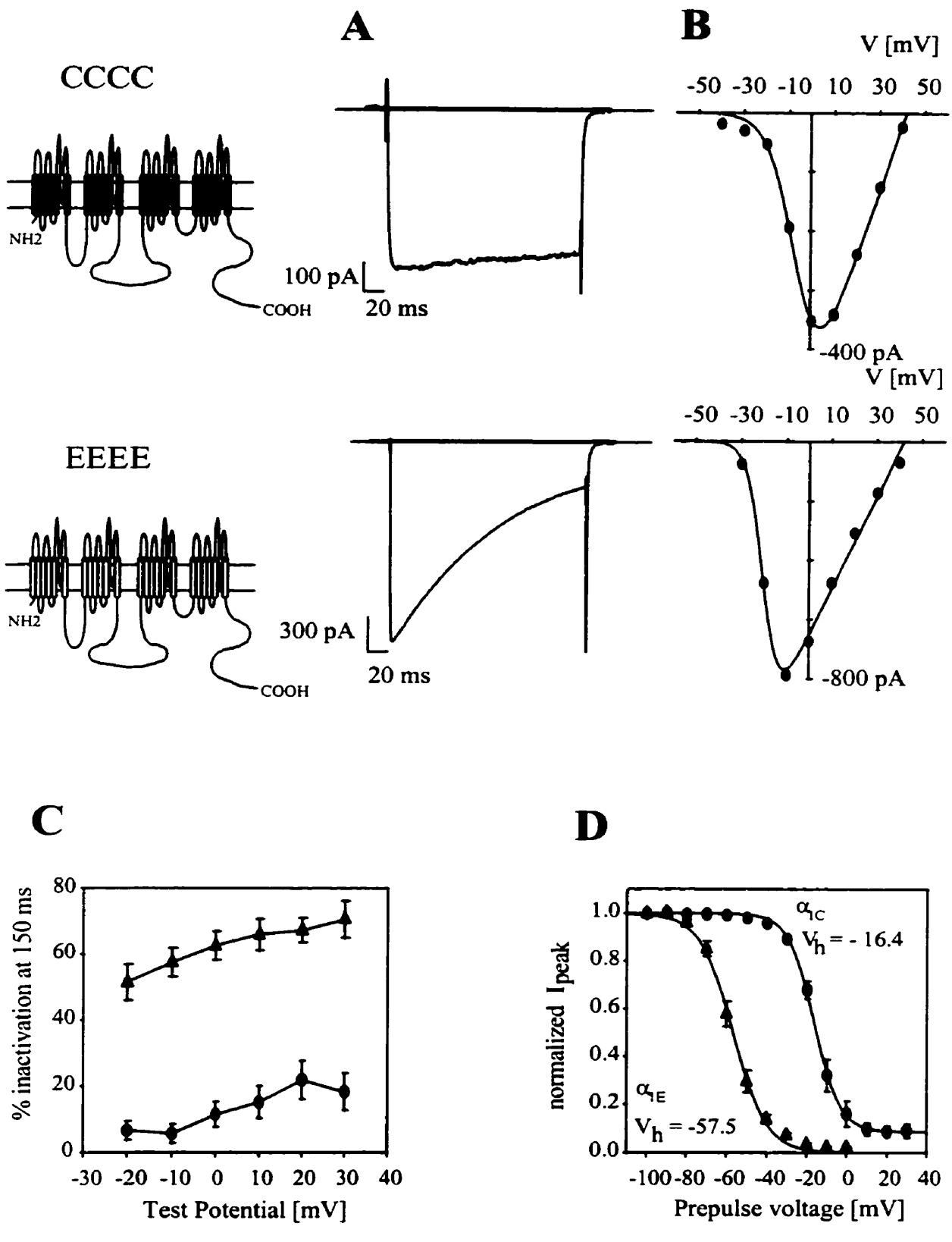
A
B
CCCC
NH2
COOH
100 pA
20 ms
V [mV]
-50 -30 -10 10 30 50
-400 pA
EEEE
NH2
COOH
300 pA
20 ms
V [mV]
-50 -30 -10 10 30 50
-800 pA
C
% inactivation at 150 ms
80
60
40
20
0
-30 -20 -10 0 10 20 30 40
Test Potential [mV]
D
normalized Ipeak
1.0
0.8
0.6
0.4
0.2
0.0
αIC
Vh = - 16.4
αIE
Vh = -57.5
-100 -80 -60 -40 -20 0 20 40
Prepulse voltage [mV]

calcium-sensitive inactivation process intrinsic to L-type calcium channels (Imredy and Yue, 1994).

In addition to their rates of inactivation, the wild type channels also exhibited pronounced differences in their half-inactivation potentials, with α_{1E} inactivating at potentials about 40 mV more negative than α_{1C} (Fig. 14D). The half-inactivation potentials were -57.5 ± 1.6 mV and -16.4 ± 1.9 mV for α_{1E} and α_{1C} respectively. In contrast, at least with 20 mM barium as the charge carrier, the half-activation potentials (estimated from Boltzman fits to current-voltage relations) of the two wild type channels differed by only about 10 mV, with a half-activation potential of -20.6 ± 3.2 mV for α_{1E} and -11.2 ± 2.4 mV for α_{1C} (Fig. 14B, see also Table 4). Overall, the differences between the inactivation properties of the two wild type channels are sufficiently large to permit a chimeric approach towards the molecular identification of the underlying structural determinants.

Inactivation Properties of α_{1E} and α_{1C} Chimeras

To investigate the molecular mechanism underlying these differences in voltage-dependent inactivation properties, a series of chimeras between wild type α_{1C} and α_{1E} calcium channels was constructed. Each chimeric construct is formed via combination of the four major transmembrane domains of the two parent channels (see illustrations in Fig. 15). As described in detail in the Methods section, the chimeras were designed such

Table 4. Activation and Inactivation Properties of Wild-Type and Chimeric Calcium Channels

Values were obtained via Boltzman fits of steady-state inactivation curves (Fig. 15) and macroscopic current-voltage relations. Note that there is no correlation between half-activation and half-inactivation potentials. Current-density measurements obtained at the peak of the current voltage relation reveal variable levels of expression among the channels.

Table 4: Activation and inactivation properties of wild-type and chimeric calcium channels

Construct	*Half-inactivation potential (mV)*	*Z*	*Half-activation potential (mV)*	*S*	*Current -Density (pA/pF)*
α_{1C}(CCCC)	- 16.4 ± 1.9 (n = 9)	3.0	- 11.2 ± 2.4 (n = 9)	5.2	14.6
α_{1E} (EEEE)	- 57.5 ± 1.6 (n = 14)	3.0	- 20.6 ± 3.2 (n = 12)	3.3	29.3
CEEC	- 66.6 ± 1.4 (n = 9)	2.6	- 15.0 ± 1.7 (n = 8)	3.8	5.1
EECC	- 58.5 ± 1.5 (n = 9)	2.7	- 21.4 ± 2.3 (n = 8)	5.7	15.3
CEEE	-47.7 ± 2.5 (n = 8)	2.9	- 27.9 ± 3.8 (n = 7)	2.6	51.8
CECC	- 44.4 ± 2.5 (n = 10)	2.2	- 13.6 ± 2.5 (n = 14)	4.0	29.9
CCEC	- 43.7 ± 2.6 (n = 10)	2.9	- 22.6 ± 2.0 (n = 8)	2.9	37.4
CCEE	-32.4 ± 2.7 (n = 8)	3.8	- 21.7 ± 2.4 (n = 12)	4.7	29.0
ECCC	- 29.8 ± 3.4 (n = 6)	1.4	- 12.5 ± 3.8 (n = 6)	11.6	8.3
ECEE	- 19.6 ± 2.8 (n = 9)	3.1	- 21.6 ± 2.2 (n = 5)	6.4	5.8
CCCE	0.4 ± 1.8 (n = 4)	2.9	5.4 ± 3.3 (n = 3)	8.6	15.9

Figure 15 - Nomenclature and Steady-State Inactivation Properties of C/E Transmembrane Domain Chimeras

Transmembrane topology of the chimeric calcium channel constructs is shown, indicating the nomenclature used throughout. The chimeras were coexpressed with $\alpha_{2\text{-}\delta}$ and β_{1b} subunits. Mean steady-state inactivation curves (right) and representative current traces (*insets*) are shown for each chimera. Current traces represent voltage steps (of 150 ms duration) to +10 mV from a holding potential of -100 mV. The experimental conditions were as outlined in Figure 14. The data were fitted with a Boltzman equation, and half-inactivation potentials (V_h in mV) are listed for each chimera. Error bars represent standard errors.

CEEE

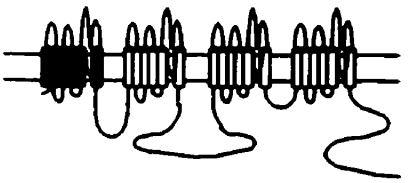

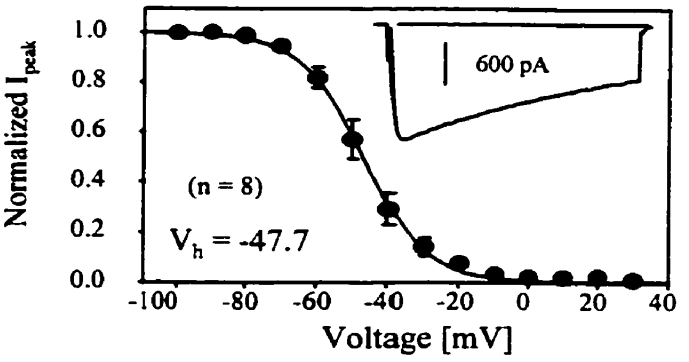

CCEE

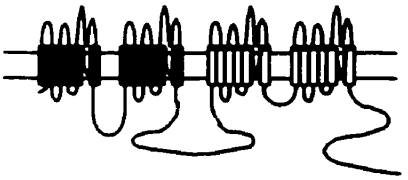

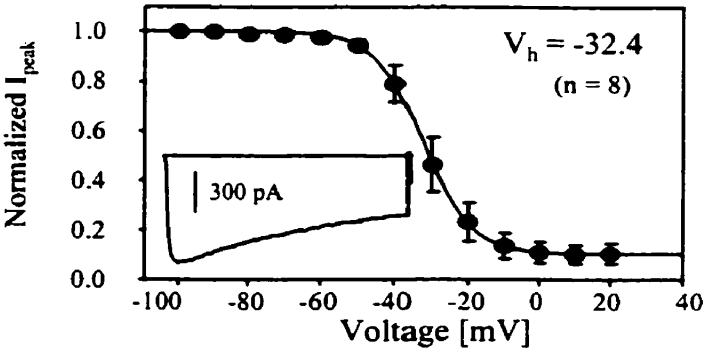

EECC

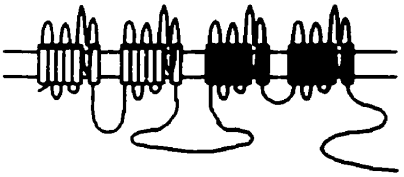

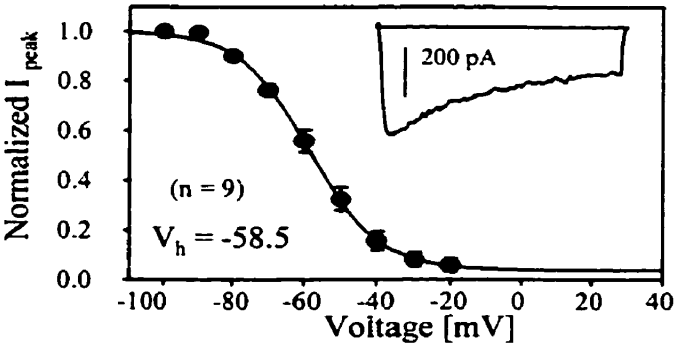

CECC

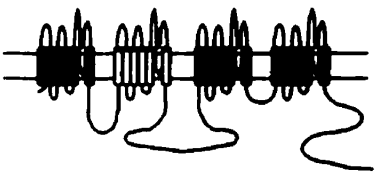

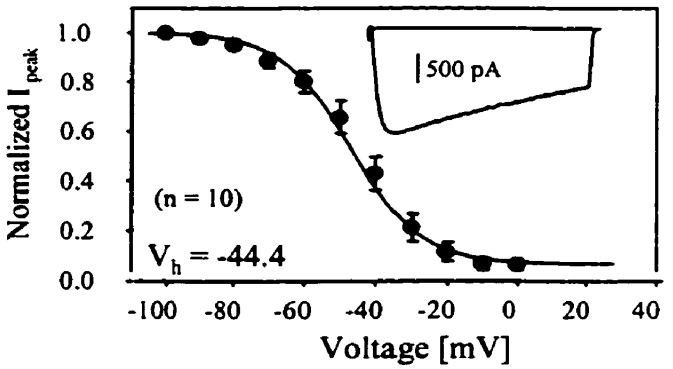

ECEE

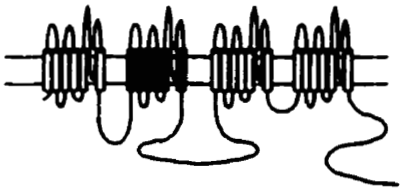

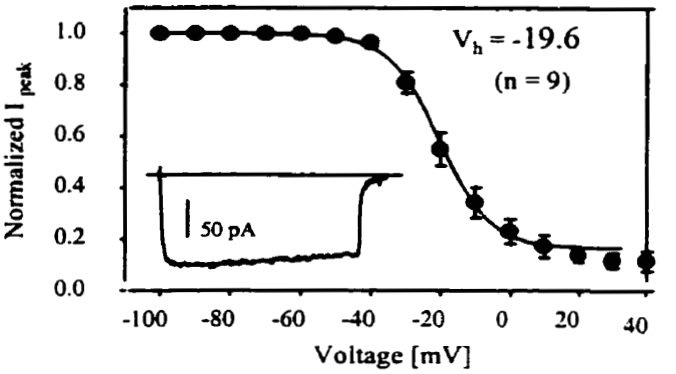

CCEC

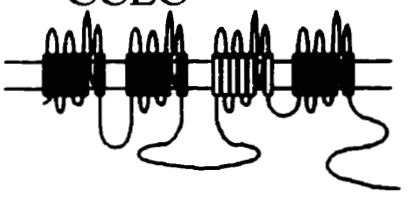

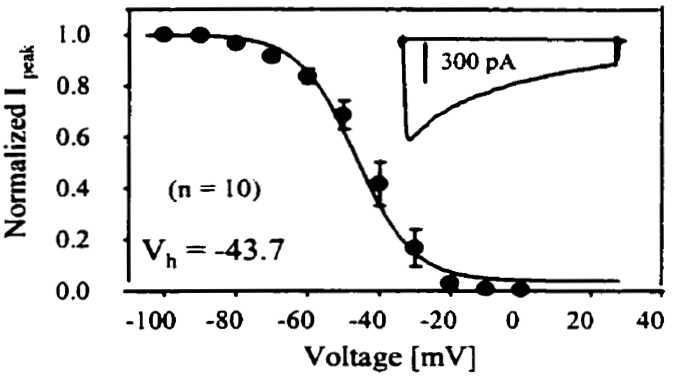

CCCE

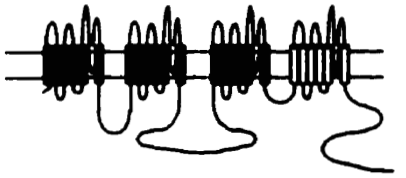

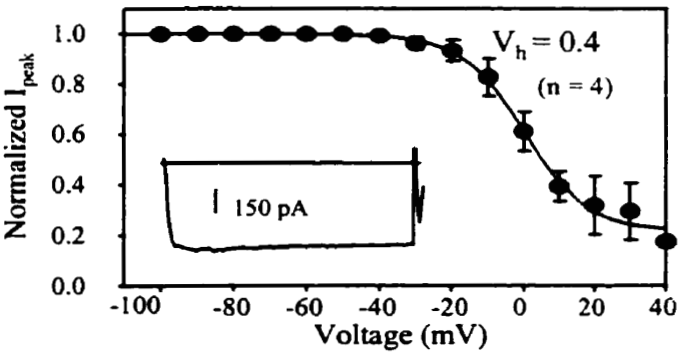

CEEC

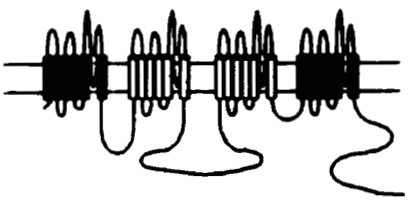

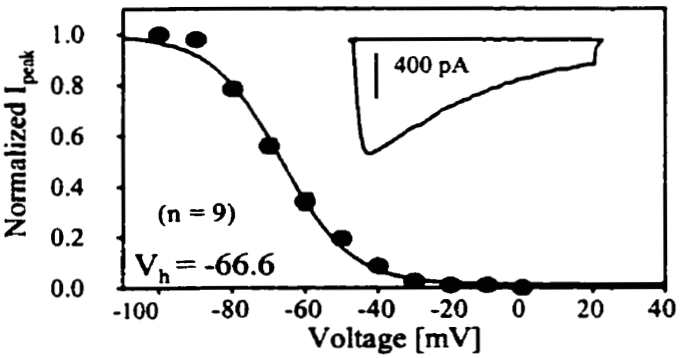

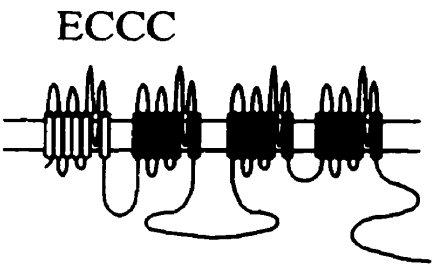
ECCC

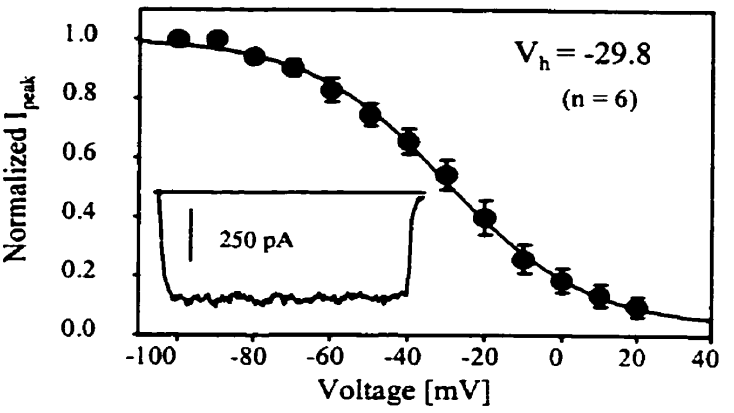
Normalized I_{peak}
1.0
0.8
0.6
0.4
0.2
0.0
V_h = -29.8
(n = 6)
250 pA
-100
-80
-60
-40
-20
0
20
40
Voltage [mV]

that switches occurred immediately after the end of the S6 segments in domains I and II, and about 30 amino acids past that of domain III, and thus, each domain remains associated with the preceding cytoplasmic linker region. Of the fourteen chimeras, nine formed functional calcium channels; CCCE, CCEC, CECC, CEEC, CEEE, CCEE, ECCC, EECC, and ECEE. Expression levels varied in these nine constructs, from very large whole cell currents (~2 nA at peak) to relatively small whole cell currents (200 - 300 pA). The nine chimeric constructs were examined electrophysiologically to assess steady-state inactivation properties and inactivation rates.

All Four Transmembrane Domains Contribute to Steady-State Inactivation

Figure 15 depicts representative current traces and ensemble steady state inactivation curves for each of the chimeras. In each case, the voltage-dependence of steady state inactivation could be accurately described with a Boltzman relation. Several of the chimeras, as well as the wild type α_{1C} channel, did not inactivate completely during the five second conditioning pulse, and hence, the Boltzman fit was modified to incorporate this non-inactivating fraction (see Methods). The half-inactivation potentials and slope factors obtained from these fits (see also Table 4), and the shapes of the current waveforms (Fig. 15) were consistent with what one might have expected based on observations of the two wild type channels. The chimera ECCC did however exhibit somewhat shallow voltage dependencies of both inactivation and activation (Table 4, Fig. 15).

Figure 16 compares the half-inactivation potentials of the nine chimeras to the wild type channels in form of a bar graph. Upon examination of Figure 16, two observations can be made: First, no single domain switch appears to be able to confer the entire steady state inactivation properties from one parent channel to another. Instead, a continuous spectrum of half-inactivation potentials spanning the range between the two wild type channels was evident. Secondly, two of the chimeras (CEEC, CCCE) exhibited half-inactivation potentials outside of that range, indicating that some of the individual domains of a particular parent channel may perhaps exert opposing effects on the position of the steady-state inactivation curve along the voltage axis. From the graph in Figure 16, it is difficult to assess the effects of individual transmembrane domain switches on half-inactivation potential. Hence, in order to isolate the individual contributions of each of the four transmembrane domains to the overall voltage-dependence of inactivation, the data of Figure 16 were divided into individual pairs of chimeras in which only a single domain was exchanged. Figure 17A examines the effect of replacement of the α_{1C} sequence in domain I with the corresponding sequence from α_{1E}. As evident from the figure, three out of the four chimera pairs examined exhibited a 10 mV to 15 mV negative shift in half-inactivation potential when domain I contained the α_{1E} sequence. Upon replacement of α_{1C} sequence in either domains II or III with that of α_{1E}, a large hyperpolarizing shift of ~20 mV was observed in every case. Thus, structures residing within each of the first three domains contribute to the more negative half-inactivation potential seen with wild type α_{1E} channels. Surprisingly, when the same type of analysis

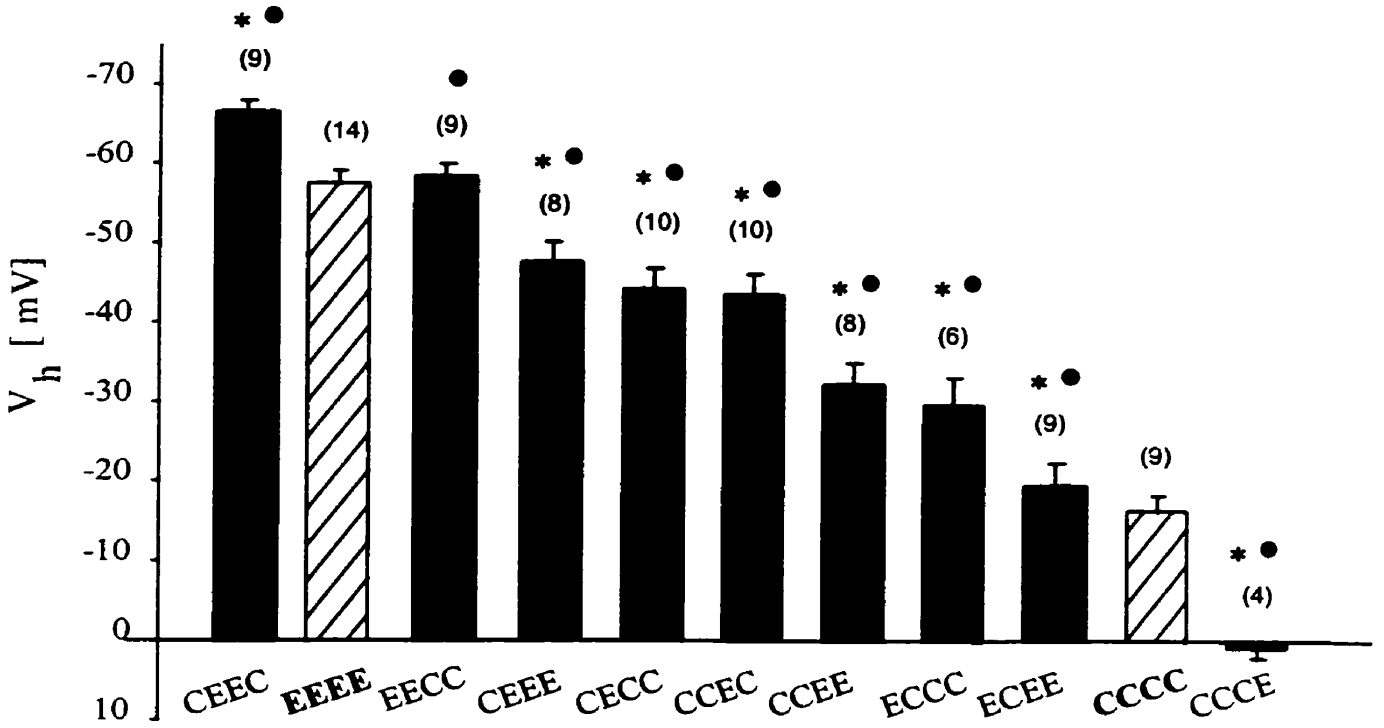

Figure 16 - Steady-State Inactivation of C/E Chimeras Spans the Range Between the Wild-Type Channels

Comparison of half-inactivation potentials for wild-type and chimerical calcium channels. In each case, steady-state inactivation curves from individual curves were fitted separately, and means and standard errors are plotted. Numbers in parentheses reflect numbers of experiments. Asterisks denote chimeras which have half-inactivation potentials which are significantly different from α_{1E}, and filled circles denote chimeras which differ significantly from α_{1C} ($p < 0.05$). For half-inactivation values for each chimera refer to Table 4.

Figure 17 - Contribution of Individual Transmembrane Domains to Steady-State Inactivation

(A) Replacement of the α_{1C} sequence in domain I with that of α_{1E} mediates a moderate (10 - 15 mV) hyperpolarizing shift in half-inactivation potential in 3 out of 4 pairs of constructs. **(B,C)** Replacement of the α_{1C} sequences in either domain II or domain III with those of α_{1E} mediates a strong (25 - 28 mV) hyperpolarizing shift in half-inactivation for all the chimeras tested. **(D)** Replacement of the α_{1C} sequence in domain IV with that of α_{1E} produces a moderate (~15 mV) depolarizing shift in half-inactivation potential. In each case, an asterisk denotes transitions for which there is a significant shift in V_h ($p < 0.05$). The numbers in parentheses reflect the ratios of the change in half-activation potential to the change in half-inactivation potential for each chimera pair.

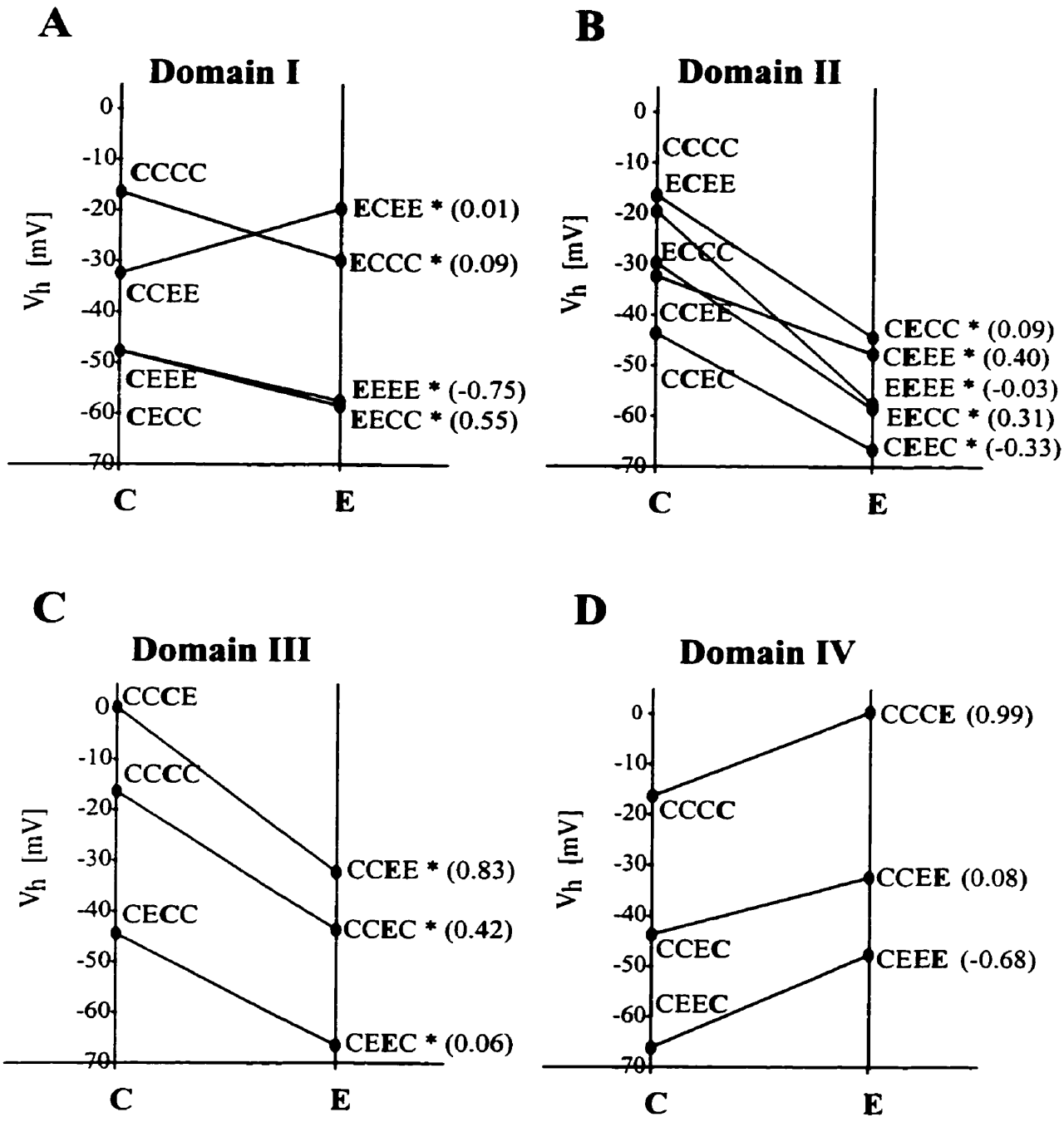
A
Domain I
0
-10
-20
-30
-40
-50
-60
-70
Vh [mV]
CCCC
CCEE
CEEE
CECC
ECEE * (0.01)
ECCC * (0.09)
EEEE * (-0.75)
EECC * (0.55)
C
E
B
Domain II
CCCC
ECEE
ECCC
CCEE
CCEC
CECC * (0.09)
CEEE * (0.40)
EEEE * (-0.03)
EECC * (0.31)
CEEC * (-0.33)
C
E
C
Domain III
CCCE
CCCC
CECC
CCEE * (0.83)
CCEC * (0.42)
CEEC * (0.06)
C
E
D
Domain IV
CCCE (0.99)
CCCC
CCEE (0.08)
CCEC
CEEE (-0.68)
CEEC
C
E

was carried out for substitutions in domain IV, the opposite effect was observed, with α_{1E} domain IV mediating a depolarizing shift in half-inactivation potential when replacing α_{1C} sequence. These data indicate that all four transmembrane domains contribute to steady-state inactivation properties of voltage-dependent calcium channels, and furthermore, that the absolute value of the half-inactivation potential for α_{1E} channels is determined through an equilibrium formed by hyperpolarizing and depolarizing structural tendencies.

Half-Inactivation Potential Shifts are Not Correlated With Activation Effects

It is known for sodium and potassium channels that inactivation can be tightly coupled to activation. Thus, the above conclusions are somewhat complicated by the notion that not all of the chimeras exhibited identical half-activation potentials (see Table 4). The wild type channels differed by less than 10 mV in their half-activation potentials, and yet, they exhibited a greater than 40 mV difference in their half-inactivation potentials. When examining the data presented in Table 4, one can identify two clusters of constructs with half-activation potentials of, respectively around -21 mV (EEEE, EECC, CCEC, CCEE, ECEE) and around -12 mV (CCCC, CEEC, CECC, ECCC), and yet, within each of these clusters the half-inactivation potentials varied by as much as 35 mV and 50 mV respectively. Overall, these considerations suggest that the distinct activation potentials of the chimeras are not correlated with the observed differences in inactivation properties. Nonetheless, it is possible that in some cases the activation

effects might skew the absolute inactivation potential changes induced by domain swapping. To assess the extent of any putative contamination by activation effects, the ratio of the change in half-activation potential to the change in half-inactivation potential was calculated for each pair of chimeras (see numbers in parentheses, Fig. 17). A value of 1 indicates that the change in half-inactivation potential parallels the changes in half-activation potential in magnitude. A value near 0 indicates that there is only little, if any, contamination by activation effects, and a negative value reflects a scenario in which a domain switch results in opposite shifts in half-activation and half-inactivation potentials. As seen from the figure, in only two out of fifteen cases did the index approach 1, and only four additional chimera pairs displayed ratios greater than 0.1. It is also noteworthy that the chimera CEEC differed from the wild type α_{1C} channel by only 4 mV in half-activation potential, while exhibiting a half-inactivation potential which was 55 mV more negative, thus further supporting the notion that domains II and III determine the bulk of the voltage dependence of inactivation. Overall these considerations suggest that for the majority of chimera pairs, differences in voltage dependent activation properties do not account for the observed changes in half-activation potentials.

The effects of individual domains on half-activation potential were not systematically examined because the difference between the two wild-type channels was relatively small (<10 mV), and perhaps with the exception of α_{1E} domain III which tended to shift the half-activation potential into the negative direction (see Table 4), none of the individual transmembrane domains appeared to have a clear cut effect on activation

range. Even with the use of more accurate tail current protocols (rather than relying on fits to macroscopic current voltage-relations), it would likely be very difficult to attribute the distinct activation ranges of the two wild type channels to individual transmembrane domains.

Transmembrane Domains II, III and IV Determine Inactivation Rates

To determine the effects of each transmembrane domain on the rate of inactivation, we compared inactivation of wild type and chimeric calcium channels by using the ratio of peak current level to the residual current level observed at the end of a 150 ms test depolarization as a single measure of all voltage-dependent inactivation processes. Figure 18 depicts the percentage of inactivation which occurred over 150 ms for three different test pulses (0 mV, +10 mV, and +20 mV). Similar to what was observed with the half-inactivation potentials, the inactivation rates of the individual chimeras formed a continuum within the range spanned by the two wild type channels. This indicates that the rate of inactivation may also be determined by multiple structural domains.

Figure 19 examines the role of each individual transmembrane domain in determining the rate of inactivation. As seen from Figure 19, in only one out of four cases did exchanges of domain I exert a significant effect, suggesting that domain I does not contribute in a substantial manner to the differences in inactivation rate between rat brain α_{1C} and α_{1E} channels. In contrast, in seven out of eight cases, replacing α_{1C}

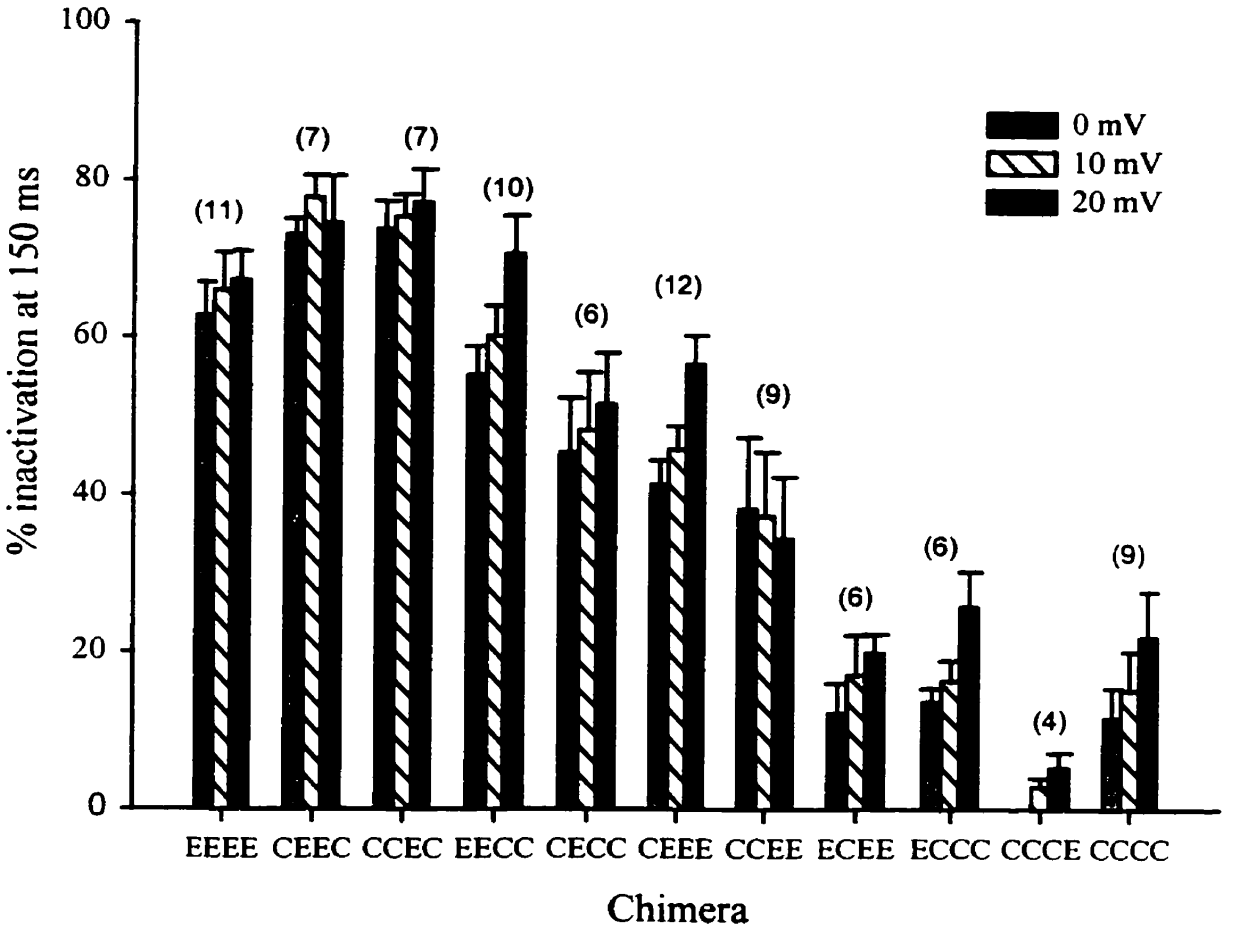

Figure 18 - Inactivation Rates for Wild-Type and Chimeric Calcium Channels

Inactivation rates for wild-type and chimeric calcium channels, indicated as the percentage of peak current that has inactivated during a 150 ms test pulse, are shown for three different test potentials (0 mV, 10 mV, and 20 mV). Error bars denote standard errors, and numbers in parentheses denote numbers of experiments. Inactivation rates observed with the chimeras are widely distributed between inactivation rates for the wild-type channels.

Figure 19 - Contribution of Individual Transmembrane Domains to Inactivation Rate

(A) Exchanging domain I has little effect on inactivation rate. **(B,C)** Replacement of α_{1C} sequence in domains II or III with the corresponding α_{1E} sequence mediates a substantial increase in the rate of inactivation. **(D)** Replacement of α_{1C} sequence in domain IV with that of α_{1E} slows the rate of inactivation. Inactivation rates were measured at +20 mV and were taken from Figure 18. Asterisks denote statistically significant changes in inactivation rates ($p < 0.05$). *Insets:* Representative whole cell current records illustrating the effects of single domain switches on inactivation rates (step depolarizations to +10 mV). Plots of the voltage-dependence of inactivation rate are depicted below the current records.

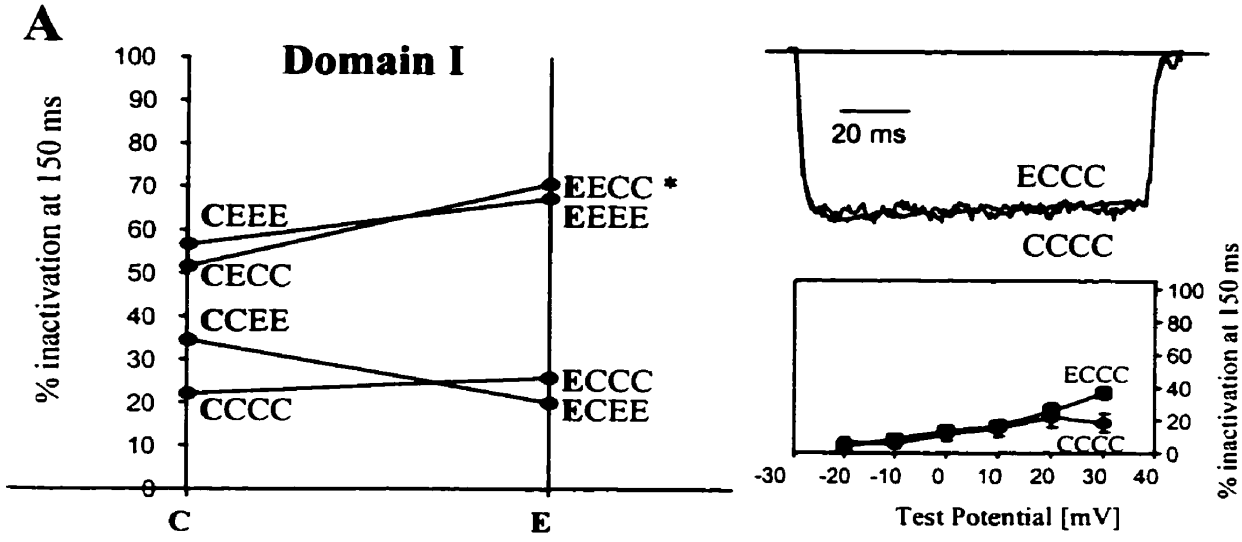
A
Domain I
% inactivation at 150 ms
100
90
80
70
60
50
40
30
20
10
0
CEEE
CECC
CCEE
CCCC
EECC *
EEEE
ECCC
ECEE
C
E
20 ms
ECCC
CCCC
ECCC
CCCC
-30 -20 -10 0 10 20 30 40
Test Potential [mV]
% inactivation at 150 ms

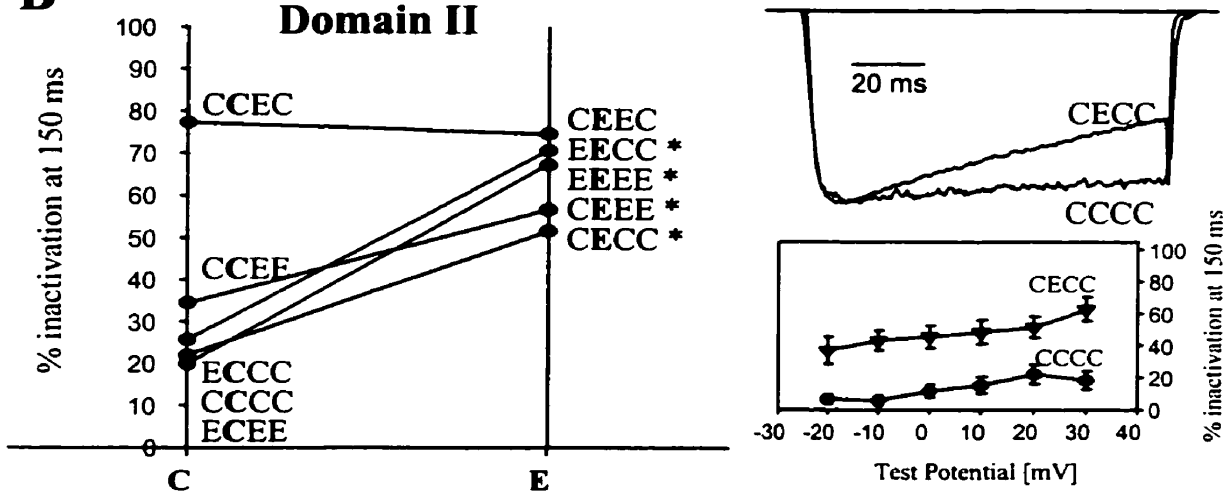
B
Domain II
% inactivation at 150 ms
100
90
80
70
60
50
40
30
20
10
0
CCEC
CCEE
ECCC
CCCC
ECEE
CEEC
EECC *
EEEE *
CEEE *
CECC *
C
E
20 ms
CECC
CCCC
CECC
CCCC
-30 -20 -10 0 10 20 30 40
Test Potential [mV]
% inactivation at 150 ms

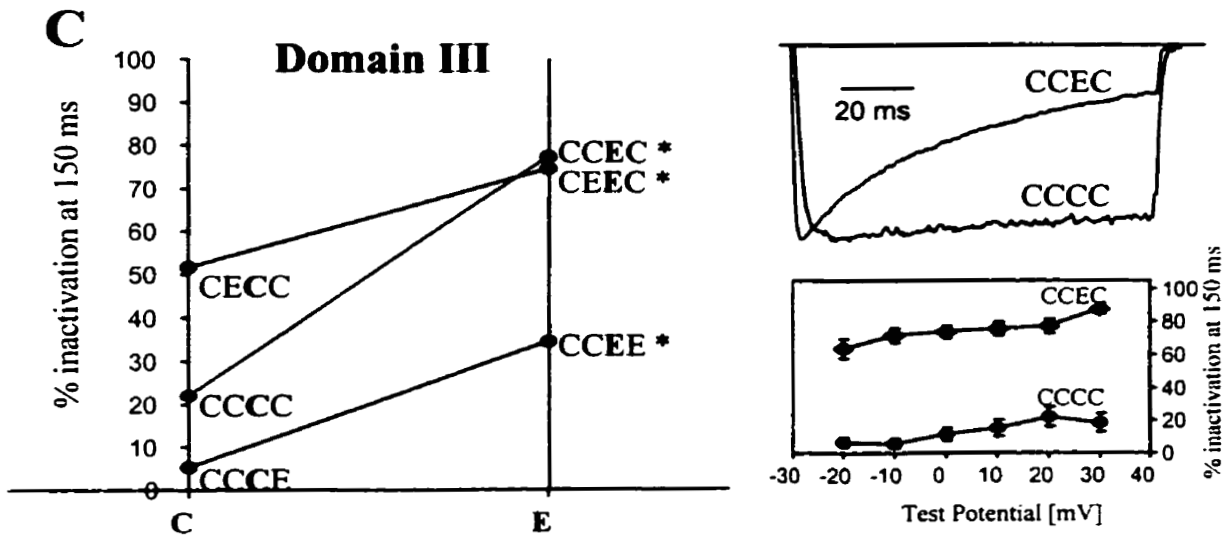
C
Domain III
% inactivation at 150 ms
100
90
80
70
60
50
40
30
20
10
0
CCEC *
CEEC *
CECC
CCEE *
CCCC
CCCE
C
E
20 ms
CCEC
CCCC
CCEC
CCCC
-30 -20 -10 0 10 20 30 40
Test Potential [mV]
% inactivation at 150 ms

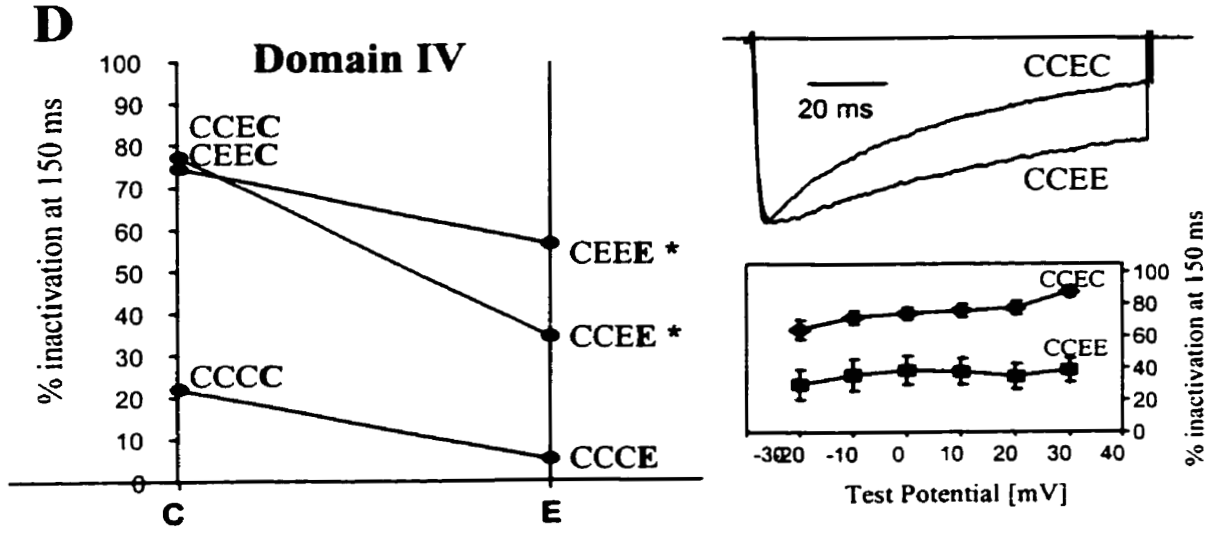
D
Domain IV
% inactivation at 150 ms
100
90
80
70
60
50
40
30
20
10
0
CCEC
CEEC
CEEE *
CCEE *
CCCC
CCCE
C
E
20 ms
CCEC
CCEE
CCEC
CCEE
-30 -20 -10 0 10 20 30 40
Test Potential [mV]
% inactivation at 150 ms

sequences in domains II or III with those corresponding to α_{1E} mediated increases in inactivation rate by 2.5 and 4-fold respectively. Replacement of the domain II sequence in CCEC with that from α_{1E} to make CEEC had no effect on inactivation rate. Consistent with the steady-state inactivation results, domain IV of α_{1E} actually slowed the rate of inactivation (by 2.5-fold). This behavior is further illustrated in Figure 19 with the current records and the voltage-dependence of the inactivation plots of selected chimera pairs. Insertion of domain I of α_{1E} into the wild type α_{1C} channel had little effect on current waveform, or on the magnitude and voltage-dependence of the rate of inactivation. Insertion of domains II or III of the wild type α_{1E} channel into α_{1C} mediated a significant speeding of inactivation at all test potentials with the chimeras CECC and CCEC inactivating with rates resembling those for α_{1E} (insets Fig. 19B and C). In fact, there was no significant difference in inactivation rate between the chimera CCEC and the wild type α_{1E} channel at any of the test potentials used, indicating that domain III might be perhaps be the most critical determinant of inactivation rate. Finally, in further support of the idea that domain IV of α_{1E} slows inactivation, the CCEE chimera inactivated significantly more slowly than CCEC at all potentials tested (Fig. 19D). A smaller difference in inactivation rate was observed between α_{1C} and the chimera CCCE because the wild-type α_{1C} already showed very little inactivation over 150 ms.

Overall, the data implicates multiple transmembrane domains in the overall voltage-dependent inactivation process of neuronal α_{1E} calcium channels, with domains II and III accounting for the bulk of the effect.

S6 Chimeras - Investigation of a "C-type"-Like Inactivation Mechanism

The finding that the voltage-dependent inactivation of calcium channels involves contributions from each transmembrane domain is reminiscent of the cooperative conformational changes that lead to inactivation of potassium channels by C-type inactivation. C-type inactivation involves, specifically, a constriction of the pore via conformational changes in the S6 segment of each of the four subunits that form the channel (Hoshi *et. al.*, 1991; Lopez *et. al.*, 1994). To investigate whether the S6 segments play a similar role in voltage-dependent inactivation of calcium channels, a second series of chimeras was constructed to assess the involvement of the II S6 and III S6 segments in the inactivation process. The S6 segments from domains II and III were selected as candidates for involvement, because the previous results showed that domains II and III had the largest effect on both inactivation rate and steady-state inactivation in the C/E transmembrane domain chimeras. The S6 chimeras contain either the II S6 or III S6 segment of α_{1E} on an α_{1C} background, and either the II S6 or III S6 segment of α_{1C} substituted on an α_{1E} background (see Figure 11). Inactivation properties of the four constructs were subsequently examined by whole cell voltage clamp to assess steady-state inactivation and inactivation rate.

Whole-cell recordings of the II S6 and III S6 chimeras (carried out by Stephanie Stotz) were performed under the same conditions as previously described (i.e., coexpressed in HEK cells with α_2-δ and β_{1b} subunits, 20 mM Ba^{2+} external solution) but with a different internal pipette solution. For the present set of experiments a cesium-

methanesulfonate (CsMS) internal solution (108 mM CsMS, 4 mM $MgCl_2$, 9 mM EGTA, 9 mM HEPES) was used rather than the cesium-chloride (CsCl) internal solution (105 mM CsCl, 25 mM TEACl, 11 mM EGTA, 10 mM HEPES), thus, permitting more stable recordings (Zhang *et. al.*, 1994b; Zamponi, 1999). Activation and inactivation properties of the wild-type α_{1E} and α_{1C} channels were reexamined under the new recording conditions. Distinct differences in activation and inactivation properties were maintained (Fig. 20) , however inactivation rates and steady-state inactivation properties were significantly changed by the new conditions. As illustrated in Figure 20A, the half-activation potentials of both α_{1E} and α_{1C} showed no dependence on composition of the internal recording solution. In contrast, the half-inactivation potentials of α_{1E} and α_{1C} were both shifted in the hyperpolarizing direction by 11 mV and 22 mV respectively when CsMS was used as the internal recording solution rather than CsCl. Slope values for steady-state inactivation and current-voltage curves were, however, not affected by the type of intracellular recording conditions (see Table 4 and 5). Inactivation rates were also dependent upon internal recording solution composition, with both α_{1E} and α_{1C} exhibiting faster inactivation kinetics at all potentials in CsMS (Figure 20B,C). Over the range from -10 mV to +30 mV, both channels displayed 15 to 30 percent faster inactivation in the new recording solution.

Figure 21 shows that despite the changes in inactivation properties induced by internal recording solution composition, distinct differences are still maintained between rat brain α_{1E} and α_{1C} calcium channels. At all potentials α_{1E} inactivates much more

Figure 20 - Inactivation Properties of α_{1E} and α_{1C} are Dependent on Internal Recording Solution Composition

(A) Half-activation and half-inactivation potentials of α_{1E} and α_{1C} in CsCl and CsMS internal recording solution. Half-activation potentials are not affected by internal recording solution composition, however the use of CsMS internal solution shifts half-inactivation potentials in the hyperpolarizing direction for both α_{1E} and α_{1C} channels in comparison to CsCl. (α_{1C} V_h: CsCl -16.4 ± 1.9 mV ; CsMS -27.5 ± 1.3 mV; α_{1E} V_h: CsCl -57.5 ± 1.6 mV; CsMS -79.5 ± 1.3 mV). The slopes of the inactivation curves were not affected by the change in internal recording solution (data not shown). In each case, curves from individual experiments were fitted separately, and the means and standard errors are plotted. An asterisk denotes a significant difference in V_a or V_h ($p<0.05$). **(B)** Voltage-dependence of inactivation rate of α_{1C} obtained using CsCl internal recording solution (closed circles, n = 9) and CsMS internal recording solution (open circles, n = 7). **(C)** Voltage-dependence of inactivation rate of α_{1E} obtained using CsCl internal recording solution (closed circles, n = 11) and CsMS internal recording solution (open circles, n = 9). Note that use of CsMS internal solution results in faster inactivation at all potentials for both α_{1E} and α_{1C}.

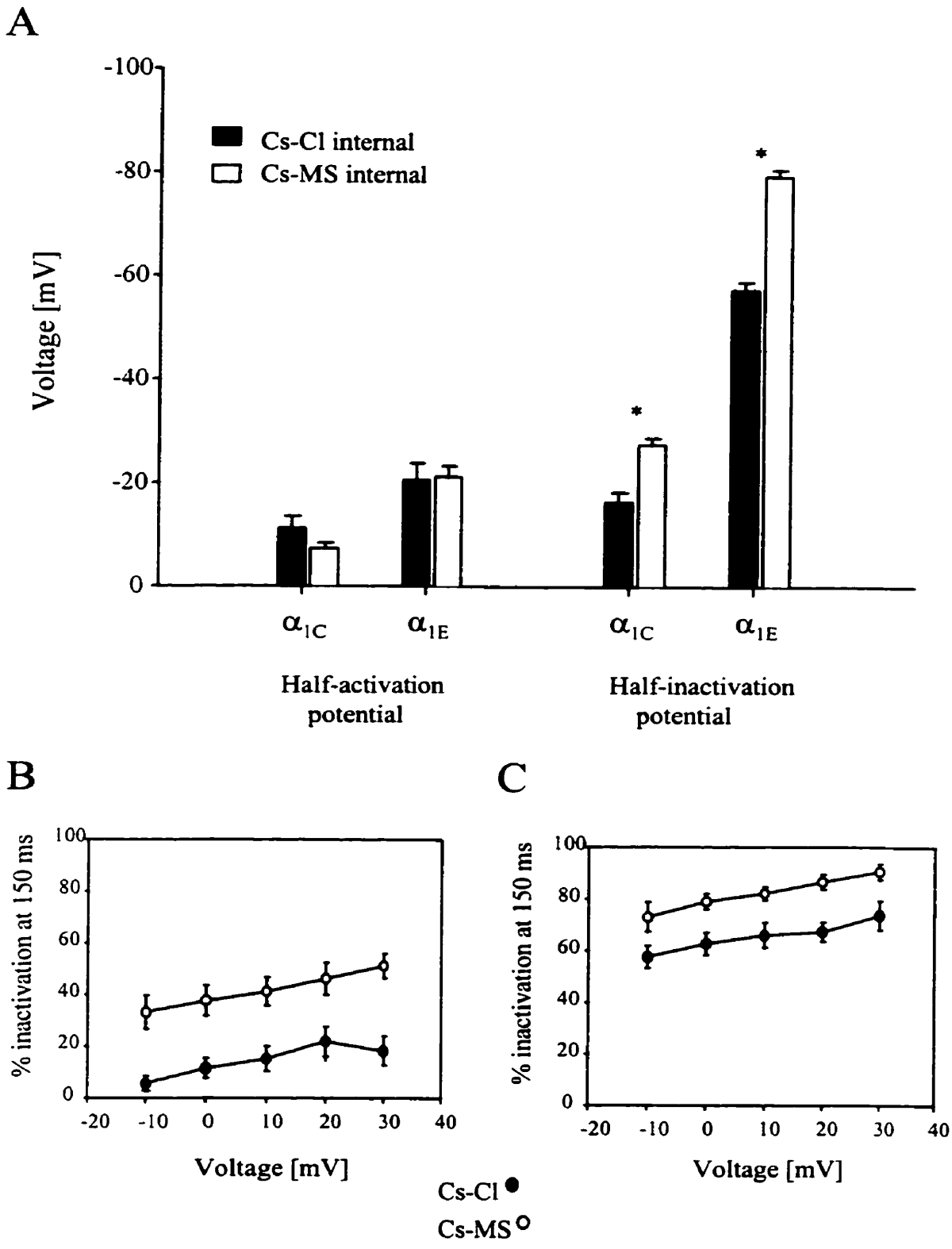
A
-100
-80
-60
-40
-20
0
Voltage [mV]
Cs-Cl internal
Cs-MS internal
*
*
α_{1C}
α_{1E}
α_{1C}
α_{1E}
Half-activation potential
Half-inactivation potential
B
% inactivation at 150 ms
100
80
60
40
20
0
-20
-10
0
10
20
30
40
Voltage [mV]
C
% inactivation at 150 ms
100
80
60
40
20
0
-20
-10
0
10
20
30
40
Voltage [mV]
Cs-Cl ●
Cs-MS ○

Construct	*Half-inactivation potential (mV)*	*Z*	*Half-activation potential (mV)*	*S*	*Current -Density (pA/pF)*
α_{1C}	- 27.5 ± 1.3 (n = 8)	4.0	- 7.3 ± 1.1 (n = 8)	5.3	21.58
α_{1E}	- 79.5 ± 1.3 (n = 9)	3.1	- 21.2 ± 2.1 (n = 9)	3.6	38.99
rbC (IIS6E)	- 35.2 ± 2.3 (n = 9)	3.3	- 6.4 ± 1.8 (n = 9)	3.5	35.96
rbC (IIIS6E)	- 42.6 ± 3.2 (n = 5)	2.6	- 7.7 ± 2.8 (n = 5)	8.3	34.69
rbE (IIS6C)	- 86.4 ± 3.2 (n = 6)	2.4	- 14.9 ± 2.0 (n = 6)	7.3	30.83
rbE (IIIS6C)	- 68.4 ± 3.8 (n = 7)	2.4	- 16.5 ± 3.0 (n = 9)	5.1	16.68

Table 5. Activation and Inactivation Properties of Wild-Type Channels and S6 Chimeras

Values were obtained via Boltzman fits of steady-state inactivation curves and macroscopic current-voltage relations. Whole cell currents were recorded in 20 mM Ba^{2+} external and Cs-MS internal recording solutions. Note that there is no correlation between current density and half-inactivation potential.

Figure 21 - Comparison of Activation and Inactivation Kinetics of Wild-Type α_{1E} and α_{1C} Channels (CsMS)

Inset: Proposed membrane topology of voltage-dependent calcium channels. Transmembrane domains of the parent α_{1C} channel are depicted in grey, and those from the parent α_{1E} channel are depicted in black. **(A)** Representative whole cell current traces (I_{Ba}) of rbC-II *(upper panel)*and rbE-II *(lower panel)* in 20mM Ba^{2+} external recording solution and CsMS internal recording solution. Currents were elicited by a 150 ms depolarization to +10 mV from a holding potential of -100 mV. Note that α_{1E} inactivated much more rapidly than α_{1C}. **(B)** Representative current-voltage relations of rbC-II *(upper panel)*and rbE-II *(lower panel)* 20mM Ba^{2+} and CsMS from a holding potential of -100 mV. The I-V plots were fitted as outlined in the Methods section. The half-activation potential of α_{1E} was typically about 14 mV more negative than that of α_{1C}. **(C)** Voltage-dependence of the inactivation rates (as determined by the fraction of current inactivated during the course of a 150 ms test depolarization) for rbC-II (circles, n = 7) and rbE-II (triangles, n = 9). **(D)** Comparison of steady-state inactivation properties of rbC-II (circles, n = 8), and rbE-II (triangles, n = 9). Peak current amplitude was measured immediately following a 5 s conditioning potential. The data were fitted using the Boltzman equation. The half-inactivation potentials obtained from the fits were, respectively -27.5 ± 1.3 mV (z = 4) and -79.5 ± 1.3 (z = 3.1) for rbC-II and rbE-II. Error bars reflect standard errors.

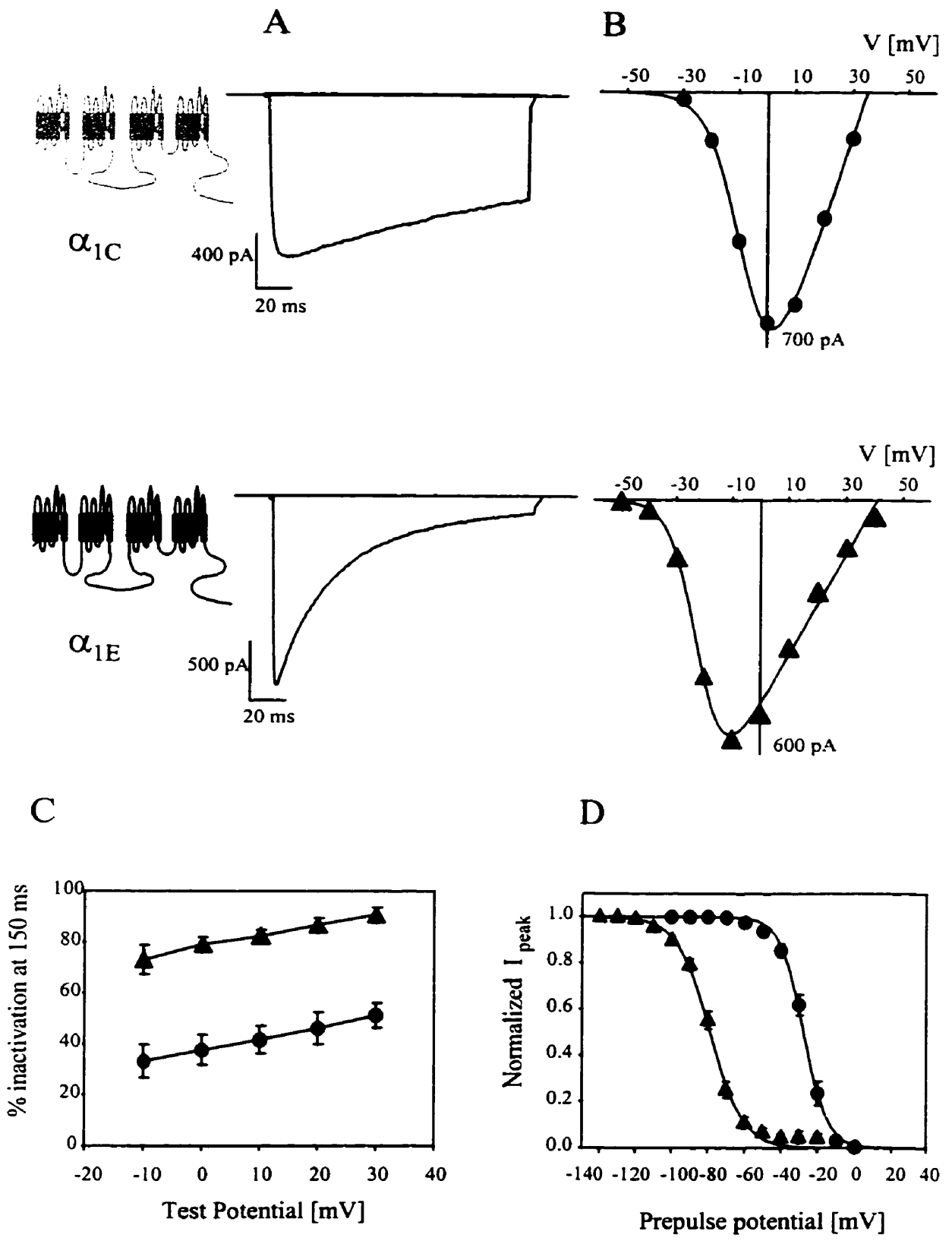
A
B
V [mV]
-50 -30 -10 10 30 50
α_{1C}
400 pA
20 ms
700 pA
V [mV]
-50 -30 -10 10 30 50
α_{1E}
500 pA
20 ms
600 pA
C
D
% inactivation at 150 ms
100
80
60
40
20
0
-20 -10 0 10 20 30 40
Test Potential [mV]
Normalized I_{peak}
1.0
0.8
0.6
0.4
0.2
0.0
-140 -120 -100 -80 -60 -40 -20 0 20 40
Prepulse potential [mV]

rapidly than α_{1C}. Over the voltage range from -10 mV to +30 mV, the inactivation rate of α_{1E} ranged from 65 to 90 percent, whereas α_{1C} exhibited inactivation rates between 33 and 51 percent. The wild-type channels also exhibit pronounced differences in steady-state inactivation properties, with α_{1E} inactivating at potentials about 50 mV more negative than α_{1C} (Fig. 21D). The half-inactivation potentials were -79.5 ± 1.3 mV and -27.5 ± 1.3 mV for α_{1E} and α_{1C} respectively. Despite the large difference in half-inactivation potential, half-activation potentials (estimated from Boltzman fits to current-voltage relations curves) of the two wild-type channels differed by only about 14 mV, with a half-activation potential of -21.2 ± 21 mV for α_{1E} and -7.3 ± 1.1 mV for α_{1C} (Fig. 21B, see also Table 4,5).

S6 Segments do Not Account for Differences in Steady-State Inactivation

Figure 22 depicts representative current traces and ensemble steady-state inactivation curves for each of the S6 chimeras. Voltage dependence of steady-state inactivation is fitted with a Boltzman relation for each construct. The half-inactivation potentials and slope factors from these fits (see also Table 5) are consistent with calcium channel characteristics based on observations of the wild-type channels. Each of the chimeras, like the parent channels, showed complete inactivation during five second conditioning prepulses.

Figure 23A compares the half-inactivation potentials of the four chimeras to the wild type channels in form of a bar graph. Several observations can be made upon

Figure 22 - Nomenclature and Steady-State Inactivation Properties of S6 chimeras

Transmembrane topology of the chimeric calcium channel S6 constructs indicating the nomenclature used throughout. The chimeras were coexpressed with α_2-δ and β_{1b} subunits and recorded in 20mM Ba^{2+} external and CsMS internal solutions. Mean steady-state inactivation curves and representative current traces (steps to +10 mV from a holding potential of -100 mV) are shown for each construct. Curves were fitted using the Boltzman equation. Error bars are standard errors.

rbC (IIS6E)

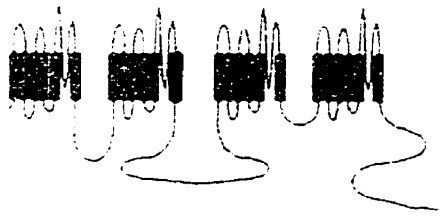

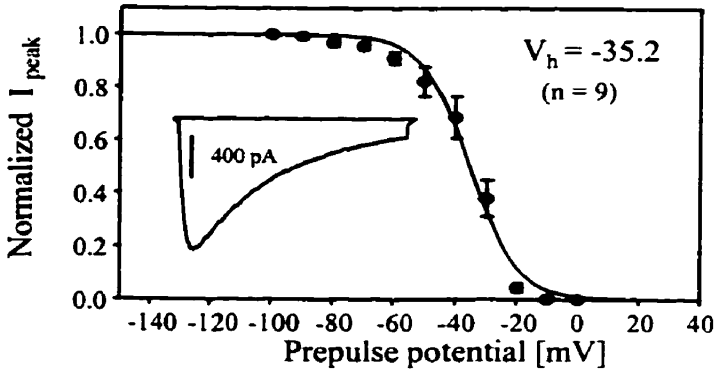

rbC (IIIS6E)

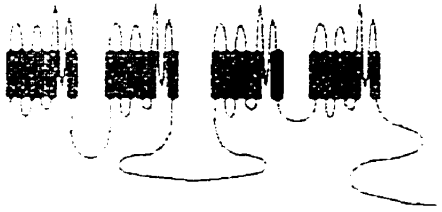

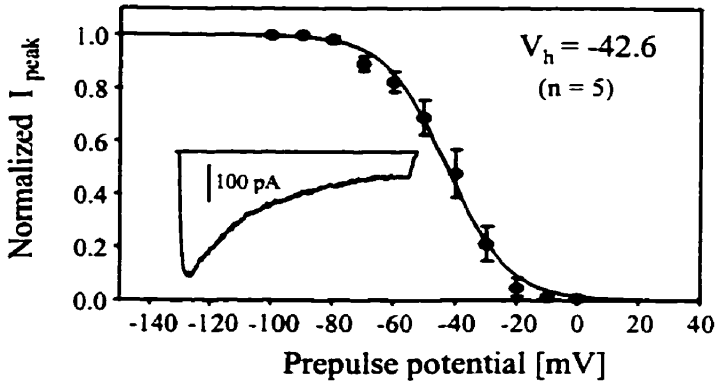

rbE (IIS6C)

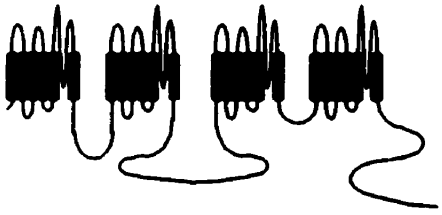

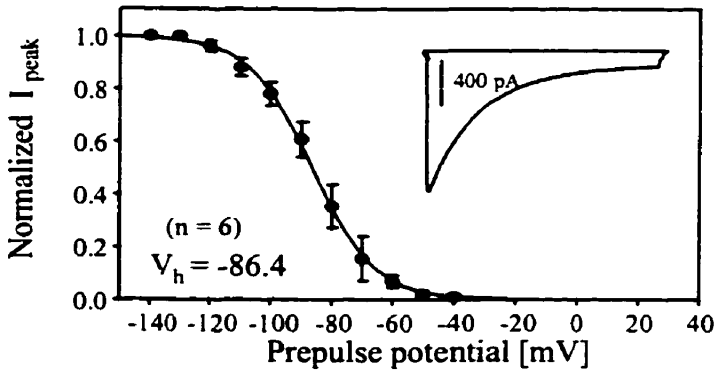

rbE (IIIS6C)

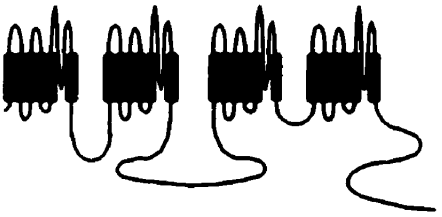

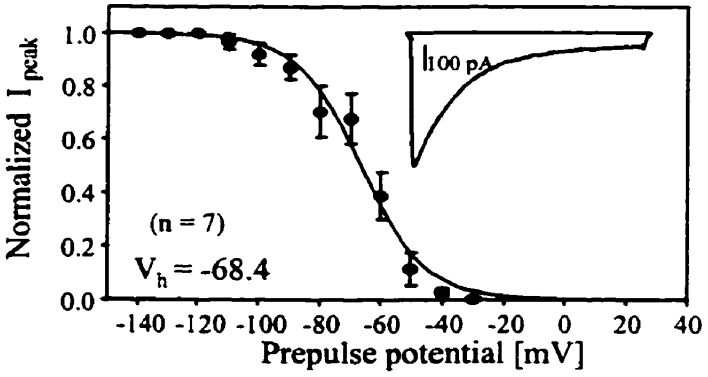

Figure 23 - Steady-State Inactivation of S6 Chimeras

(A) Comparison of half-inactivation potentials for wild-type and chimeric calcium channels. In each case, steady-state inactivation curves from individual curves were fitted separately, and the means and standard errors are plotted. [V_h α_{1E} = -79.5 ± 1.3; rbE (IIS6C) = -86.4 ± 3.2; rbE (IIIS6C) = -68.4 ± 3.8; α_{1C} = -27.5 ± 1.3; rbC (IIS6E) = -35.2 ± 2.3; rbC (IIIS6E) = -42.6 ± 3.2]. An asterisk denotes V_h values which are significantly different than those obtained from α_{1E} ($p < 0.05$), and the number sign denotes V_h values which are significantly different from the ones observed with α_{1C}. Numbers in parentheses indicate numbers of experiments. **(B)** Shifts in V_h produced by the IIS6 and IIIS6 segments in comparison to those caused by the entire transmembrane domains (including the preceding linker region). Note that the values of ΔV_h given for domains II and III from α_{1E} and α_{1C} are average values of ΔV_h for the chimera pairs in Fig. 17B,C. Also recall that recordings of C/E transmembrane domain chimeras used CsCl internal recording solution rather than CsMS.

A

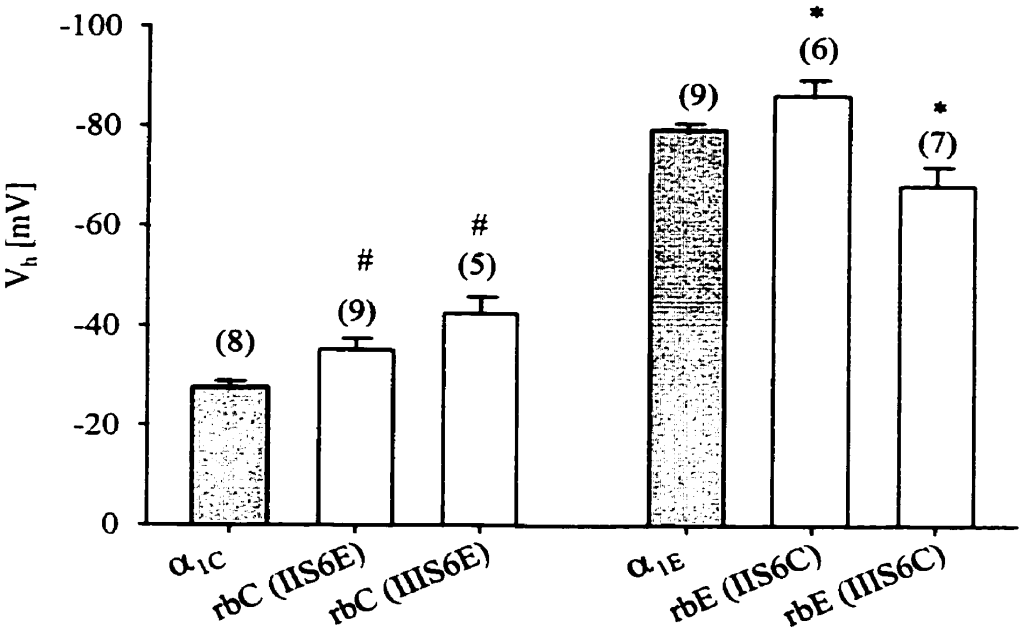
-100
-80
-60
-40
-20
0
V_h [mV]
(8)
#
(9)
#
(5)
(9)
*
(6)
*
(7)
α_{1C}
rbC (IIS6E)
rbC (IIIS6E)
α_{1E}
rbE (IIS6C)
rbE (IIIS6C)

B

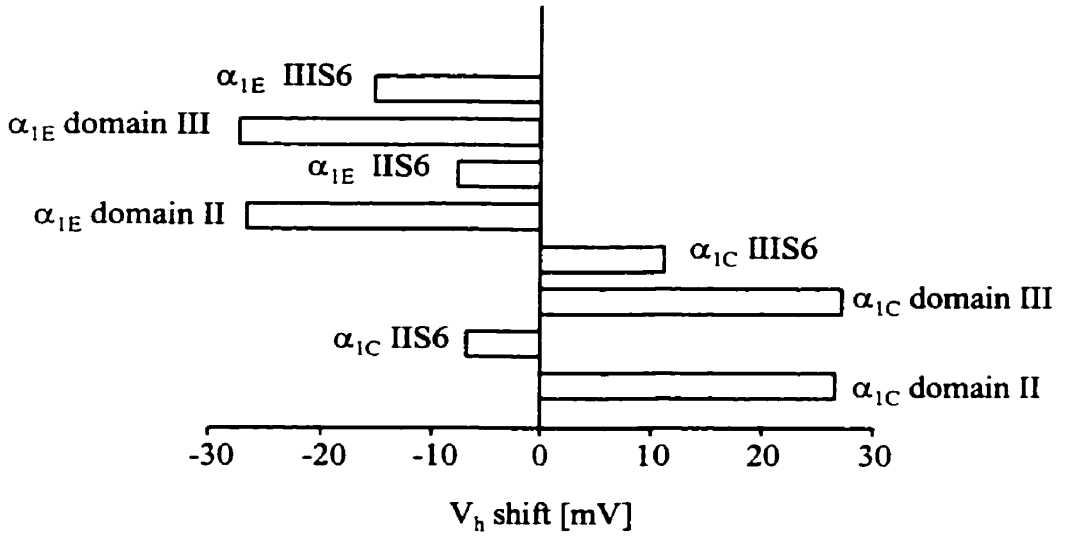
α_{1E} IIIS6
α_{1E} domain III
α_{1E} IIS6
α_{1E} domain II
α_{1C} IIIS6
α_{1C} domain III
α_{1C} IIS6
α_{1C} domain II
-30
-20
-10
0
10
20
30
V_h shift [mV]

examination of this figure. First, each of the four S6 segments (II S6 and III S6 from α_{1E} and α_{1C}) have small, yet significant effects on the steady-state inactivation properties of the parent channels. Segments II S6 and III S6 of the α_{1E} channel similarly shift the half-inactivation potential of α_{1C} in the hyperpolarizing direction by about 10 mV. The hyperpolarizing shifts observed with the S6 segments of α_{1E} are not as prominent as the effects observed after switching entire transmembrane domains (including the preceding cytoplasmic linker) (Fig. 23B), remembering, however, that recordings of transmembrane domain chimeras were done under slightly different conditions. Also shown in Figure 23 are the half-inactivation potentials of rbE (IIS6C) and rbE (IIIS6C). The α_{1C} III S6 segment causes an 11 mV positive shift in half-inactivation potential of α_{1E}, whereas the II S6 α_{1C} segment exerts an opposite effect, causing α_{1E} to inactivate 7 mV more negatively. Again, these shifts are of a smaller magnitude than those observed after complete domain swapping. Thus, although the S6 segments of domains II and III do contribute to the half-inactivation voltage, there are likely other parts of domains II and III which determine the bulk of the steady-state inactivation profile.

The observed shifts in half-inactivation potentials caused by the II S6 and III S6 segments cannot be attributed to underlying shifts in half-activation. Of the four constructs, only rbE (IIS6C) showed any significant difference in half-activation potential in comparison to the wild-type channel, yet the half-inactivation potentials of all four constructs differed significantly from those of the wild-type channels. Furthermore, the ratio of change in half-activation potential to change in half-inactivation potential for the

pair α_{1E} and rbE (IIS6C) had a value of -0.91, indicating that shifts in half-activation and half-inactivation potentials were opposite to each other. These considerations suggest that differences in voltage-dependent activation properties cannot explain the observed changes in half-inactivation potentials of the S6 chimeras.

Role of the II S6 and III S6 Regions in Controlling Inactivation Rate

To determine the role of the II S6 and III S6 segments on the rate of inactivation, the inactivation properties of the wild-type and chimeric channels were compared by using the ratio of peak current levels to residual current level at the end of a 150 ms test depolarization. Figure 24 depicts the percentage of inactivation occurring over 150 ms for three different test pulses (0 mV, +10 mV, and +20 mV). As seen from Figure 24, each of the four chimeric constructs showed α_{1E}-like inactivation rates. Hence, exchange of either the II S6 or III S6 segment from α_{1E} with the corresponding fragment of α_{1C} had no effect on inactivation rate or inactivation kinetics, whereas the insertion of only a single S6 segment of α_{1E} (either domain II or III) was sufficient to confer α_{1E} like inactivation properties onto α_{1C}. This is further demonstrated in Figure 25A, where no difference in inactivation rate between α_{1E}, rbE (IIS6C), and rbE (IIIS6C) in the voltage range from -10 to +30 mV can be observed. These data suggest that, at least individually, the II S6 and III S6 regions of α_{1C} cannot override the inactivation rates of α_{1E}. In contrast to the lack of effect by α_{1C} S6 segments, both the II S6 and III S6 segments of α_{1E} are able to completely confer α_{1E}-like inactivation properties onto the slowly inactivating

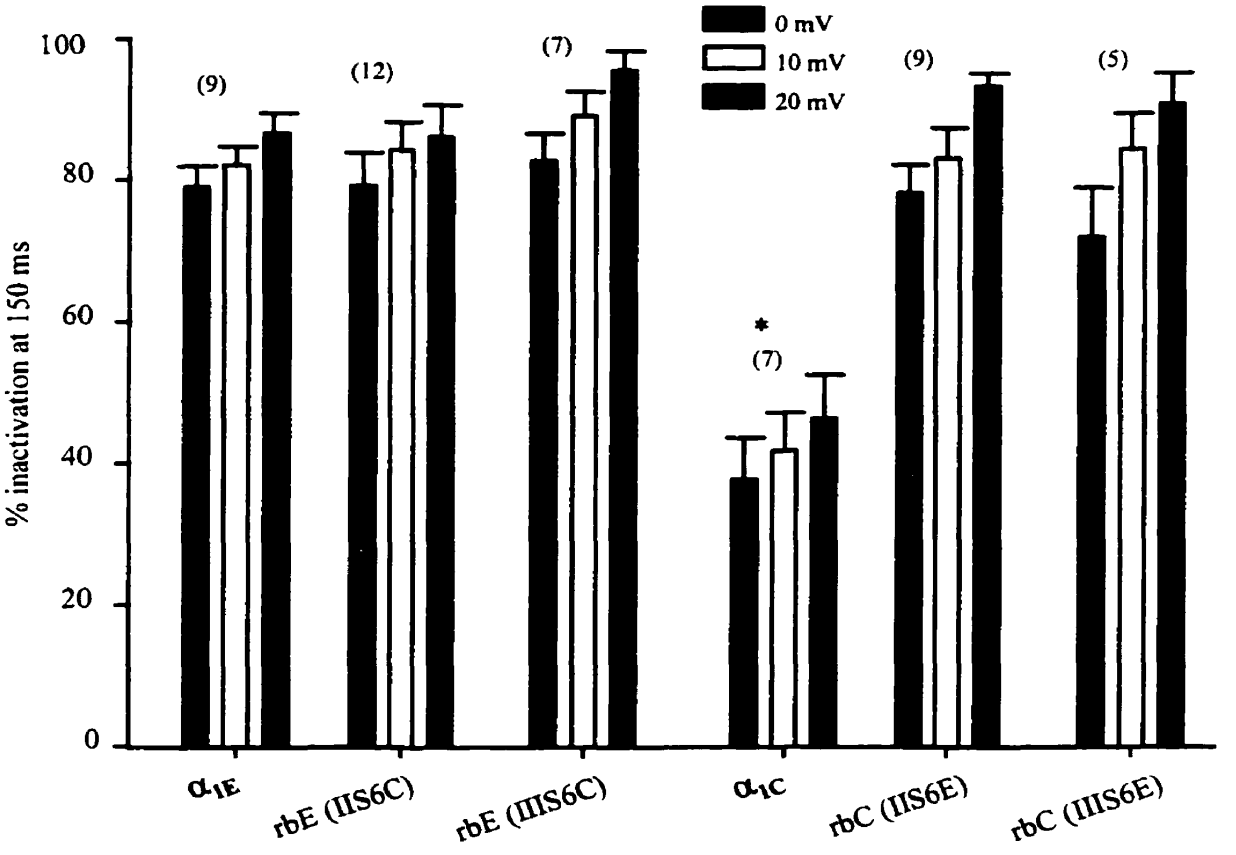

Figure 24 - Inactivation Rates for Wild-Type α_{1E} and α_{1C} Channels and S6 Chimeras

Mean inactivation rates of wild-type and chimeric channels, reflected as the percentage of peak current that has inactivated during 150 ms test pulse, are shown for 3 different test potentials (0 mV, 10 mV, and 20 mV). Error bars denote standard errors, numbers in parentheses denote numbers of experiments. An asterisk denotes inactivation rates (measured at +10 mV) which are significantly different from α_{1E} ($p < 0.05$). Note that α_{1C} constructs containing α_{1E} S6 segments from domain II or III exhibit α_{1E}-like inactivation kinetics.

Figure 25 - Contribution of Domain II and III S6 Segments to Inactivation Rate

(A) Voltage-dependence of inactivation rate of wild-type α_{1E} and α_{1C}, and constructs containing S6 segments from α_{1C} (α_{1C} - closed circles, n = 7; α_{1E} - closed triangles, n = 9; rbE (IIS6C) - closed diamonds, n = 12; rbE (IIIS6C) - closed squares, n = 7). Note that α_{1C} S6 segments from domains II and III do not affect the inactivation rate of α_{1E}. **(B)** Voltage dependence of inactivation rate of wild-type α_{1E} and α_{1C}, and constructs containing S6 segments from α_{1E} (α_{1C} - closed circles, n = 7; α_{1E} - closed triangles, n = 9; rbC (IIS6E) - open diamonds, n = 9; rbC (IIIS6E) - open squares, n = 5). An α_{1E} S6 segment from either domain II or III confers α_{1E}-like inactivation kinetics onto α_{1C} channels. **Inset:** representative whole cell current records illustrating the effects of single S6 segment switches on inactivation rate (step depolarizations to +10 mV from a holding potential of -100 mV). Current traces are scaled to the same peak amplitude to allow for comparison of inactivation rates.

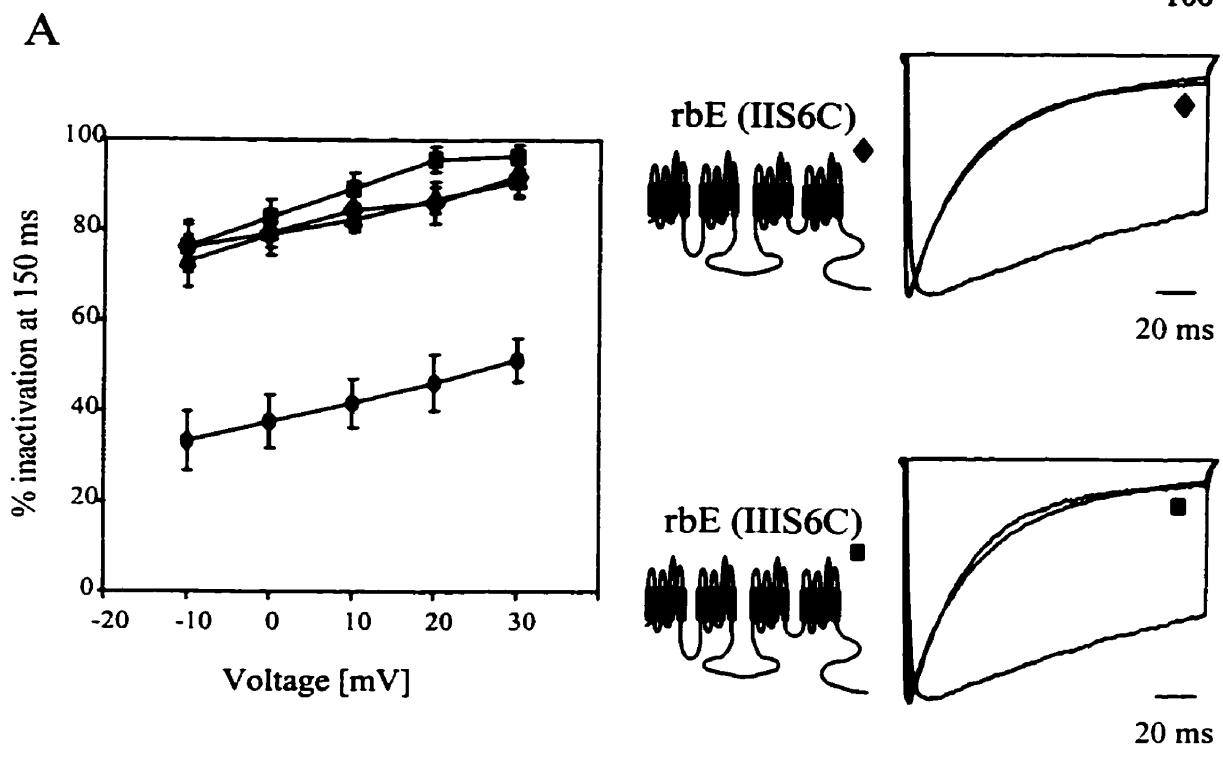
A
% inactivation at 150 ms
100
80
60
40
20
0
-20
-10
0
10
20
30
Voltage [mV]
rbE (IIS6C)
20 ms
rbE (IIIS6C)
20 ms

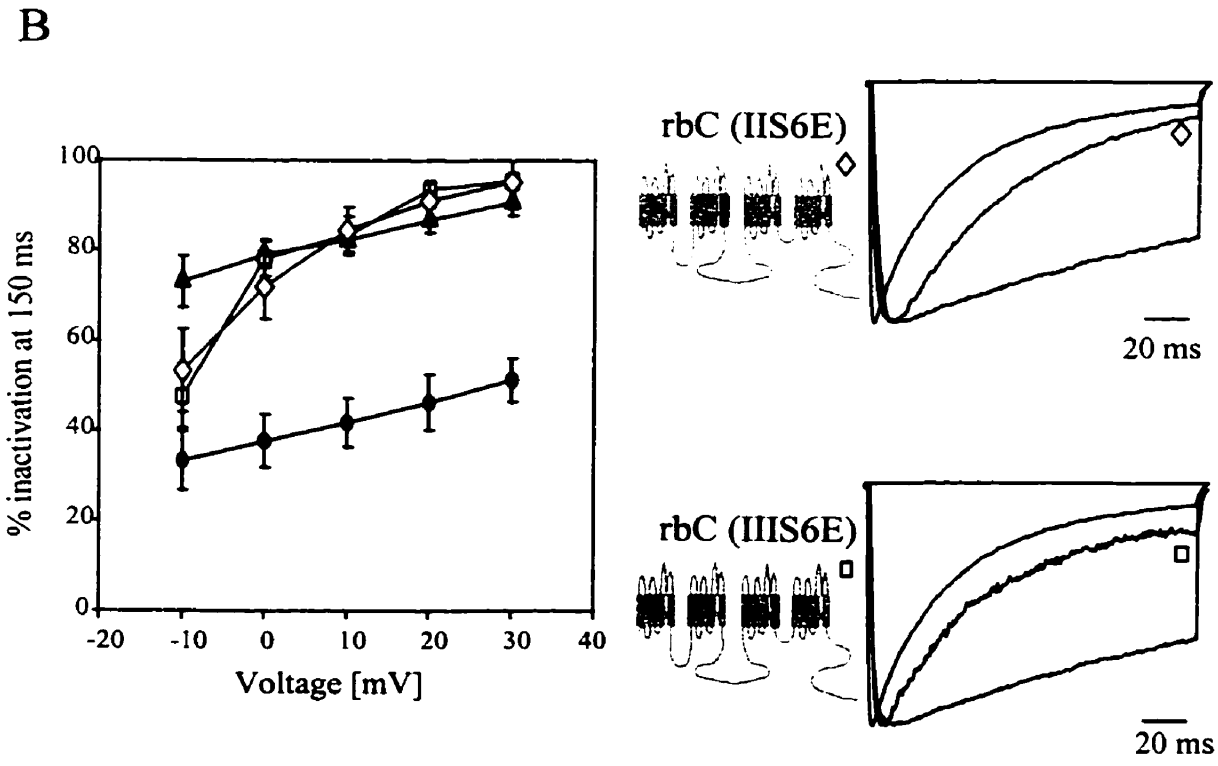
B
% inactivation at 150 ms
100
80
60
40
20
0
-20
-10
0
10
20
30
40
Voltage [mV]
rbC (IIS6E)
20 ms
rbC (IIIS6E)
20 ms

α_{1C} channel for potentials more positive than -10 mV (Fig 24 and Fig 25B). At potentials between 0 mV and 30 mV, there is no significant difference between the inactivation rates of α_{1E}, rbC (IIS6E) and rbC (IIIS6E). Current records of voltage steps to +10 mV show that although the slower activation properties of α_{1C} are retained in these two chimeras, each show similar levels of residual current at the end of the 150 ms test pulse (Fig. 25B). At more negative test potentials however (i.e., -10 mV), the constructs containing the II S6 and III S6 segments of α_{1E} show inactivation rates which fall between the two parent channels (Fig 25B). Overall these data indicate that both the α_{1E} II S6 and III S6 regions are critical mediators of voltage dependent inactivation. The notion that either of these segments alone are able to confer rapid inactivation onto the α_{1C} channel may account for the observation that the corresponding α_{1C} segments are not able to abolish rapid inactivation of the α_{1E} channel. In each of the rbE (IIS6C) and rbE (IIIS6C) constructs, the III S6E and II S6E segments respectively, remain intact, and alone are sufficient to maintain fast inactivation as demonstrated in Figure 25B.

These results are consistent with results obtained with the CECC and CCEC chimeras. Both chimeras showed accelerated inactivation rates in comparison to the α_{1C}, and in fact CCEC did not inactivate with significantly different rates than α_{1E} (Fig. 18 and 19). In contrast, the ECEE chimera (which also includes the I-II linker of α_{1C}) showed very slow α_{1C}-like inactivation properties (Fig. 18). Since the α_{1C} II S6 region by itself does not appear to be able to reduce the inactivation rate of α_{1E}, this observation might

suggest that perhaps the I-II linker and/or areas of domain II other than II S6 may help determine the slow rate of inactivation in the chimera ECEE.

Overall, examination of inactivation properties of the S6 constructs reveals a role for the S6 segments from domains II and III in mediating voltage-dependent inactivation processes. The S6 segments exert small effects on determination of steady-state inactivation properties, but do not contribute in a substantial manner to the differences in steady-state inactivation between rat brain α_{1C} and α_{1E} calcium channels. The II S6 and III S6 segments are however, critical determinants of the rapid inactivation rate in α_{1E} calcium channels, with either segment alone able to maintain rapid inactivation in the α_{1E} channel, or confer rapid inactivation onto the α_{1C} channel.

DISCUSSION

Calcium Channel Inactivation is Fundamentally Different From That of Other Voltage-Dependent Ion Channels

The molecular mechanisms of fast voltage-dependent inactivation of voltage-dependent sodium and potassium channels have been subject to extensive study, and are now well understood. In voltage-dependent sodium channels, fast inactivation appears to be caused by occlusion of the pore by three hydrophobic residues (I,F,M) located in the domain III-IV linker region of the sodium channel α_1 subunit (Vassilev *et. al.*, 1988; 1989; West *et. al.*, 1992; Eaholtz *et. al.*, 1994). Cleavage of the domain III-IV linker region by proteolytic enzymes such as pronase or trypsin abolishes fast inactivation (Armstrong *et. al.*, 1973). In voltage-dependent potassium channels, fast inactivation appears to be mediated by physical occlusion of the pore by a cluster of about 20 amino acids (termed inactivation ball) located either at the N-terminal of the α_1 subunit (Hoshi *et. al.*, 1990; Zagotta *et. al.*, 1990; Demo and Yellen, 1991), or by structural homologs of this ball peptide located on the associated β subunit molecule (Rettig *et. al.*, 1994). Due to the tetrameric structure of these channels, the presence of four identical inactivation particles has been proposed (MacKinnon *et. al.*, 1993). Voltage-dependent calcium channels do not contain analogous structural elements, and no evidence for a pore-blocking mechanism has been presented. Furthermore, unlike with sodium channels, proteolytic enzymes are not able to eliminate voltage-dependent inactivation of calcium

channels, suggesting that calcium channel inactivation is not mediated exclusively by any of the cytoplasmic regions of the channel (but see below). Zhang *et. al.* (1994a) have provided compelling evidence that the differences between the inactivation rates of marine ray α_{1E} and rabbit brain α_{1A} channels can be exclusively located to the domain I S6 region. However, more recently, individual point mutations in the domain I-II linker region (Herlitze *et. al.*, 1996; Bourinet *et. al.*, 1999), and the S6 regions of domains III and IV (Hering *et. al.*, 1996, 1997, 1998) have been shown to attenuate, or abolish voltage-dependent inactivation of α_{1A} calcium channels, perhaps suggesting the possibility that inactivation of neuronal calcium channels might involve a more diffusely located effect.

Here, the roles of each of the four transmembrane domains in voltage-dependent inactivation of α_{1E} channels has been systematically investigated. The chimeric approach was designed to be constructive, i.e., the goal was to confer the inactivation properties from a rapidly inactivating channel onto a relatively non-inactivating one, rather than simply to destroy inactivation. However, while certain aspects of voltage-dependent inactivation of α_{1E} could be conferred onto α_{1C} channels through the insertion of individual domains, the mechanism underlying voltage-dependent inactivation could not be attributed to a single transmembrane domain. Instead, the data indicate that all four transmembrane domains contribute to varying degrees to fast inactivation. The overall half-inactivation potential appeared to be determined through an equilibrium between hyperpolarizing (α_{1E} domains I, II, and III) and depolarizing (α_{1E} domain IV) elements.

Similarly, the differences in inactivation rate between the two wild-type channels appeared to involve predominantly domains II and III with some contribution from domain IV. Thus, consistent with previous suggestions, the molecular mechanisms which mediate fast inactivation of voltage-dependent calcium channels appear to differ fundamentally from those observed with other types of voltage-gated cation channels.

It is important to note that there are limitations in the use of chimeras as a method for studying functional aspects of ion channel physiology. In exchanging primary amino acid sequences between parent channels, it is possible that the global three-dimensional folding of the channel could also become altered. The effect of such changes on channel function and the extent to which they influence the studied property are difficult to isolate. For example, there is the potential for a change in one domain to affect the conformation of the protein such that the contribution of a second domain is altered. This has the potential to obscure the observed relative contributions of individual domains. Despite these considerations, the chimeric approach provides a useful tool in differentiating structural aspects of a particular ion channel function and paves the way for future studies to further isolate specific residues and/or regions responsible for mediating the channel function.

Putative Effects of Differential Activation Properties

In principle, it is possible that some of the differences in half-inactivation potentials observed with the C/E transmembrane chimeric calcium channels might be secondarily due to intrinsic differences in their activation properties. In a case where

inactivation was coupled directly to activation, structural changes that lead to shifts in the voltage-dependence of activation would also induce shifts in voltage-dependence of inactivation. In 20 mM barium, an approximate 10 mV difference in the half-activation potentials of wild-type α_{1E} and α_{1C} channels was observed. In contrast, their difference in alf-inactivation potential was more than four fold larger. Furthermore, with the exception of 2 out of 15 chimera pairs, no correlation between shifts in half-activation and half-inactivation potentials resulting from the switching of individual, or multiple domains was found, suggesting that changes in half-activation potential cannot account for the observed changes in half-inactivation potentials. These factors imply that the effects observed with the transmembrane domain chimeras are indeed due to structural changes in the voltage-dependent inactivation machinery.

The effects of individual domain exchanges on the inactivation rate were examined at the same test potential (+20 mV). Because the rate of inactivation may be coupled to channel activation, any variability in half-activation potential among the chimeras/wild type channels might affect the comparison of inactivation rate measured at a single arbitrary potential. However, this variability in half-activation potential was fairly small (9 of the 11 chimeras activated within the 10 mV window), and thus, given the shallow voltage-dependencies of the inactivation rates, the interpretations are not likely to be affected.

The issue of activation effects contributing to changes in inactivation properties is not as conspicuous with the S6 chimeras. As previously mentioned, three of the four

chimeras showed no difference in activation properties in comparison to the wild type channels, despite their shifts in steady-state inactivation. In the fourth chimera, rbE (IIS6C), which did show significantly different activation properties compared with α_{1E}, the shift in half-activation potential was in the opposite direction as compared to the shift in half-inactivation potential, thus ruling out any possible correlation between half-activation and half-inactivation potential shifts.

Role of Cytoplasmic Constituents in Voltage-Dependent Inactivation

An additional finding of this study was that internal cytoplasmic constituents can modify inactivation properties of calcium channels. The voltage clamp conditions under which the first set of chimeras (C/E transmembrane chimeras) were recorded included a CsCl internal solution. For the S6 chimeras, conditions were changed such that a CsMS internal recording solution was used instead. The new conditions were favorable because they permitted more stable whole-cell recordings of calcium channels. Both Zhang *et. al.* (1994b) and Kay (1992) have reported that cesium-methanesulfonate salts are effective replacements for cesium-chloride salts in whole-cell patch clamping of calcium channels. Use of the CsMS internal pipette solution did not, however, only affect the stability of the recordings. It also altered biophysical channel properties. Dependence of calcium channel properties on internal recording solution composition has been previously demonstrated in a study by Zamponi (1999), where it was shown that CsMS changes the blocking affinity of piperidine for N-type channels. Here, it was observed that the

intracellular recording solution was an important determinant of the inactivation properties of both the wild-type α_{1E} and α_{1C} channels. For both channels, when using the CsMS solution, inactivation rate was accelerated and steady-state inactivation was shifted towards more hyperpolarizing potentials. In contrast, the activation properties were not affected. The differences in inactivation observed under the two conditions may have resulted from one of, or a combination of three factors which differ between the two solutions used. The most apparent difference is the replacement of chloride anions with methanesulfonate ($MeSO_3^-$). Methanesulfonate is inert and does not interact with divalent cations, as compared to chloride, a chaotropic anion, which is very reactive and might interact with the cytoskeleton or the calcium channel itself to reduce inactivation. Alternatively, differential surface charge effects of internal ions could result in changes in the basic gating properties of the channel. This however, seems unlikely since no effects on half-activation potential were observed. In addition to the replacement of chloride ions, the CsMS solution lacks TEACl (although the pH of CsMS is still adjusted with TEAOH, so TEA is not completely eliminated), and contains an additional 4 mM Mg^{2+}. So it is also possible that the differences in TEA and/or Mg^{2+} concentration could be the factors which modulate the inactivation properties of the channels. Magnesium ions are known to modulate the functions of a number of other ion channels, including NMDA receptors (Burnashev *et. al.*, 1992; Mori *et. al.*, 1992) and inward rectifier potassium channels. Overall, the notion that cytoplasmic constituents are able to affect voltage-dependent inactivation may suggest that regions of the channels accessible to the

cytoplasmic aqueous solution may participate in the inactivation processes. Any putative action of intracellular ions within the inner vestibule of the pore would be consistent with the inactivation hypothesis outlined below if the inner vestibule were involved in the inactivation process.

Influence of Ancillary Subunits on Observed Transmembrane Contributions

In theory, it is possible that the observed contributions of each of the four transmembrane domains to the inactivation process might be influenced by unique interactions of ancillary subunits with the two wild type α_{1E} and α_{1C} channels. The β subunit, specifically, has pronounced effects on the inactivation properties of calcium channels (see introduction). It binds at a site in the I-II linker that is highly conserved amongst all the high voltage activated calcium channels (Pragnell *et. al.*, 1994). Despite the conserved binding motif, it is possible that the β subunit induces distinct conformational changes for each of the HVA channels which may, in part, influence the inactivation properties of the channels. If the is the case, then the transfer of individual domains between α_{1E} and α_{1C} could alter the conformational changes produced by the bound β subunit. Therefore, the observed inactivation properties could be dependent on the β subunit interaction with specific transmembrane domains, rather than the transmembrane domains themselves evoking the effect.

It is also possible that the β subunit might have other minor interaction sites along the calcium channel α_1 subunit which are important in determining its modulatory

actions. With the combination of different transmembrane domains, it is possible that the β subunit might be prevented from accessing other interaction domains, and therefore the influence of the β subunit could alter the apparent contribution of a specific transmembrane domain.

Theoretically, similar effects could be conferred by α_2-δ, however little evidence exists to suggest that this subunit plays a significant role in inactivation of calcium channels. Nonetheless, because little is known about the actual interaction between α_2-δ and the α_1 subunit, the influence of this subunit on calcium channel inactivation cannot be ruled out.

For the present set of experiments, we attempted to control for the interaction of the ancillary subunits by using the same accessory subunits in all recordings (β_{1b} and α_2-δ). Further experiments could be performed using different β subunits or no β subunit to examine whether the relative contribution of transmembrane domains is dependent on the β subunit interaction. Studying calcium channel inactivation in the absence of ancillary subunits would be difficult however, as it is unlikely that expression levels of the wild type and chimeric calcium channels would allow for these experiments to be carried out.

Comparison with Previous Work

At first glance, the results presented here appear to contradict those of Zhang *et. al.* (1994a) who have provided the only other systematic examination of calcium channel

inactivation. Zhang *et. al.* (1994a) reported that the differences in inactivation between the rapidly inactivating marine ray doe-I channel (α_{1E}) and the more slowly inactivating rabbit brain α_{1A} channel could be exclusively attributed to the domain I S6 segment. In the present study the role of the entire domain I was examined (as well as the amino terminal portion of the channel which is connected to domain I), and it was found that that domain I had a moderate impact on the steady-state inactivation of calcium channels, but played no role in the inactivation rate. In contemplating the contradictions between these two studies, two issues must be taken into consideration. First, wild-type α_{1E} and α_{1C} channels used in the present study exhibit much more pronounced differences in inactivation rate and half-inactivation potential compared to the channels used by Zhang *et. al.* to create their chimeras. α_{1E} and α_{1A} are phylogenetically much more closely related (54 - 64% identity) than the α_{1E} and α_{1C} channels which show only about 40% identity (de Waard *et. al.*, 1996). Thus, it is possible that both parent channels may carry similar "inactivation" motifs in domains II, III and IV, but differ predominantly in domain I. In the present study, due to the lower degree of overall identity between α_{1E} and α_{1C} channels, the regions critical for inactivation might perhaps be more divergent, thus revealing the contributions of additional domains to the overall inactivation process. A second fundamental difference between the present study and that of Zhang *et. al.* (1994a) lies in the type of transient expression system used, with Zhang *et. al.* using *Xenopus* oocytes as compared with the HEK cells which were used in this study. It is well established that the type of host system frequently affects the functional and

pharmacological properties of transiently expressed ion channels (e.g., Zamponi, 1999), and it will be interesting to examine the properties of the C/E chimeras and S6 chimeras in *Xenopus* oocytes. Lastly, the data from this study do support some contribution of domain I to the overall inactivation properties, as substitution of α_{1C} sequence in domain I with that corresponding to α_{1E} mediated a 10 mV to 15 mV negative shift in half-inactivation potential.

Many groups have pinpointed the domain I-II linker, as well as individual amino acid residues in the I-II linker, as critical determinants of voltage-dependent inactivation. An alternative splice variant of the rat brain α_{1A} channel which carries a single valine insertion in the I-II linker completely lacks voltage-dependent inactivation (Bourinet *et. al.*, 1999). Herlitze *et. al.* (1997) identified a single amino acid residue (arginine) in the domain I-II linker of α_{1A} which can confer positive inactivation properties onto L-type calcium channels. Chimeras containing transferred I-II linkers of α_{1B} or α_{1A} onto α_{1E}, and one containing a transferred I-II linker from α_{1S} onto α_{1C} all showed slower inactivation rates than the parent channels (Adams and Tanabe, 1997; Page *et. al.*, 1997). Also, acceleration of inactivation was demonstrated in a study in which the I-II linkers of α_{1A} and α_{1C} were overexpressed (Cens *et. al.*, 1999), but this may have been due to a quenching of the available ancillary β subunits which are known to bind to this region of the channel and are critical modulators of inactivation properties. In the present study, the domain I-II linker was always associated with domain II in the C/E transmembrane chimeras. Thus, although Zhang *et. al.* (1994a) showed that exchanging the I-II linker

region between doe-I and α_{1A} channels did not affect inactivation rate, it cannot be ruled out that the effects which are attributed to "domain II" may be contained, in part, in the domain I-II linker rather than the actual domain II region *per se*. The actions of the I-II linker could explain why the transfer of α_{1C} sequence from domain II (including the I-II linker) onto the α_{1E} channel (ECEE chimera) is able to virtually eliminate fast inactivation, yet transfer of just the II S6 segment of α_{1C} onto α_{1E} has no effect on inactivation rate. Given the substantial evidence showing that the I-II linker is an important determinant of inactivation in calcium channels, it seems likely that the I-II linker, at least in part, may be the structure responsible for slowing inactivation in the ECEE chimera. Ultimately, swapping of the I-II linker alone will be required to establish its role in determining inactivation of α_{1E} and α_{1C} channels. The same consideration applies in principle to domain III which is associated with the II-III linker, and to domain IV which is associated with the III-IV linker and the carboxyl terminal region. No evidence has been presented to date to implicate either the II-III linker or the III-IV linker in voltage-dependent inactivation of calcium channels, however swapping of the individual cytoplasmic linker regions would be required to rule out any contribution by these regions to the effects which have been attributed to domains III and IV in this study.

One of the surprising findings of this study is the role of domain IV in governing inactivation properties. Interestingly, the insertion of the domain IV sequence of the rapidly inactivating α_{1E} did not result in a transfer of the faster α_{1E}-type kinetics onto the slowly inactivating α_{1C}. Unexpectedly, the sequence substitution slowed the inactivation

kinetics compared to that of α_{1C}, and resulted in a positive shift in steady-state inactivation. Conversely, upon replacement of the α_{1E} domain IV with the corresponding α_{1C} sequence, acceleration of inactivation rate and a negative shift in steady-state inactivation was observed. This finding suggests that inactivation properties are determined through a balance between structures which accelerate inactivation and structures which slow inactivation, or through an equilibrium between hyperpolarizing and depolarizing elements, as is the case with steady-state inactivation. Doring *et. al.* (1996) also observed that regions of domain IV had antagonistic effects on the rate of inactivation in α_{1A} and L-type α_{1S} calcium channels. In their study, an α_{1A} construct containing the IV S6 segment of α_{1S}, did not result in the transfer of the faster α_{1A}-like inactivation kinetics, but instead resulted in a decreased inactivation rate. Thus, it appears that an antagonistic role for domain IV could be a universal feature of calcium channels, and is not just confined to the α_{1E} and α_{1C} channels. These findings give examples where kinetic properties of calcium channels are not simply conferred by swapping sequences from different α_1 subunits. The conclusions of the study by Doring *et. al.* (1996) as well as studies by Hering *et. al.* (1996), and Yatani *et. al.* (1994) which implicate the IV S6 segment and the pore-forming regions of domain IV, suggest that the effects of "domain IV" in the current study might be ascribed specifically to the IV S6 segment, although involvement of the carboxyl terminal, III-IV linker and other parts of domain IV cannot be ruled out. Additional S6 chimeras with exchanged IV S6 segments would be necessary to prove this.

As stated earlier, no other studies have shown any involvement of the domain II S6 segment in governing calcium channel inactivation, so the findings here that the II S6 segment from α_{1E} can confer rapid inactivation kinetics onto the α_{1C} channel are entirely novel. On the other hand, three studies have demonstrated that the III S6 segment (at least in α_{1A} and α_{1C}) is involved in inactivation. The observation that the III S6 region of α_{1E} mediates fast inactivation is consistent with the findings of Tang *et. al.* (1993), Hockerman *et. al.* (1997), and Hering *et. al.* (1997), all of which implicated amino acids within the III S6 segment, or parts of the III S6 segment in inactivation. In addition to the S6 segments themselves from domain III, the pore-forming regions attached to III S6 are also important factors for calcium channel inactivation (Yatani *et. al.*, 1994), and so it would be of interest to investigate how these regions are involved in the different inactivation rates of α_{1E} and α_{1C}.

What Might Be the Molecular Mechanism of Fast Calcium Channel Inactivation?

The observation that each of the four transmembrane domains appeared to affect voltage-dependent inactivation suggested that calcium channel inactivation might involve a complex global conformational change in the channel protein. Most of the structures or amino acid residues which have been linked to changes in voltage-dependent inactivation of various types of calcium channels have so far been located to the S6 regions of domains I, III and IV (Tang *et. al.*, 1993; Yatani *et. al.*, 1994b; Zhang *et. al.*, 1994a; Doring *et. al.*, 1996; Hering *et. al.*, 1996; 1997; Hockerman *et. al.*, 1997; Hering *et. al.*,

1998), or to cytoplasmic regions directly linked to these S6 segments such as the domain I-II linker or the carboxyl terminal region (Herltize *et. al.*, 1996; Adams and Tanabe, 1997; Page *et. al.*, 1997; Soldatov *et. al.*, 1997; Bernatchez *et. al.*, 1998; Soldatov *et. al.*, 1998; Bourinet *et. al.*, 1999; Cens *et. al.*, 1999). In addition, cytoplasmic proteins such as ancillary β subunits and syntaxin which physically bind to the domain I-II linker (Pragnell *et. al.*, 1994) and II-III linker regions, respectively, have been shown to affect voltage-dependent inactivation properties. In view of the current understanding of the slower C-type inactivation process in certain types of voltage-dependent potassium channels (Yellen *et. al.*, 1994; Ogielska *et. al.*, 1995; Panyi *et. al.*, 1995; Liu *et. al.*, 1996; Durrell *et. al.*, 1998; Holmgren *et. al.*, 1998;), it is tempting to speculate that voltage-dependent inactivation of calcium channels could perhaps involve a physical constriction of the pore via a mechanism similar to that which mediates C-type inactivation of potassium channels. C-type inactivation depends strongly on residues located in the channel pore and in the extracellular mouth of the channel; regions which correspond particularly to the S6 segments of each of the four subunits that form the potassium channel. The hypothesis that calcium channel inactivation could resemble C-type inactivation was therefore investigated by the creation and electrophysiological examination of an additional set of chimeras which examined the role of the S6 segments of domains II and III in channel inactivation. The S6 segments of domains II and III were considered suitable candidates to test because these two domains mediated the most significant changes in the rates of inactivation and in half-inactivation potential among

the C/E transmembrane domain chimeras. Previous studies have already indicated that the III S6 segment mediates some role in voltage-dependent inactivation. Alanine substitutions in the III S6 region of both α_{1A} and α_{1C} channels altered inactivation rate and also affected steady-state inactivation, and transfer of part of the III S6 segment of α_{1A} onto α_{1C} has been shown to cause a speeding of inactivation (Yatani *et. al.*, 1994; Hering *et. al.*, 1997; Hockerman *et. al..*, 1997). There has been no evidence to date however, demonstrating any involvement of the II S6 segment in governing inactivation properties.

The chimeric approach was once again designed to be constructive, so that the goal was both to confer the inactivation properties of α_{1E} onto α_{1C}, and vice versa through transfer of either the II S6 or III S6 segments. Rapid inactivation kinetics of α_{1E} were conferred onto the α_{1C} channel through transfer of either the α_{1E} II S6 or III S6 segment, however, transfer of the S6 segment from domains II or III of α_{1C} had no significant effect on the inactivation rate of α_{1E}. Nonetheless, these results imply that the S6 segments of domain II and III are important determinants of fast inactivation kinetics. That either of the α_{1E} domain II or III S6 segments are alone able to confer rapid inactivation onto the α_{1C} channel could account for the observation that the corresponding α_{1C} segments are not able to abolish rapid inactivation of the α_{1E} channel. In the rbE-II constructs which contain α_{1C} S6 segments of domain II, compensation by the α_{1E} domain III S6 segment allows rapid inactivation kinetics to be maintained. Similarly, in constructs in which α_{1E} III S6 is replaced by the corresponding α_{1C} sequence, the α_{1E} domain II S6 region would be sufficient to maintain the rapid inactivation kinetics.

Preliminary observations from a new construct in which the α_{1E} S6 segments of domains II and III were simultaneously replaced with α_{1C} sequence show that this double chimera yields a channel with inactivation rates that are similar to the wild-type α_{1E} channel. That both the II S6 and III S6 segment from α_{1C} together are not able to eliminate the fast inactivation kinetics of α_{1E} suggests that perhaps there are additional regions of the channel which may contribute in some form to the overall rate of inactivation. Clearly, for calcium channels, conferring fast inactivation kinetics is much more readily accomplished than the destruction of fast inactivation properties. Nonetheless, these preliminary results do not rule out the possibility that the S6 segments (at least of the α_{1C} channel) may be cooperatively responsible for determining the inactivation phenotype of the channel, and that several non-inactivating structures are necessary to override the structures which mediate fast inactivation.

While the S6 segments do seem to play a role in determining inactivation rate they do not contribute extensively to determining the half-inactivation potential. Although each of the four chimeras exhibited significant shifts of steady-state inactivation in comparison to the wild-type channels, these shifts were small (7-15 mV) compared with the 52 mV difference in half-inactivation potentials between α_{1E} and α_{1C} channels. Interestingly, the apparent coupling of steady-state inactivation properties with inactivation rate, which was seen with all the C/E transmembrane domain chimeras (i.e., more negative half-inactivation potentials were accompanied by fast inactivation rates),

was not evident in the S6 chimeras. The rbC (IIS6E) and rbC (IIIS6E) chimeras both displayed α_{1C}-like steady-state inactivation, and yet exhibited α_{1E}-like inactivation rates.

Although the determinants of steady-state inactivation were not assigned to any one delimited region of the calcium channel α_1 subunit, the combined results of both sets of chimeras suggest that all four domains play a role in the process. The primary determinants of steady-state inactivation could be localized to regions other than the S6 segments of domains II and III, as well as domains I and IV, which were also shown to have smaller effects on steady-state inactivation. Further experiments will be required to determine the exact structures which set the half-inactivation potential.

A Model for Calcium Channel Voltage-Dependent Inactivation

Overall, the data presented here, and the collective evidence of previous studies that have given insight into the calcium channel structures which govern inactivation, suggest that calcium channel inactivation might occur via a mechanism which is consistent with C-type inactivation of potassium channels. That all four domains contribute to inactivation, and that the S6 segments (particularly in domains II and III) play a critical role suggests a possible conformational change throughout the protein which leads to a constriction of the pore to inactivate the channel. A key role for residues in S6 segments, that are localized to the inner mouth of the pore, in inactivation gating of calcium channels is supported by recently available crystal structure of the KcsA potassium channel (Doyle *et. al.*, 1998). Crystallization of the channel shows that both

membrane spanning segments are α-helices, with a peripheral and an inner helix that run almost parallel through the membrane. The inner helix corresponds to the S6 segment in the *Shaker* potassium channels and forms the lining of the inner part of the pore. The pore-forming S6 segments in potassium channels are packed against each other near the intracellular mouth of the channel pore to form an inverted teepee structure, which is widely separated near the outer membrane surface and converges toward a narrow zone near the inner surface. Doyle *et. al.* point out that sequence conservation among potassium channels is strongest for the amino corresponding to the pore region and the pore-lining S6 segments, and that sodium and calcium channels also show high levels of relatedness over these segments. It is suggested that the teepee-like architecture of the potassium channel is likely a feature of all P-loop cation channels (Moczydlowski, 1998), with four inner helices (corresponding to the S6 segments) arranged like poles of a teepee to enclose the pore region of the channel. During calcium channel inactivation the cytoplasmic and/or extracellular ends of the S6 segments might come together by voltage-induced conformational changes to constrict the pore, thereby preventing the passage of permeant ions through the permeation pathway (Fig. 26). Such a mechanism could account for the previously reported mutagenesis data in the both the S6 regions and the associated linker regions. For example, the structural changes in the linker regions might affect the mobility or flexibility of the associated S6 regions, and thus the overall inactivation properties. Furthermore, in such a model, one would expect to observe some contribution from each transmembrane domain and from the pore-lining S6 regions as

Figure 26 - Proposed Mechanism of Calcium Channel Inactivation

(A) Cartoon showing the possible arrangement of the six transmembrane segments from three of the major transmembrane domains of a calcium channel. S6 segments (black and white checkered cylinder) are proposed to line the pore of the calcium channel. **(B)** Extracellular view of the calcium channel S6 segments from each domains. The S6 segments are packed against each other near the intracellular mouth of the channel pore in an inverted teepee structure (Doyle, *et. al.*, 1998). *i.* In the open state the S6 segments are arranged such that calcium is able to permeate the channel. A calcium ion is shown in the vestibule of the channel (black circle). *ii.* During inactivation, a constriction of the pore brings the S6 segments brings closer together, thereby preventing calcium permeation. Note that the present set of data does not distinguish between closure of the extracellular or intracellular mouth of the pore during inactivation. The mechanism shown here is one of two possibilities.

A

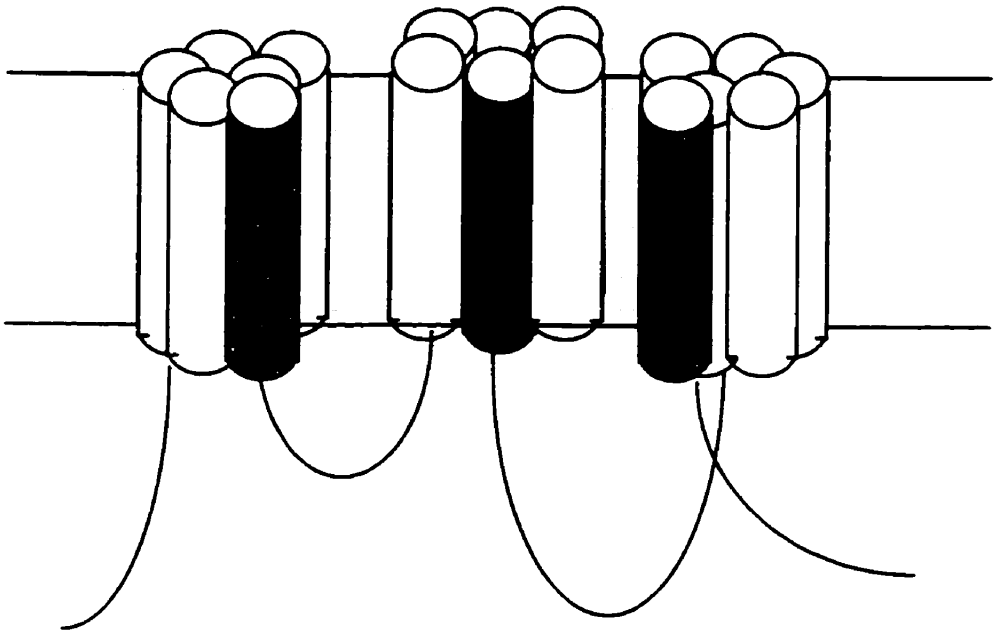

B

i

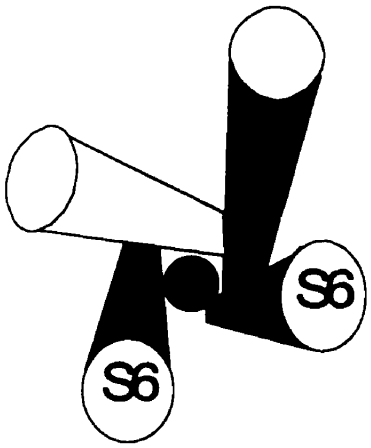

ii

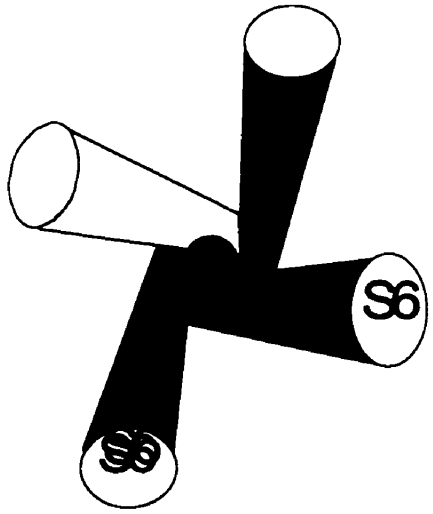

reported here. Hence, a mechanism similar to that proposed to underlie C-type inactivation of potassium channels is an attractive possibility for fast voltage-dependent inactivation of calcium channels. While C-type inactivation has been shown to be mediated through movement of the extracellular regions of the S6 segments, the present data does not distinguish which specific regions of the S6 segments mediate inactivation in calcium channels. Further experiments, using site-directed mutagenesis of specific amino acid residues, will be needed to answer this question.

Calcium Channel Inactivation: Modification of a Common Mechanism

It is not altogether surprising to find that ion channels inactivate by common mechanisms. Fast inactivation of sodium channels and potassium channels similarly occur via intracellular block of the pore by an inactivation particle. Perhaps a second fundamentally different mechanism of inactivation also evolved early on in ion channel evolution. C-type inactivation is best characterized in potassium channels, where in most cases it is a slower form of inactivation than N-type "ball and chain" inactivation. Constriction of the pore, mediated by S6 segments, is also encountered in sodium channels where it also causes a slow form of inactivation (Balser *et. al.*, 1996; Wang and Wang, 1997). It is not inconceivable that a similar mechanism also exists in calcium channels to bring about inactivation. In this case though, it is modified to occur on a much faster time scale than is observed with sodium and potassium channels.

Future Directions

Future experiments will be needed to further elucidate the exact mechanisms of calcium channel voltage-dependent inactivation. Chimeras containing exchanged IV S6 segments should be examined to determine whether this region plays a role in inactivation, and whether its role is antagonistic as the C/E transmembrane domain chimeras would predict. As mentioned earlier, the construct which contains both the II S6 and III S6 segments of α_{1C} on the α_{1E} channel will be an important construct to examine in further detail. Another important experiment will be to look at the role of the I-II linker in isolation, and also in combination with the S6 segments to try and confer the voltage-dependent inactivation properties of α_{1C} onto α_{1E}. Ultimately, single point mutations by site-directed mutagenesis may be used to pinpoint the critical residues in the S6 segments that participate in and mediate constriction of the pore leading to inactivation.

FOOTNOTE

Parts of this study have been published in The Journal of Biological Chemistry in a paper entitled "*Multiple Structural Domains Contribute to Voltage-dependent Inactivation of Rat Brain* α_{1E} *Calcium Channels*" by Renée Spaetgens and Gerald Zamponi. (Volume 274, No. 32, August 6, 1999; 22428-22436)

REFERENCES

Adams B, Tanabe T (1997) Structural regions of the cardiac calcium channel α_{1C} subunit involved in calcium-dependent inactivation. J Gen Physiol 110: 379-389.

Armstrong CM, Bezanilla F, Rojas E (1973) Destruction of sodium conductance inactivation in squid axons perfused with pronase. J Gen Physiol 62: 375-391.

Balser JR, Nuss HB, Chiamvimonvat N, Perez-Garcia MT, Marban E, Tomaselli GF (1996) External pore residue mediates slow inactivation in MU-I rat skeletal muscle sodium channels. J Physiol (Lond) 494: 431-442.

Bean BP (1991) Pharmacology of calcium channels in cardiac muscle, vascular muscle, and neurons. Am J Hypertens 4: 406S-411S.

Bech-Hansen NT, Naylor MJ, Maybaum TA, Pearce WG, Koop B, Fishman GA, Mets M, Musarella MA, Boycott KM (1998) Loss-of-function mutations in a calcium-channel alpha 1-subunit gene in Xp11.23 cause incomplete X-linked congenital stationary night blindness. Nat Genet 19: 264-7.

Bernatchez G, Talwar D, Parent L (1998) Mutations in the EF-hand motif impair the inactivation of barium currents of the cardiac α_{1C} channel. Biophys J 75: 1727-1739.

Birnbaumer L, Campbell KP, Catterall WA, Harpold MM, Hofmann F, Horne WA, Mori Y, Schwartz A, Snutch TP, Tanabe T (1994) The naming of voltage-dependent calcium channels. Neuron 13: 505-506.

Bourinet E, Soong TW, Sutton K, Slaymaker S, Mathews E, Monteil A, Zamponi GW, Nargeot J, Snutch TP (1999) Phenotypic variants of P-and Q-type calcium channels are generated by alternative splicing of the α_{1A} subunit gene. Nat Neurosci 2: 1-9.

Branchaw JL, Banks MI, Jackson MB (1997) Calcium- and voltage-dependent inactivation of calcium channels in nerve terminals of the neurohypophysis. J Neurosci 17: 5772-5781.

Brice NL, Berrow NS, Campbell V, Page KM, Brickley K, Tedder I, Dolphin AC (1997) Importance of the different β subunits in the membrane expression of the alpha1A and alpha2 calcium channel subunits: studies using a depolarization sensitive alpha1A antibody. Eur J Neurosci 9: 749-759.

Burnashev N, Schoepfer R, Monyer H, Ruppersberg JP, Gunther W, Seeburg PH, Sakmann B (1992) Control by asparagine residues of calcium permeability and magnesium blockade in the NMDA receptor. Science 257: 1415-1419.

Catterall WA (1988) Structure and function of voltage-sensitive ion channels. Science 242: 50-61.

Catterall WA (1991) Excitation-contraction coupling in vertebrate skeletal muscle: A tale of two calcium channels. Cell 64: 871-874.

Catterall WA, Striessnig J (1992) Receptor sites for calcium channel antagonists. Trends Pharm Sci 13: 256-262.

Cens T, Restituito S, Galas S, Charnet P (1999) Voltage and calcium use the same molecular determinants to inactivate calcium channels. J Biol Chem 274: 5483-5490.

Chein AJ, Gao T, Perez-Reyes E, Hosey MM (1998) Membrane targeting of L-type calcium channels. Role of palmitoylation in the subcellular localization of the β_{2a} subunit. J Biol Chem 273: 23590-23597.

Choi DW (1988) Calcium-mediated neurotoxicity: relationship to specific channel types and role in ischemic damage. Trends Neurosci 11: 465-469.

Choi KL, Aldrich RW, Yellen G (1991) Tetraethylammonium blockade distinguishes two inactivation mechanisms in voltage-activated potassium channels. Proc Natl Acad Sci USA 88: 5092-5095.

Cribbs LL, Lee JH, Yang J, Satin J, Zhang Y, Daud A, Barclay J, Williamson MP, Fox M, Rees M, Perez-Reyes E (1998) Cloning and characterization of alpha1H from human heart, a member of the T-type calcium channel gene family. Circ Res 83: 103-109.

De Jongh KS, Warner C, Catterall WA (1990) Subunits of purified calcium channels. J Biol Chem 265: 14738-14741.

de Leon M, Wang Y, Jones L, Perez-Reyes E, Wei X, Soong TW, Snutch TP, Yue DT (1995) Essential calcium-binding motif for calcium-sensitive inactivation of the L-type calcium channels. Science 270: 1502 - 1506.

Demo SD, Yellen G (1991) The inactivation gate of the *Shaker* potassium channel behaves like an open-channel blocker. Neuron 7: 743-753.

De Waard M, Campbell KP (1995) Subunit regulation of the neuronal alpha-1A calcium channel. J Physiol 485: 619-634.

De Waard M, Gurnett CA, Campbell KP (1996) Structural and functional diversity of voltage-activated calcium channels. Ion Channels. 4: 41-87.

De Waard M, Liu H, Walker D, Scott VE, Gurnett CA, Campbell KP (1997) Direct binding of G-protein βγ complex to voltage-dependent calcium channels. Nature 385: 446-450.

Doring F, Degtiar VE, Grabner M, Striessnig J, Hering S, Glossmann H (1996) Transfer of L-type calcium channel IVS6 segment increases phenylalkylamine sensitivity of α_{1A}. J Biol Chem 271: 11745-11749.

Doyle DA, Morais J, Pfuetzner RA, Kuo A, Gulbis JM, Cohen Sl, Chait BT, MacKinnon R (1998) The structure of the potassium channel: Molecular basis of potassium conduction and selectivity. Science 280; 69-77.

Dubel SJ, Starr TV, Hell J, Ahlijanian MK, Enyeart JJ, Catterall WA, Snutch TP (1992) Molecular cloning of the alpha-1 subunit of an omega-conotoxin-sensitive calcium channel. Proc Natl Acad Sci USA 89: 5058-5062.

Durrell SR, Hao Y, Guy HR (1998) Structural models of the transmembrane region of voltage-gated and other K^+ channels in open, closed, and inactivated conformations. J Struct Biol 73: 157-167.

Eaholtz G, Scheuer T, Catterall WA (1994) Restoration of inactivation and block of open sodium channels by an inactivation gate peptide. Neuron 12(5): 1041-1048.

Eberst R, Dai SP, Klugbauer N, Hofmann F (1997) Identification and functional characterization of a calcium channel gamma subunit. Pflugers Arch 433: 633-637.

Ellinor PT, Zhang JF, Randall AD, Zhou M, Schwartz TL, Tsien RW (1993) Functional expression of a rapidly inactivating neuronal calcium channel. Nature 363: 455-458.

Ellinor PT, Yang J, Sather WA, Zhang JF, Tsien RW (1995) Calcium channel selectivity at a single locus for high-affinity calcium interactions. Neuron 15: 1121-1132.

Ellis SB, Williams ME, Ways NR, Brenner R, Sharp AH, Leung AT, Campbell KP, McKenna E, Koch WJ, Hui A, Schwartz A, Harpold MM (1988) Sequence and expression and mRNA's encoding the alpha1 and alpha2 subunits of a DHP sensitive calcium channel. Science 241: 1661-1664.

Felix R, Gurnett CA, De Waard M, Campbell KP (1997) Dissection of functional domains of the voltage-dependent calcium channel α_2-δ subunit. J Neurosci 17: 6884-6891.

Forsythe ID, Tsujimoto T, Barnes-Davies M, Cuttle MF, Takahashi T (1998) Inactivation of presynaptic calcium current contributes to synaptic depression at a fast central synapse. Neuron 20: 797-807.

Fujita Y, Mynlieff M, Dirksen RT, Kim MS, Niidome T, Nakai J, Friedrich T, Iwabe N, Miyata T, Furuichi T, Furutama D, Mikoshiba K, Mori Y, Beam KG (1993) Primary structure and functional expression of the omega-conotoxin-sensitive N-type calcium channel from rat brain. Neuron 10:585-598.

Gurnett CA, De Waard M, Campbell KP (1996) Dual function of the voltage-dependent calcium channel α_2-δ subunit in current stimulation and subunit interaction. Neuron 16: 431-440.

Guy HR, Conti F (1990) Pursuing the structure and function of voltage-gated ion channels. Trends Neurosci 13: 201-206.

Hagiwara N, Irisawa H, Holtzhauser M, Vetter R, Glossmann H (1988) Contribution of two types of calcium channels to the pacemaker potentials of rabbit sino-atrial node cells. J Physiol 395: 233-253.

Heinemann SH, Terlau H, Stuhmer W, Imoto K, Numa S (1992) Calcium channel characteristics conferred on the sodium channel by single mutations. Nature 356: 441-443.

Hell JW, Westenbroek RE, Warner C, Ahlijanian MK, Prystay W, Gilbert MM, Snutch TP, Catterall WA (1993) Identification and differential subcellular localization of neuronal class C and D L-type calcium channel alpha1 subunits. J Cell Biol 123: 949-962.

Hering S, Aczel S, Grabner M, Doring F, Berjukow S, Mitterdorfer J, Sinnegger MJ, Striessnig J, Degtiar VE, Wang Z, Glossmann H (1996) Transfer of high sensitivity for benzothiazepines from L-type to class A (BI) calcium channels. J Biol Chem 271: 24471-24475.

Hering S, Aczel S, Kraus RL, Berjukow S, Striessnig J, Timin EN (1997) Molecular mechanism of use-dependent calcium channel block by phenylalkylamines: role of inactivation. Proc Natl Acad Sci USA 94: 13323-13328.

Hering S, Berjukow S, Aczel S, Timin EN (1998) Calcium channel block and inactivation: common molecular determinants. Trends Pharm Sci 19: 439-443.

Herlitze S, Garcia DE, Mackie K, Hille B, Scheuer T, Catterall WA (1996) Modulation of calcium channels by G protein βγ subunits. Nature 21: 258-262.

Herlitze S, Hockerman GH, Scheuer T, Catterall WA (1997) Molecular determinants of inactivation and G protein modulation in the intracellular loop connecting domains I and II of the calcium channel α_{1A} subunit. Proc Natl Acad Sci USA 94:1512-1516.

Hescheler J, Trautwein W (1988) Modification of L-type calcium current by intracellularly applied trypsin in guinea-pig ventricular myocytes. J Physiol (Lond) 404: 259-274.

Hille B (1992) Ionic Channels of Excitable Membranes (Sinauer, Sunderland, MA)

Hirning LD, Fox AP, McClesky EW, Olivera BM, Thayer SA, Miller RJ, Tsien RW (1988) Dominant role of N-type calcium channels in evoked release of norepinephrine from sympathetic neurons. Science 239: 57-60.

Hockerman GH, Johnson BD, Abbott MR, Scheuer T, Catterall WA (1997) Molecular determinants of high affinity phenylalkylamine block of L-type calcium channels in transmembrane segment IIIS6 and the pore region of the alpha1 subunit. J Biol Chem 272: 18759-18765.

Holmgren M, Shin KS, Yellen G (1998) The activation gate of a voltage-gated K^+ channel can be trapped in the open state by an intersubunit metal bridge. Neuron 21:617-621.

Hoshi T, Zagotta WN, Aldrich RW (1990) Biophysical and molecular mechanisms of *Shaker* potassium channel inactivation. Science 250: 533-538.

Hoshi T, Zagotta WN, Aldrich RW (1991) Two types of inactivation in *Shaker* potassium channels: effects of alterations in the carboxyl terminal. Neuron 7: 574-556.

Huguenard JR (1996) Low threshold calcium currents in central nervous system neurons. Annu Rev Physiol 58: 329-348.

Hullin R, Singer-Lahat D, Freichel M, Biel M, Dascal N, Hofmann F, Flockerzi V (1992) Calcium channel β subunit heterogeneity: Functional expression of cloned cDNA from heart, aorta, and brain. EMBO J 11: 885-890.

Imredy JP, Yue DT (1994) Mechanism of calcium-sensitive inactivation of L-type calcium channels. Neuron 12: 1301-1318.

Isacoff EY, Jan YN, Jan LY (1991) Putative receptor for the cytoplasmic inactivation gate in the *Shaker* potassium channel. Nature 353: 86-90.

Jay SD, Sharp AH, Kahl SD, Vedvick TS, Harpold MM, Campbell KP (1991) Structural characterization of the dihydropyridine-sensitive calcium channel alpha2 subunit and the associated delta peptides. J Biol Chem 266: 3287-3293.

Josephson IR, Varadi G (1996) The β subunit increases calcium currents and gating charge movements of human cardiac L-type calcium channels. Biophys J 70: 1285-1293.

Kamp TJ, Perex-Garcia MT, Marban E (1996) Enhancement of ionic current and charge movement by coexpression of calcium channel β_{1a} subunit with α_{1C} subunit in human embryonic kidney cell line. J Physiol (Lond) 492 (I): 89-96.

Kay AR (1992) An intracellular medium fomulary. J Neurosci Methods 44: 91-100.

Klugbauer N, Lacinova L, Marais E, Hobom M, Hofmann F (1999) Molecular diversity of the calcium channel α_2-δ subunit. J Neurosci 19: 684-691.

Kukuljan M, Lebarca P, Latorre R (1995) Molecular determinants of ion conduction and inactivation in potassium channels. Am J Physiol 268: C535-C556.

Letts VA, Felix R, Biddlecome GH, Arikkath J, Mahaffey CL, Valenzuela A, Bartlett II FS, Mori Y, Campbell KP, Frankel WN (1998) The mouse stargazer gene encodes a neuronal calcium channel γ subunit. Nat Genet 19: 340-347.

Liu Y, Jurman E, Yellen G (1996) Dynamic rearrangement of the outer mouth of a K^+ channel during gating. Neuron 16: 859-867.

Lopez GA, Jan YN, Jan LY (1994) Evidence that the S6 segments of the *Shaker* voltage-gated potassium channel comprises part of the pore. Nature 367: 179-182.

Lopez-Barneo J, Hoshi T, Heinemann SH, Aldrich RW (1993) Effects of external cations and mutations in the pore region on C-type inactivation of *Shaker* potassium channels. Receptors & Channels 1: 61-71.

MacKinnon R, Aldrich RW, Lee AW (1993) Functional stoichiometry of *Shaker* potassium channel inactivation. Science 262: 757-759.

Marty A (1989) The physiological role of calcium-dependent channels. Trends Neurosci. 12: 420-424.

McDonald TF, Pelzer S, Trautwein W, Pelzer DJ (1994) Regulation and modulation of calcium channels in cardiac, skeletal, and smooth muscle cells. Physiol Rev 74: 365-507.

McPhee JC, Ragsdale DS, Scheuer T, Catterall WA (1994) A mutation in segment IVS6 disrupts fast inactivation of sodium channels. Proc Natl Acad Sci 91: 12346-12350.

McPhee JC, Ragsdale DS, Scheuer T, Catterall WA (1995) A critical role for transmembrane segment IVS6 of the sodium channel alpha subunit in fast inactivation. J Biol Chem 270: 12025-12034.

Mintz IM, Adams ME, Bean BP (1992a) P-type calcium channels in rat central and peripheral neurons. Neuron 9: 85-95.

Mintz IM, Venema VJ, Swiderek K, Lee T, Bean BP (1992b) P-type calcium channels blocked by spider toxin ω-Aga-IVA. Nature 355: 827-829.

Moczydlowski E (1998) Chemical basis for alkali cation selectivity in potassium channel proteins. Chem Biol 5; R291-301.

Mori H, Masaki H, Yamakura T, Mishina M (1992) Identification by mutagenesis of a Mg^{2+}-block site of the NMDA receptor channel. Nature 358: 673-675.

Mori Y, Friedrich T, Kim MS, Mikami A, Nakai J, Ruth P, Bosse E, Hofmann F, Flockerzi V, Furuichi T, Mikoshiba K, Imoto K, Tanabe T, Numa S (1991) Primary structure and functional expression from complementary DNA of a brain calcium channel. Nature 350: 398-402.

Morton ME, Froehner SC (1989) The alpha1 and alpha2 polypeptides of the dihydropyridine-sensitive calcium channel differ in developmental expression and tissue distribution. Neuron 350: 398-402.

Murphy BJ, Rogers CA, Sunahara RK, Lemaire S, Tuana BS (1990) Identification, characterization, and photoaffinity labeling of the dihydropyridine receptor associated

with the L-type calcium channel from bovine adrenal medulla. Mol Pharmacol 37: 173-181.

Ogielska EM, Zagotta WN, Hoshi T, Heinemann SH, Haab J, Aldrich RW (1995) Cooperative subunit interactions in C-type inactivation of potassium channels. Biophys J 69: 2449-2457.

Orrenius S, McConkey DJ, Bellomo G, Nicotera P (1989) Role of calcium in toxic cell killing. Trends Pharmacol Sci 10: 281-285.

Orrenius S, Nicotera P (1994) The calcium ion and cell death. J Neural Transm Suppl 43: 1-11.

Page KM, Stephens GJ, Berrow NS, Dolphin AC (1997) The intracellular loop between domains I and II of the B-type calcium channel confers aspects of G-protein sensitivity to the E-type calcium channel. J Neurosci 17: 1330-1338.

Panyi G, Sheng Z, Tu L, Deutsch C (1995) C-type inactivation of a voltage-gated K^+ channel occurs by a cooperative mechanism. Biophys J 69: 896-903.

Parent L, Gopalakrishnan M, Lacerda AE, Wei X, Perez-Reyes E (1995) Voltage-dependent inactivation in a cardiac-skeletal chimeric calcium channel. FEBS Lett 360: 144-150.

Patil PG, Brody DL, Yue DT (1998) Preferential closed-state inactivation of neuronal calcium channels. Neuron 20: 1027-1038.

Pelzer D, Pelzer S, McDonald TF (1990) Properties and regulation of calcium channels in muscle cells. Rev Physiol Biochem Pharmacol 114: 107-207.

Perez-Reyes E, Cribbs LL, Daud A, Lacerda AE, Barclay J, Williamson MP, Fox M, Rees M, Lee JH (1998) Molecular characterization of a neuronal low-voltage-activated T-type calcium channel. Nature 391: 896-900.

Peterson BZ, DeMaria CD, Yue DT (1999) Calmodulin is the calcium sensor for calcium-dependent inactivation of L-type calcium channels. Neuron 22: 549-558.

Plummer MR, Logothetis DE, Hess P (1989) Elementary properties and pharmacological sensitivities of calcium channels in mammalian peripheral neurons. Neuron 2: 1453-1463.

Pragnell M, DeWaard M, Mori Y, Tanabe T, Snutch TP, Campbell KP (1994) Calcium channel beta-subunit binds to a conserved motif in the I-II cytoplasmic linker of the alpha 1-subunit. Nature 368: 67-70.

Qin N, Olcese R, Bransby M, Lin T, Birmbaumer L (1999) Calcium-induced inhibition of the cardiac calcium channel depends on calmodulin. Proc Natl Acad Sci USA 96: 2435-2438.

Randall AD, Wendland B, Schweizer F, Miljanich G, Adams ME, Tsien RW (1993) Five pharmacologically distinct high voltage-activated calcium channels in cerebellar granule cells. Soc Neurosci Abstr 19: 1478.

Regan LJ, Sah DWY, Bean BP (1991) Calcium channels in rat central and peripheral neurons: High threshold current resistant to dihydropyridine blocker and ω-conotoxin. Neuron 6: 269-280.

Rettig J, Heinemann SH, Wunder F, Lorra C, Parcej DN, Dolly JO, Pongs O (1994) Inactivation properties of voltage-gated potassium channels altered by presence of a beta-subunit. Nature 26; 289-294.

Robitaille R, Adler EM, Charlton MP (1990) Strategic location of calcium channels at transmitter release sites of frog neuromuscular synapses. Neuron 5: 773-779.

Sather WA, Tanabe T, Zhang JF, Mori Y, Adams ME, Tsien RW (1993) Distinctive biophysical properties of class A (BI) calcium channel alpha 1 subunits. Neuron 11: 291-303.

Sather WA, Yang J, Tsien RW (1994) Structural basis of ion channel permeation and selectivity. Curr Opin Neurobiol 4: 313-323.

Schmid R, Seydl K, Baumgartner W, Groschner K, Romanin C (1995) Trypsin increases availability and open probability of cardiac L-type Ca^{2+} channels without affecting inactivation induced by Ca^{2+}. Biophys J 69: 1847-1857.

Sheng ZH, Rettig J, Takahashi M, Catterall WA (1994) Identification of a syntaxin-binding site on N-type calcium channels. Neuron 13: 1303-1313.

Soldatov NM (1988) Purification and characterization of dihydropyridine receptor from rabbit skeletal muscle. Eur J Biochem 173: 327-338.

Soldatov NM, Zuhlke RD, Bouron A, Reuter H (1997) Molecular structures involved in L-type calcium channel inactivation. Role of the carboxyl-terminal region encoded by

exons 40-42 in alpha1C subunit kinetics and calcium dependence of inactivation. J Biol Chem 272: 3560-3566.

Soldatov NM, Oz M, O'Brien KA, Abernethy DR, Morad M (1998) Molecular determinants of L-type calcium channel inactivation. Segment exchange analysis of the carboxyl-terminal cytoplasmic motif encoded by exons 40-42 of the human α_{1C} subunit gene. J Biol Chem 273: 957-963.

Sollner T, Whiteheart SW, Brunner M, Erdjument-Bromage H, Germanos S, Tempst P, Rothman JE (1993) SNAP receptors implicated in vesicle targeting and fusion. Nature 362: 318-324.

Soong TW, Stea A, Hodson CD, Dubel SJ, Vincent SR, Snutch TP (1993) Structure and functional expression of a member of the low voltage-activated calcium channel family. Science 260: 1133-1136.

Stea A, Dubel SJ, Pragnell M, Leonard JP, Campbell KP, Snutch TP (1993) A β-subunit normalizes the electrophysiological properties of a cloned N-type calcium channel alpha-1 subunit. Neuropharm 32: 1103-1116.

Stea A, Tomlinson WJ, Soong TW, Bourinet E, Dubel SJ, Vincent SR, Snutch TP (1994) Localization of functional properties of a rat brain alpha 1A calcium channel reflect similarities to neuronal Q- and P-type channels. Proc Natl Acad Sci USA 91: 10576-10580.

Striessnig J, Glossman H, Catterall WA (1990) Identification of a phenylalkylamine binding region within the aplha1 subunit of skeletal muscle calcium channels. Proc Natl Acad Sci USA 87: 9108-9112.

Stuhmer W, Conti F, Suzuki H, Wang XD, Yahagi N, Kubo H, Numa S (1989) Structural parts involved in activation and inactivation of the sodium channel. Nature 339: 597-603.

Sutton KG, Zamponi GW, Bourinet E, Soong TW, Snutch TP (1998) Alternative splicing of the α_{1A} gene generates distinct P- or Q-type sensitivity to ω-agatoxin IVA. Soc Neurosci Abstracts 24: 21.

Takahashi T, Momiyama A (1993) Different types of calcium channels mediate central synaptic transmission. Nature 366: 156-168.

Talley EM, Cribbs LL, Lee JH, Daud A, Perez-Reyes E, Bayliss DA (1999) Differential distribution of three members of a gene family encoding low voltgae-activated (T-type) calcium channels. J Neurosci 19: 1895-1911.

Tanabe T, Beam KG, Adams BA, Niidome T, Numa S (1990) Regions of the skeletal muscle dihydropyridine receptor critical for excitation-contraction coupling. Nature 346: 567-579.

Tang S, Yatani A, Bahinski A, Mori Y, Schwartz A (1993) Molecular localization of regions in the L-type calcium channel critical for dihydropyridine action. Neuron 11: 1013-1021.

Tomlinson WJ, Stea A, Bourinet E, Charnet P, Nargeot J, Snutch TP (1993) Functional properties of a neuronal class C L-type calcium channel. Neuropharm 32: 1117-1126.

Tottene A, Moretti A, Pietrobon D (1996) Functional diversity of P-type and R-type calcium channels in rat cerebellar neurons. J Neurosci 16: 6353-6363.

Tsien RW, Lipscombe D, Madison DV, Bley RK, Fox AP (1988) Multiple types of neuronal calcium channels and their selective modulation. Trends Neurosci 11: 431-438.

Vassilev PM, Scheuer T, Catterall WA (1988) Identification of an intracellular peptide segment involved in sodium channel inactivation. Science 241: 1658-1661.

Vassilev P, Scheuer T, Catterall WA (1989) Inhibition of inactivation of sodium channels by a site-directed antibody. Proc Natl Acad Sci USA 86: 8147-8151.

Walker D, De Waard MD (1998) Subunit interaction sites in voltage-dependent calcium channels: role in channel function. Trends Neurosci 21: 148-154.

Wang SY, Wang GK (1997) A mutation in segment I S6 alters slow inactivation of sodium channels. Biophys J 72: 1633-1640.

Wheeler DB, Randall A, Tsien RW (1994) Roles of N-type and Q-type calcium channels in supporting hippocampal synaptic transmission. Science 264: 107-111.

West JW, Patton DE, Scheuer T, Wang Y, Goldin AL, Catterall, WA (1992) A cluster of hydrophobic amino acid residues required for fast sodium channel inactivation. Proc Natl Acad Sci 89: 10910-10914.

Westenbroek RE, Ahlijanian MK, Catterall WA (1990) Clustering of L-type calcium channels at the base of major dendrites in hippocampal pyramidal neurons. Nature 347: 281-284.

Westenbroek RE, Hell J, Warner C, Dubel S, Snutch TP Catterall WA (1992) Biochemical properties and subcellular distribution of an N-type calcium channel aplha1 subunit. Neuron 9: 1099-1115.

Williams ME, Feldman DH, McCue AF, Brenner R, Velicelebi G, Ellis SB, Harpold MM (1992a) Structure and functional expression of alpha 1, alpha 2, and beta subunits of a novel human neuronal calcium channel subtype. Neuron 8:71-84

Williams ME, Brust PF, Feldman DH, Patthi S, Simerson S, Maroufi A, McCue AF, Velicelebi G, Ellis SB, Harpold MM (1992b) Structure and functional expression of an omega-conotoxin-sensitive human N-type calcium channel. Science 257:389-395.

Williams ME, Marubio LM, Deal CR, Hans, M, Brust PF, Philipson LH, Miller RJ, Johnson EC, Harpold MM, Ellis SB (1994) Structure and functional characterization of neuronal alpha 1E calcium channel subtypes. J Biol Chem 269: 22347-22357.

Yang J, Ellinor PT, Sather WA, Zhang JF, Tsien RW (1993) Molecular determinants of calcium selectivity and ion permeation in L-type calcium channels. Nature 366: 158-161.

Yatani A, Bahinski A, Mikala G, Yamamoto S, Schwartz A (1994a) Single amino acid substitutions within the ion permeation pathway alter single-channel conductance of the human L-type cardiac calcium channel. Circ Res 75: 315-323.

Yatani A, Bahinski A, Wakamori M, Tang S, Mori Y, Kobayashi T, Schwartz A (1994b) Alteration of channel characteristics by exchange of pore-forming regions between two structurally related calcium channels. Mol Cell Biochem 140: 93-102.

Yellen G, Sodickson D, Chen TY, Jurman ME (1994) An engineered cysteine in the external mouth of the K^+ channel allows inactivation to be modulated by metal binding. Biophys J 66: 1068-1075.

You Y, Pelzer DJ, Pelzer S (1995) Trypsin and forskolin decrease the sensitivity of L-type calcium current to inhibition by cytoplasmic free calcium in guinea pig heart muscle. Biophys J 69: 1838-1846.

Zagotta WN, Hoshi T, Aldrich RW (1990) Restoration of inactivation in mutants of *Shaker* potassium channels by a peptide derived from ShB. Science 250: 506-507.

Zamponi GW, Soong TW, Bourinet E, Snutch TP (1996) Beta subunit coexpression and the alpha1 subunit domain I-II linker affect piperidine block of neuronal calcium channels. J Neurosci 16: 2430-2443.

Zamponi GW, Bourinet E, Nelson D, Nargeot J, Snutch TP (1997) Crosstalk between G proteins and protein kinase C mediated by the calcium channel alpha1 subunit. Nature 385: 442-446.

Zamponi GW (1999) Cytoplasmic determinants of piperidine blocking affinity for N-type calcium channels. J Membr Biol 167: 183-192.

Zhang JF, Randall AD, Ellinor PT, Horne WA, Sather WA, Tanabe T, Schwartz TL, Tsien RW (1993) Distinctive pharmacology and kinetics of cloned neuronal calcium channels and their possible counterparts in mammalian CNS neurons. Neuropharm 32: 1075-1088.

Zhang JF, Ellinor PT, Aldrich RW, Tsien RW (1994a) Molecular determinants of voltage-dependent inactivation in calcium channels. Nature 372: 97-100.

Zhang L, Weiner JL, Valiante TA, Velumian AA, Watson PL, Jahromi SS, Schertzer S, Pennfeather P, Carlen PL (1994b) Whole-cell recording of the calcium-dependent slow afterhyperpolarization in hippocampal neurones: effects of internally applied anions. Pflugers Arch 426: 247-253.

Zuhlke RD, Pitt GS, Deisseroth K, Tsien RW, Reuter H (1999) Calmodulin supports both inactivation and facilitation of L-type calcium channels. Nature 393: 159-162